SANDIA REPORT

SAND2001-1842
Unlimited Release
Printed July 2001

Visualization and Quantification of Heterogeneous Diffusion Rates in Granodiorite Samples by X-Ray Absorption Imaging

Susan J. Altman, Masahiro Uchida, Vincent C. Tidwell, Craig M. Boney, and Bryan P. Chambers

Prepared by
Sandia National Laboratories
Albuquerque, New Mexico 87185 and Livermore, California 94550

Sandia is a multiprogram laboratory operated by Sandia Corporation, a Lockheed Martin Company, for the United States Department of Energy under Contract DE-AC04-94AL85000.

Issued by Sandia National Laboratories, operated for the United States Department of Energy by Sandia Corporation.

Available to DOE and DOE contractors from
U.S. Department of Energy
Office of Scientific and Technical Information
P.O. Box 62
Oak Ridge, TN 37831

Telephone: (865)576-8401
Facsimile: (865)576-5728
E-Mail: reports@adonis.osti.gov
Online ordering: http://www.doe.gov/bridge

Available to the public from
U.S. Department of Commerce
National Technical Information Service
5285 Port Royal Rd
Springfield, VA 22161

Telephone: (800)553-6847
Facsimile: (703)605-6900
E-Mail: orders@ntis.fedworld.gov
Online order: http://www.ntis.gov/ordering.htm

SAND2001-1842
Unlimited Release
Printed July 2001

Visualization and Quantification of Heterogeneous Diffusion Rates in Granodiorite Samples by X-Ray Absorption Imaging

Susan J. Altman
Vincent C. Tidwell
Craig M. Boney
Bryan P. Chambers
Geohydrology Department
Sandia National Laboratories
P.O. Box 5800
Albuquerque, NM 87185-0735

Masahiro Uchida
Repository Systems Analysis Group
Japan Nuclear Cycle Development Institute
Tokai Works, Tokai-mura, Ibaraki-ken
319-1194, Japan

Abstract

Heterogeneous diffusion in different regions of Cretaceous granodiorite samples from Japan has been observed directly through the use of X-ray absorption imaging. These regions of interest include gouge-filled fractures, recrystallized fracture-filling material and hydrothermally altered matrix. With the X-ray absorption imaging technique, porosity and relative concentration and mass of an iodine tracer can be imaged over the samples in two-dimensions with a sub-millimeter pixel scale. Based on the relative mass estimates, diffusion coefficients for these different regions were also estimated using both an analytical and numerical technique. The numerical solution estimated both a single diffusion rate and a log-normal multirate distribution for diffusion coefficients for each region. The different methods provided consistent estimates of diffusion coefficients showing different rates of diffusion for the different materials of interest. Estimates of diffusion coefficients from the gouge-filled fractures, fracture-filling material, and altered matrix ranged from 4.5×10^{-10} to 1.2×10^{-9} m^2/s, 9.6×10^{-11} to 4.3×10^{-10} m^2/s, and 3.6×10^{-11} to 3.8×10^{-11} m^2/s, respectively. Diffusion rates for the gouge-filled fractures have not been measured previously due their small aperture and fragility. It was also determined that the imaging technique as applied to these experiments cannot be used quantitatively for regions where the porosity is less than 3% – 4%. Thus

diffusion rates for unaltered matrix and healed fractures were not estimated. The results of these experiments provide evidence that diffusion from advective zones in fractures through the gouge-filled fractures and recrystallized fracture-filling material could increase the surface area available for matrix diffusion. This evidence is important for understanding the performance of potential nuclear waste repositories in crystalline rocks as diffusion is thought to be an important retardation mechanism for radionculides.

ACKNOWLEDGMENTS

This paper was improved through reviews by Sean McKenna and Erik Webb. Chris Rautman provided the geological descriptions of samples. Irene Farnham was responsible for analyzing the outflow-solution for iodide concentrations. Bob Hardy provided much appreciated advice in the sample preparation.

This project was funded by Japan Nuclear Cycle Development Institute (JNC). This work was conducted jointly between Sandia National Laboratories (SNL) and JNC under a joint JNC/U. S. Department of Energy (DOE) work agreement. The experiments were conducted and analyzed at the Flow Visualization and Processes Laboratory at SNL with a large amount of input from JNC to make sure the results would be relevant for the Japanese nuclear waste program.

This page is intentionally left blank

CONTENTS

LIST OF TABLES

This page is intentionally left blank

LIST OF FIGURES

This page is intentionally left blank

1 INTRODUCTION

Matrix diffusion of radionuclides during transport is thought to be an important factor in delaying potential releases from deep geologic waste repositories [*Neretnieks*, 1980]. The safety assessment study of the geological disposal system in Japan found the rock matrix retardation parameters to be one of the most important parameters effecting maximum dose [*JNCb*, 2000]. These parameters include the proportion of the fracture surface from which the nuclides can diffusion into the matrix and the maximum depth into the matrix in which radionuclides can diffuse. In the performance assessment calculations it is assumed that radionuclides can only diffuse into matrix in direct contact with the areas of the fractures where water is flowing, the flow-wetted surface (FWS). The proportion of the fractures with flowing water was 50% for the reference case with a range of 10% to 100% for sensitivity studies. There is a two-order of magnitude range in released dose over the sensitivity-study range.

In reality, field and laboratory studies have shown that the crystalline rocks over which the safety assessment study was designed are extremely heterogeneous. Examination of crystalline rocks commonly shows an altered rim (or halo) along the entire fracture surface, which is often indicated by orange, pink or white coloring. The presence of this altered matrix gives evidence that there is access via diffusion along the entire fracture surface. Therefore most of the rock matrix adjacent to the fracture could be available for matrix diffusion. It is therefore possible that due to diffusion in the fractures the FWS could be increased to 100% in the performance-assessment time scale, making the 50% value used in the reference case over-conservative.

The conceptual model of a water-conducting fracture contains four distinct zones: gouge-filled fractures, recrystallized fracture-filling material, altered matrix and unaltered matrix (Figure 1). Through-diffusion experiments have shown that diffusion rates in the recrystallized fracture-filling material, altered and unaltered matrix different from each other [*Ota et al.*, 1998]. However, these materials are fragile and cover small areas and are thus difficult to measure.

The purpose of this study is to quantify the heterogeneous nature of the diffusion rates through the different materials by use of X-ray absorption imaging. X-ray absorption imaging allows for quantitative measurements of porosity and relative concentration and mass in two dimensions with pixel sizes on the sub-millimeter scale [*Tidwell and Glass*, 1994; *Tidwell et al.*, 2000]. Relative concentration and mass are measured over time as a tracer diffuses through the samples. This information can then be used to estimate diffusion coefficients for the regions of interest. The analyses of the experiments will provide relative differences between the effective diffusion coefficients in the region of interest (gouge-filled fractures, recrystallized fracture-filling material, and altered and unaltered matrix). In addition, this technique is being applied to low-porosity materials for the first time. Therefore, an evaluation of the minimum sample porosity needed to obtain quantitative results is also evaluated.

This study is meant to provide information on the effectiveness of the geological environment (in this case fractured-crystalline rock) to act as a natural barrier to radionuclide migration in the case that radionuclides are released from the engineered barrier system (EBS) of a nuclear waste

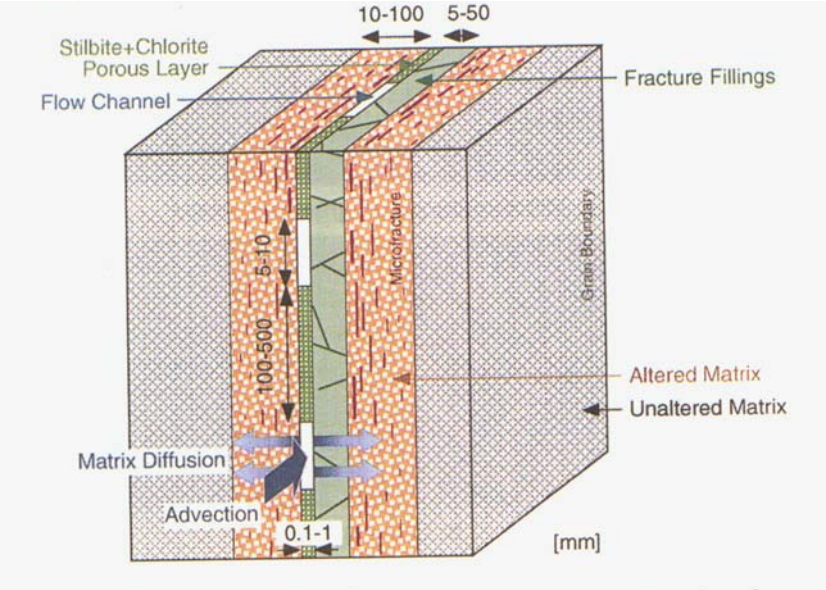

Figure 1: Small-scale conceptual model of a water-conducting fracture in the Kurihashi granodiorite at the Kamaishi mine (from JNCa, 2000). The stilbite and chlorite porous layer is the gouge filling.

repository. Currently, a site for high-level waste disposal has not been selected in Japan. Both fractured crystalline rocks and sedimentary rocks are being studied and evaluated for the safety assessment case. It is proposed that in order to isolate waste from the human environment for long periods of time, the waste will be solidified into a stable vitrified waste form and disposed of in a stable, deep geological environment. In addition, an EBS will be placed around the waste package to further isolate the waste. The geological environment can act as a natural barrier due to slow movement of groundwater from the repository to the accessible environment and retardation mechanisms along the transport pathway. Retardation mechanisms include diffusion into the rock matrix and sorption. Diffusion without sorption leads to a decrease in peak concentration and delay in time to peak concentration. Diffusion alone, however, will not change the total mass released. Matrix diffusion with sorption would lead to additional retardation. If the sorption is irreversible, then the total mass released would be reduced. *Osawa et al.* [1995] reported the results of batch sorption experiments that suggest the materials, especially the recrystallized fracture-filling materials, have the potential to sorb radionuculcides

2 EXPERIMENT DESCRIPTION

Each sub-section in this section describes a step in the experimental set-up in the order they need to be taken. Each step is also shown schematically in Figure 2. The steps are sample selection (Section 2.1), sample preparation (Section 2.2), sample descriptions (Section 2.3), test cell preparation (Section 2.4), tracer solution (Section 2.5), sample saturation (Section 2.6), setting up and running the diffusion experiment (Section 2.7), X-ray absorption imaging (Section 2.8), and X-ray film digitizing (Section 2.9). The analyses of outflow solution (Section 2.10) and potential sources of error (Section 2.11) are also described. The steps taken in analyzing the experiment are described in Sections 3 and the results presented in Section 4. At what steps the data that are needed to make the specific analyses are also shown in Figure 2.

2.1 Sample Selection

Four samples were selected for the purpose of gaining an understanding of the variation in diffusion rates in these different materials of interest: gouge-filled fractures, recrystallized fracture-filling materials, altered and unaltered matrix (Figure 3). More detailed descriptions of each sample after preparation are presented in Section 2.3. The sample naming convention was as follows: "K" indicates the samples came from the Kamaishi mine, and "C" and "B" indicate the samples were extracted from a core or block, respectively. The numbers indicate which core or block the samples came from (in this case 1, since there was only one core and one block) and the letters before the hyphen are an indication of the slice from which the samples were extracted. The information after the hyphen indicates the materials of interest in the sample. For example, the name KC1c-FF explains the sample was extracted from the third slice taken from the first core the came from the Kamaishi mine. "FF" indicates that the fracture-filling materials were what was being examined from the sample. Use of KC1c-FF focused on evaluating diffusion rates through the recrystallized fracture-filling material. Test Cells KC1a-alt and KC1a-unalt were selected to assess diffusion through the altered matrix and unaltered matrix, respectively. Results from KB1am-1 were used to look at diffusion through fractures. The two predominant fractures in KB1am-1 were partially opened and partially filled with gouge material. There were also healed fractures in the sample.

Samples KC1c-FF, KC1a-alt and KC1a-unalt were extracted from a core approximately 15 cm in diameter taken from the Kamaishi mine located in the northern part of Honshu (the main island of Japan). The core sample consisted of fracture-filling material as well as altered and unaltered matrix. The fracture in the core was characterized as a Type-B fracture, meaning it contains a zone of fracture fillings, altered and unaltered matrix [*Osawa et al.*, 1995]. Damage from shipping and handling of the core might have caused fracturing in the fracture-filling material along the plane of the fracture.

Sample KB1am-1 was obtained from a block, approximately 50 cm on a side, also obtained from the Kamaishi mine. Several fractures running perpendicular to the diffusion face were observed. Some of the fractures were filled with high-porosity fault gouge and others were healed. Rock bolts were used to protect the integrity of the fractures during shipping. Altered granodiorite was

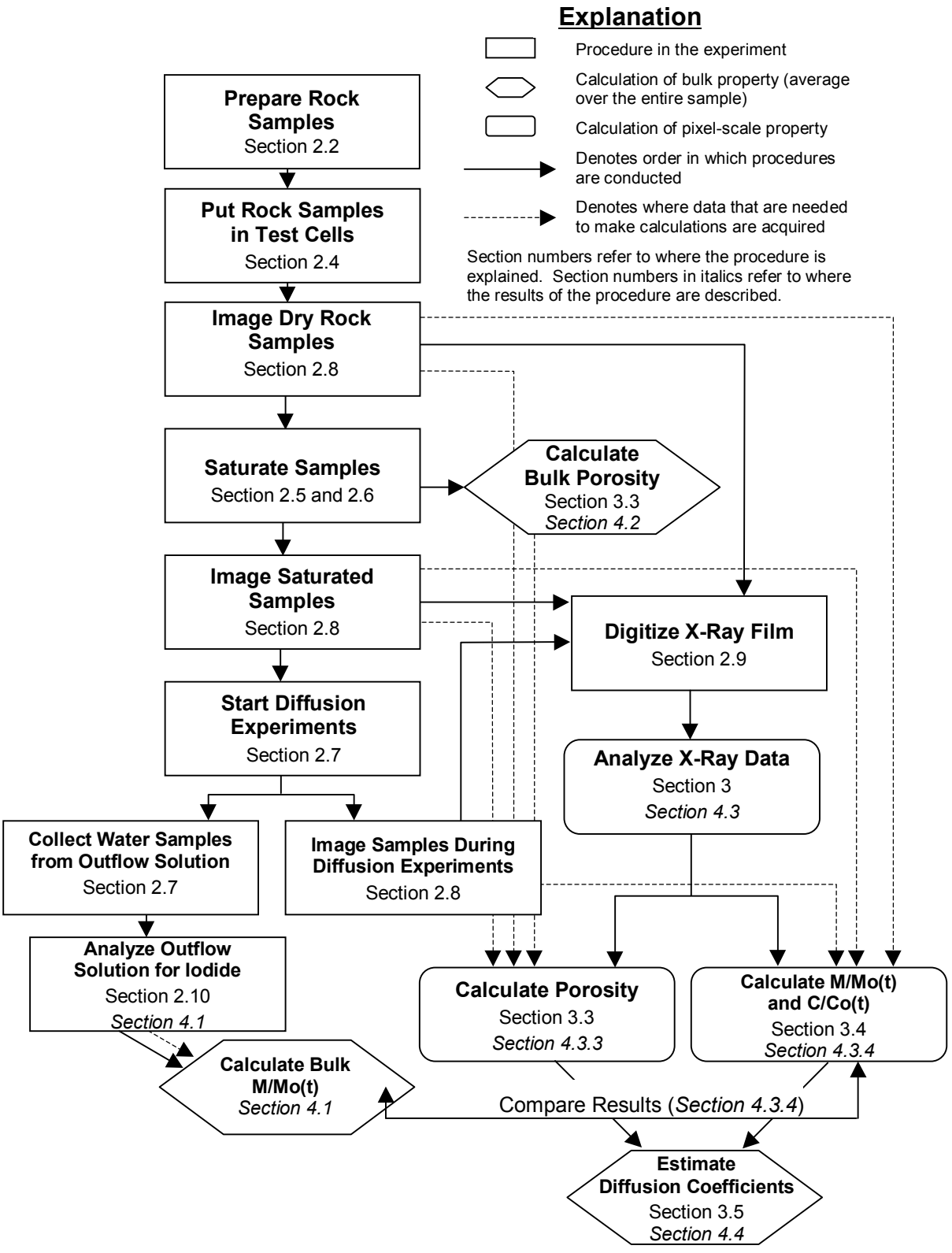

Figure 2: Schematic of the steps in setting up and analyzing the X-ray absorption imaging experiment with corresponding sections showing where the step is described and the results are presented.

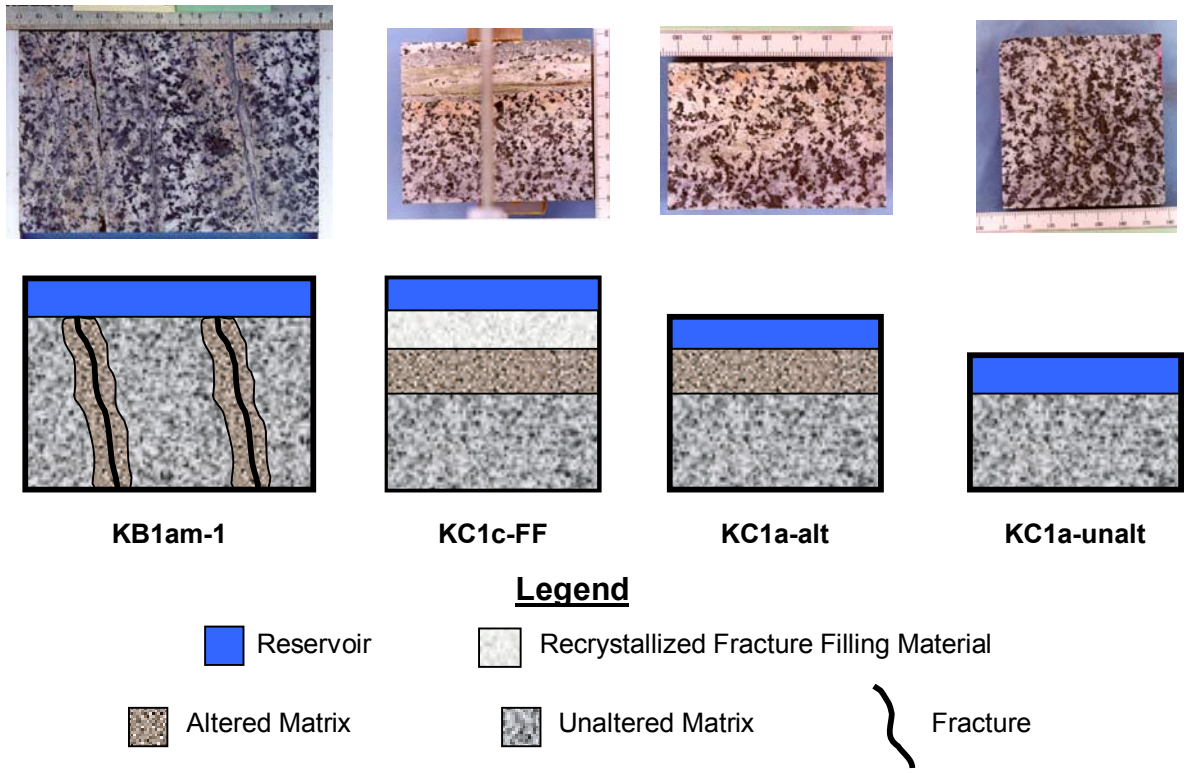

Figure 3: Photographs of rock samples and schematic of the different test cells for the experiments showing how the configuration of the materials with the source terms differs. The regions of interest analyzed for this experiment are the gouge-filled fractures in KB1am-1, the recrystallized fracture-filling material in KC1c-FF, the altered matrix in KC1a-alt, and the unaltered matrix in KC1a-unalt. Scales are in millimeters.

also present in the sample in the vicinity of several of the fractures. One of the advantages of this block over the core described above is that there was less damage to the block during shipping. Therefore, the fractures have been left intact and disturbance or loss of the high-porosity gouge material was probably minimal.

2.2 Sample Preparation

Preparing rock samples to put in the test cell was a time consuming and difficult process for these fragile samples. For each step, care was taken so to not damage the sample. This includes clamping or epoxying the sides of the sample to hold the fractures together. Also, in order not to dissolve any of the sample or have materials precipitate (thus changing the internal pore structure), cutting and grinding was done with as little water as possible.

Sample preparation for samples KC1c-FF, KC1a-alt and KC1a-unalt consisted of:

- Cutting slab from core
- Cutting rectangular piece from slab
- Grinding sample so that thickness is uniform and edges are square with each other.

All three steps were done without using water.

Sample preparation KB1am-1 from the 50 cm block consisted of the following steps:

- Cutting manageable-sized piece from the block
- Cutting rectangular piece for experimental sample from smaller, manageable piece
- Grinding sample so that thickness is uniform and edges are square with each other.

The manageable-sized pieces were extracted from the large block, as depicted in Figure 4, using a large band saw. Minimal water was sprayed on the saw blade as it was exiting the sample. Air was blown on the blade as it re-entered the sample to attempt to minimize the water that entered the sample. As further cutting and grinding was needed to finish the sample, use of water in this step of cutting was not thought to affect the sample. The three pieces extracted from the large block were held together with steel straps. To cut the samples, these steel straps had to be removed from block KB1am. A fiberglass cloth was epoxied on each face of the block to give strength to the sample during the next step of cutting. Care was taken to make sure the epoxy did not seep into the fractures of the sample. Once the cutting was completed the sample was ground so that thickness was uniform and edges were square with each other. In the process the epoxy and fiberglass was ground off the sample. The second stage of cutting and grinding was done without water.

The sample preparation for KB1am-1 was difficult due to the open fractures and loose gouge material. Preparation proceeded successfully until the last step of grinding. Unfortunately, in grinding the final face some gouge material was lost from the sample. It was decided to proceed with this sample as it was thought that there was sufficient gouge material in the sample for the preliminary experiments. It was decided not to refill the fractures with the gouge material because many of the *in-situ* fractures are partially opened and partially gouge-filled.

It should be noted that during the grinding it was difficult to avoid chipping along mineral boundaries. The chips were generally small relative to the size of the sample (approximately 1 mm or less). Chipping was especially prevalent in the fracture filling material. As this chipping exists only along the boundaries of the samples, it is not expected to affect the experimental results significantly.

Final dimensions of samples used in the experiments were measured with electronic digital calipers (Table 1).

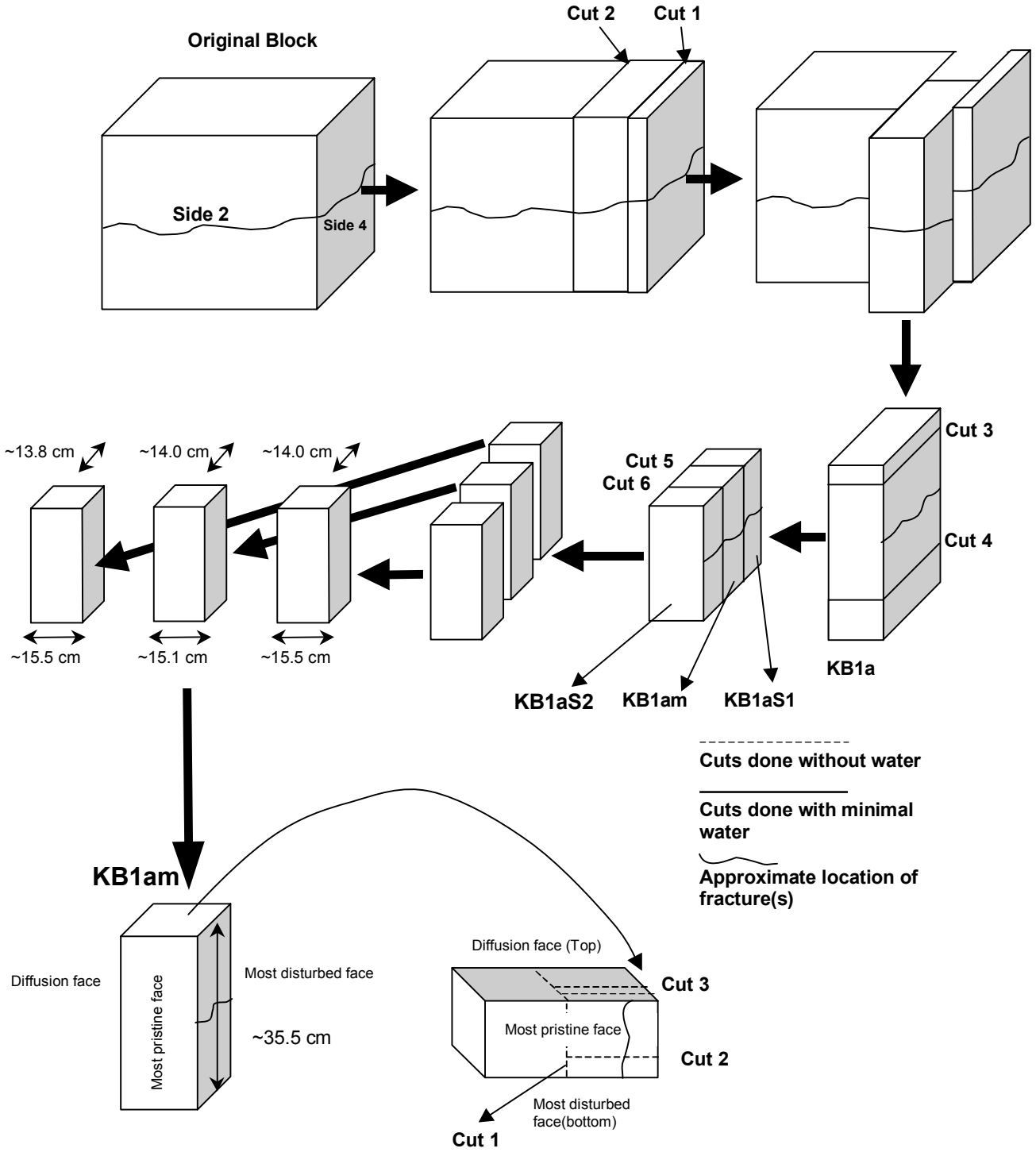

Figure 4: Schematic of cutting of the large block into pieces that can be used for sample KB1am-1.

Table 1: Dimensions of samples

Sample ID	Description	Length (cm)	Width (cm)	Thickness (cm)	Volume (cm^3)
KB1am-1	Fractured sample	10.024	14.989	2.423	364.010
KC1c-FF	Fracture-Filling	7.840	9.241	2.289	165.787
KC1a-alt	Altered matrix	4.940	7.330	2.625	95.034
KC1a-unalt	Unaltered matrix	7.240	6.861	2.641	131.187

2.3 Sample Descriptions

The descriptions of the samples used in the experiments are as follows:

Sample KB1am (Figure 5) — This sample is a composite of variably altered coarse-grained granodiorite, similar to samples KC1a-unalt and KC1a-alt, cut by 4 to 6 prominent fractures, two of which are "open" with an apparent aperture of 1-3 mm. These two open fractures are associated with fine-grained gray siliceous material 1–5-mm thick, and are bordered by a fine-grained mass of white to light-greenish alteration material. Primary feldspar crystals outside these two fractured/veined intervals exhibit gradational changes in color from salmon- pink to white to clear over zones extending 25–30 mm from the center. The largest fracture opening was impregnated with grayish epoxy.

There are also 3–5 less-prominent "healed" fractures, consisting of fine-grained, light gray siliceous material containing streaks and wisps of what may be greenish chlorite. Some of these features exhibit microbreccia fabrics with a clast size typically much finer than 1 mm. Some of these veinlets form weakly anastomosing networks.

A unique feature of this sample in comparison to others in this group is that the entire rock has been flooded with disseminated, brassy-yellow pyrite. Pyrite is present as small cubes and small numbers of octahedral crystals, typically on the order of 1 mm across. Most such occurrences appear associated with biotite crystals, but some cubes and irregular masses are associated with the gray siliceous veining. One large clot of biotite-plus-pyrite exceeds 10–12 mm across.

Sample KC1a-FF (Figure 6) — This sample consists of unaltered and altered material similar to that in samples KC1a-unalt and KC1a-alt, with an alterated zone extending 3–4 cm from a complex, composite fracture/vein system. K-feldspars exhibit gradation from clear to white to salmon-pink approaching the principal fracture that appears to control the alteration. The contact of altered-but- relatively-intact granodiorite with the complex fracture/vein system is quite sharp. Material with a coarse-grained igneous texture transitions to a 1-2 mm medium gray siliceous veinlet, which in turn transitions to a 1-2-mm open fracture, bounded on the opposite side by 5-7 mm of very fine grained unidentifiable micaceous material. This fine-grained, micaceous material appears to be part of a 20-plus mm zone of sheared granodiorite and medium-gray

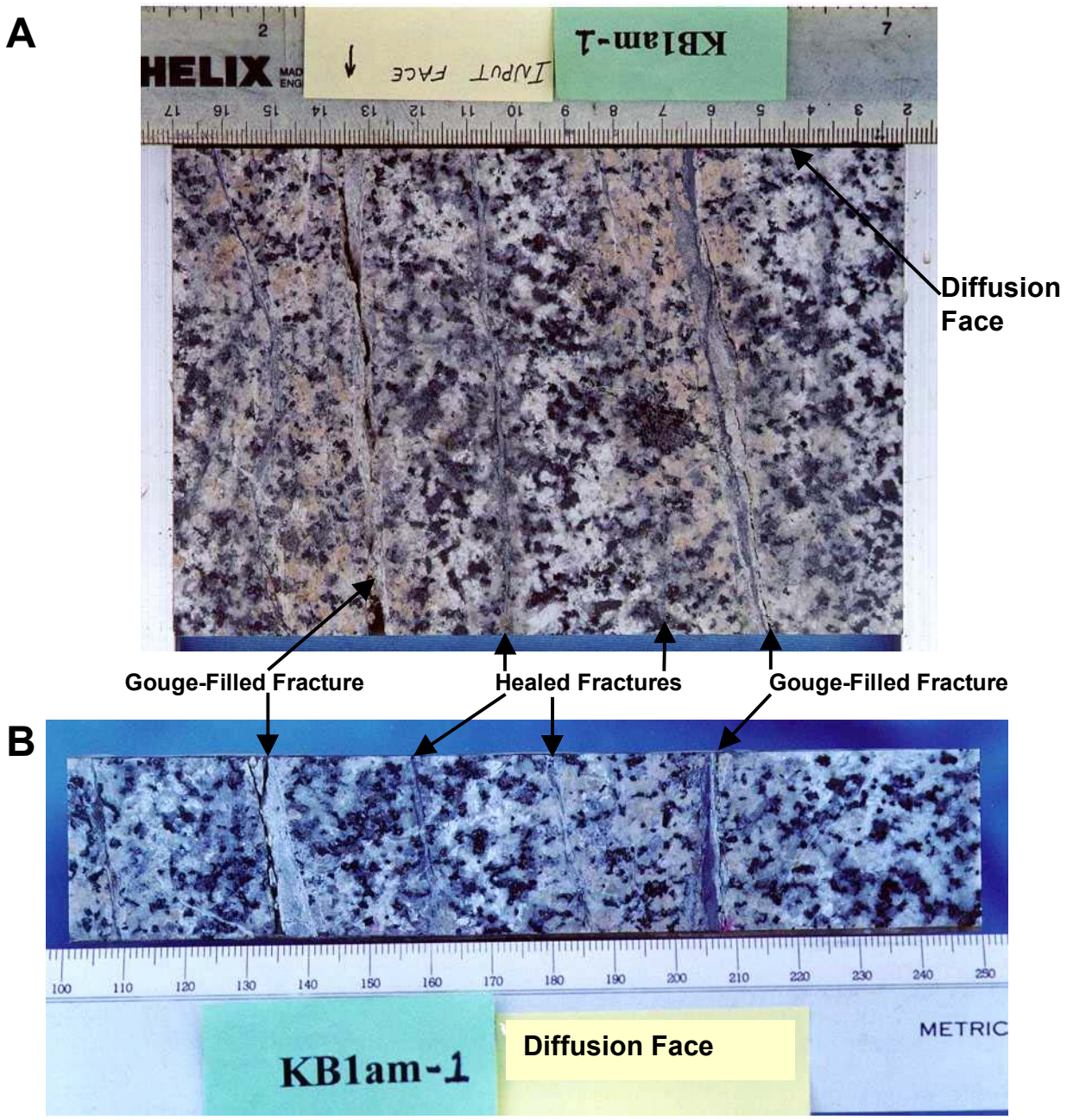

Figure 5: Photograph of two faces of sample KB1am-1. The upper face is the face over which the X-ray images are taken (A). The lower face is the face where the diffusion boundary is located (B). Note gouge-filled and healed fractures. The scale is in millimeters.

siliceous material. The fracture/vein system locally exhibits a microbreccia fabric of finely comminuted material with subrounded to subangular fragments of likely feldspar and/or quartz in the size range of 1–0.1 mm. Traces of pistachio-yellow epidote can be observed along narrow microfractures trending normal to the main fracture plane and along grain boundaries elsewhere in the sample. Medium-gray siliceous veinlets locally cut through feldspar and biotite crystals.

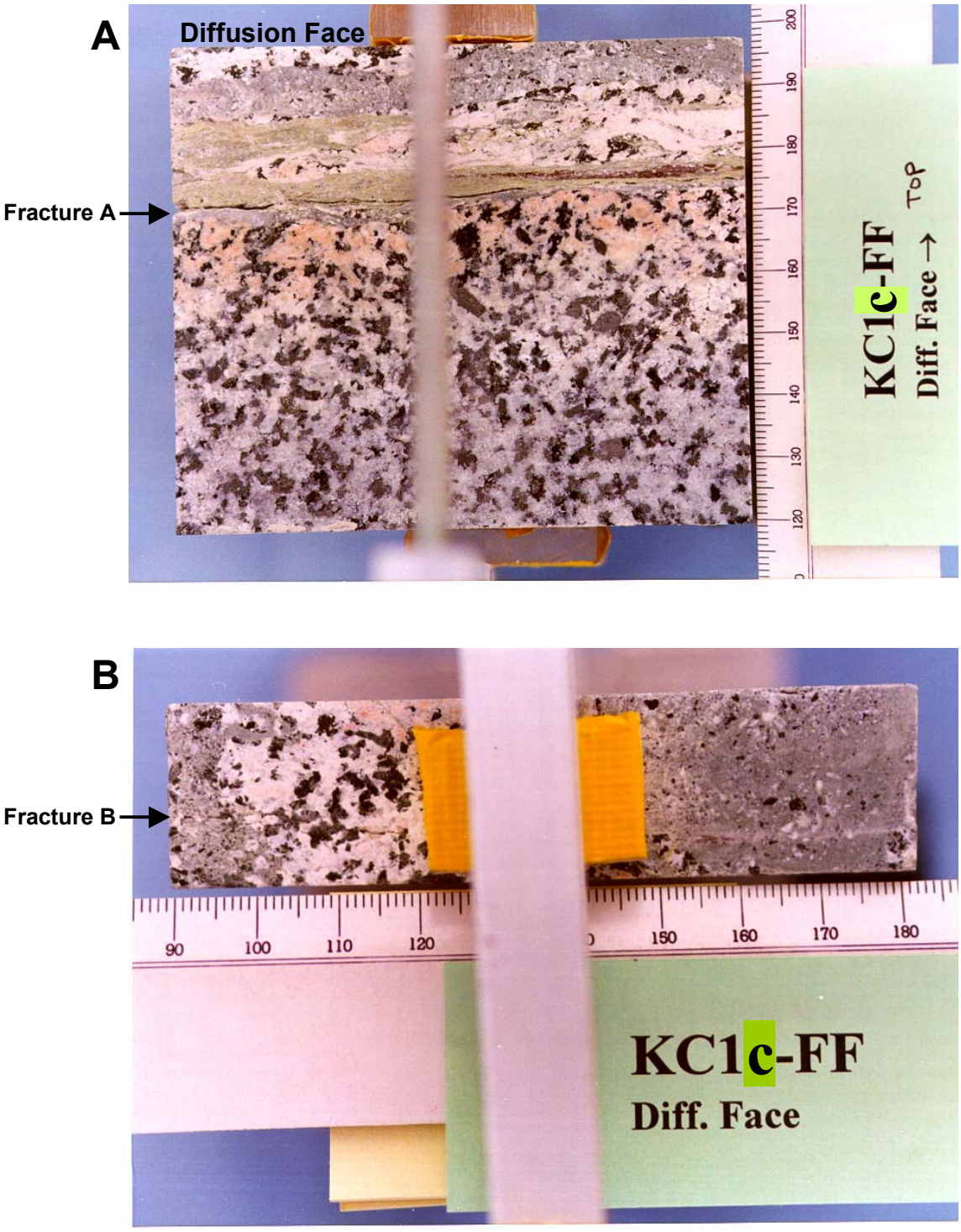

Figure 6: Photograph of two faces of sample KC1c-FF. The upper face is the face over which the X-ray images are taken (A). The lower face is the face where the diffusion boundary is located (B). The portion of the sample above "Fracture A" is the recrystallized fracture-filling material. Fractures A and B could be artificial. The scale is in millimeters.

Rounded blebs of magnetite up to 2-mm across are associated with centers of biotite crystals; some of these blebs appear altered to brassy, yellow pyrite or other sulphide opaque mineral.

Sample KC1a-alt (Figure 7) — This sample consists of a coarse-grained (2–5 mm) rock consisting mostly of subhedral to anhedral crystals of plagioclase, K-feldspar, quartz, biotite, and probable hornblende, basically similar to sample KC1a-unalt. The sample exhibits a strong zonation across its full width from what appears to be unaltered material identical to sample KC1a-unalt to altered material similar to that associated with the hairline fracture in that same sample. Unaltered feldspars are clear to light gray and transparent, whereas in the more altered portions of the rock, the feldspars are white, somewhat chalky and more translucent. The altered feldspars become light salmon-pink and relatively "opaque" in a 1-cm band along one edge of the sample. The salmon-colored material may represent zeolitic alteration to laumontite-stilbite-prehnite, although this sort of material has been seen in potassic-altered intrusive rocks elsewhere ("Kspar flooding"). Complex intergrowths of quarts and K-feldspar are quite evident in the intermediate-altered areas, and there are a small number of weak siliceous veinlets less than 0.1 mm across. There is minor weak epidote staining associated with some biotite crystals, and likely chloritic alteration is also associated with mafic minerals. Rounded blebs of opaque magnetite are associated with some biotite crystals, and there appears to be a trace of brassy, yellow pyrite alteration from magnetite.

Sample KC1a-unalt (Figure 8) — This sample is a coarse-grained (2–5 mm) rock consisting mostly of subhedral to anhedral crystals of plagioclase, K-feldspar, quartz, and biotite with some small subhedral to euhedral crystals of amphibole (hornblende). Rounded blebs of magnetite less than 1-mm in diameter are commonly associated with the centers of biotite crystals. The feldspars are mostly clear to light gray and appear "transparent," becoming distinctly milky-white and more translucent in appearance along a band extending 3–5 mm symmetrically away from a healed hairline fracture containing probable siliceous material. The rock also contains minor pistachio yellow- green epidote in association with (altering from?) biotite. Greenish, probable chlorite is associated with the primary mafic minerals and most likely represents an alteration product.

The following features of the samples should be noted:

- The fracture near the bottom of the fracture filling material in sample KC1c-FF is most likely not natural (Figure 6a, Fracture A). As the diffusion face is on the other end of this material, we hope to be able to characterize the fracture-filling material before the fracture affects the experimental results.

- The fracture along the diffusion face of the KC1c-FF could strongly divert diffusion along the fracture rather than through the matrix causing an effect in the third dimension that may effect experimental interpretation. (Figure 6b, Fracture B)

- Healed fracture exist in samples KB1am-1 and KC1a-unalt (Figures 5 and 8).

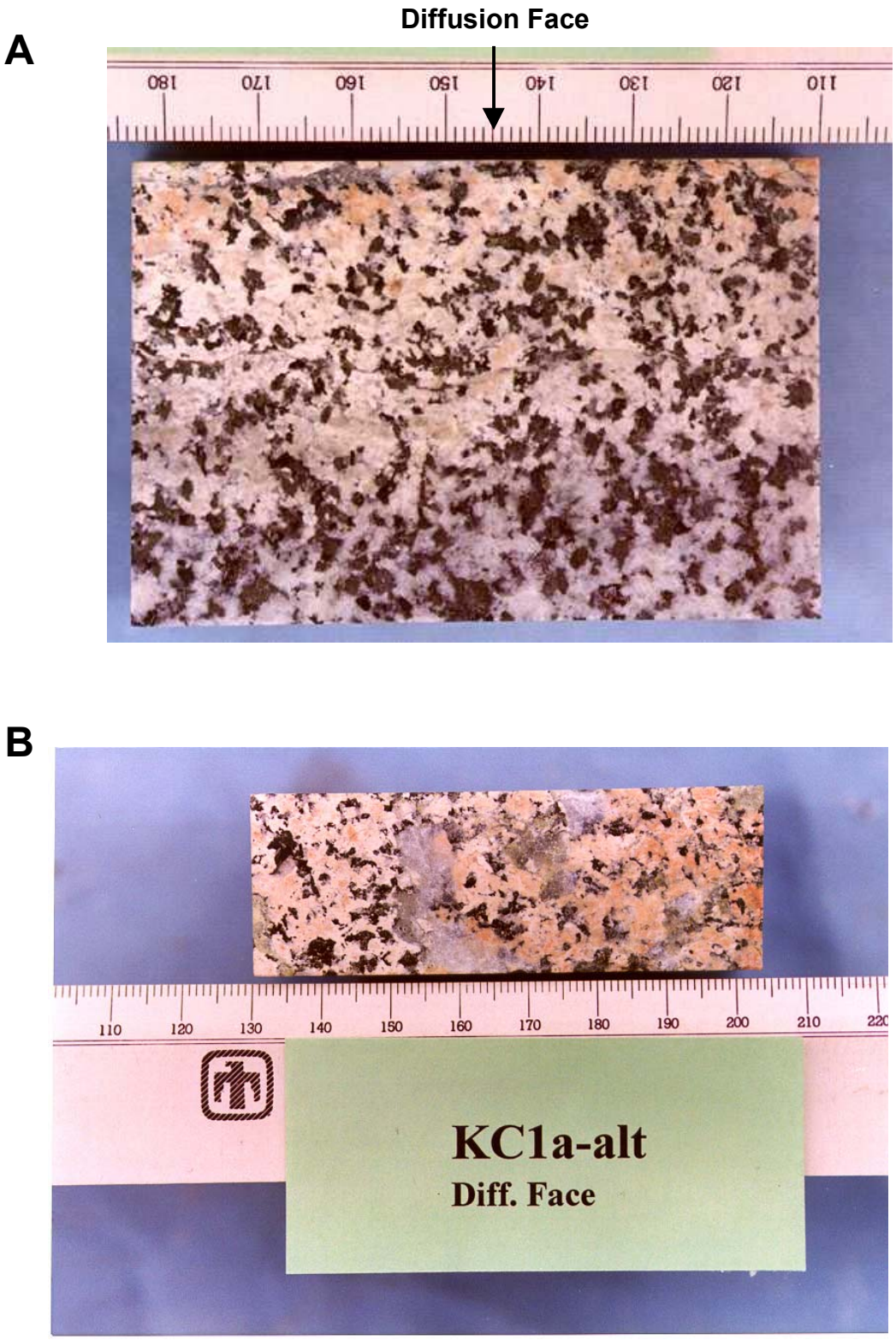

Figure 7: Photograph of two faces of sample KC1a-alt. The upper face is the face over which the X-ray images are taken (A). The lower face is the face where the diffusion boundary is located (B). Note that the pink and bleached white portions are altered matrix. The scale is in millimeters.

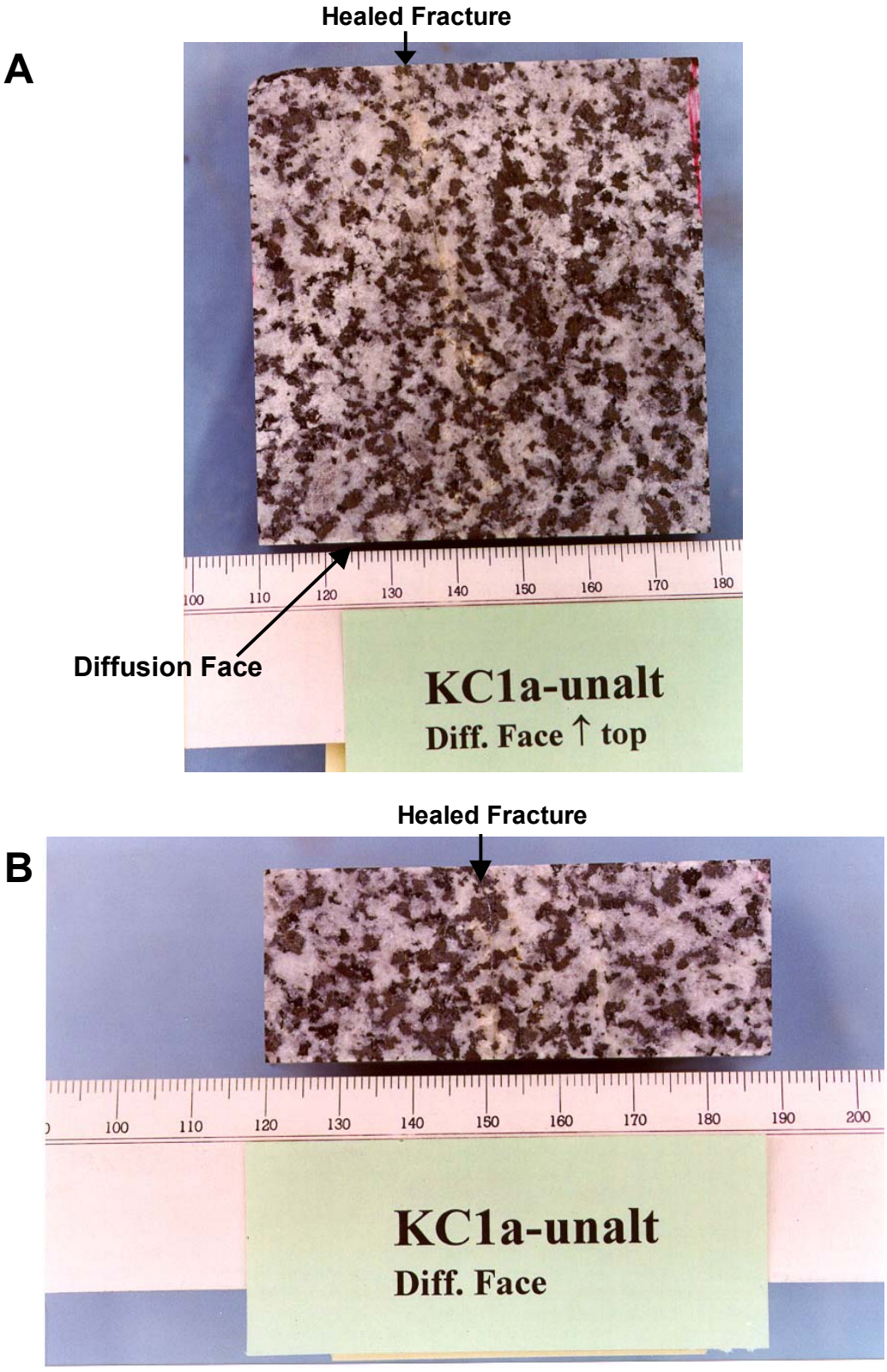

Figure 8: Photograph of two faces of sample for test cell KC1a-unalt. The upper face is the face over which the X-ray images are taken (A). The lower face is the face where the diffusion boundary is located (B). Note healed fractures. The scale is in millimeters.

2.4 Test Cell Preparation

A schematic of the test cells used in the diffusion experiment is shown in Figure 9. Each sample was housed in a separate test cell. Four bars of aluminum were cut to fit around the four edges of each sample. The frame was used to provide rigidity to the test cell, minimize X-ray scatter around the edges of the sample, and provide no-flux boundaries. A reservoir was milled out of one of the aluminum bars, the top of the test cell. Another aluminum bar, the base of the test cell, consisted of two pieces. The piece in contact with the sample has a hole providing access to tracer during saturating process (Figure 9, Piece A). The second piece was constructed so that it would fit in the hole for final assembly (Figure 9, Piece B). By inserting plumber's putty (a

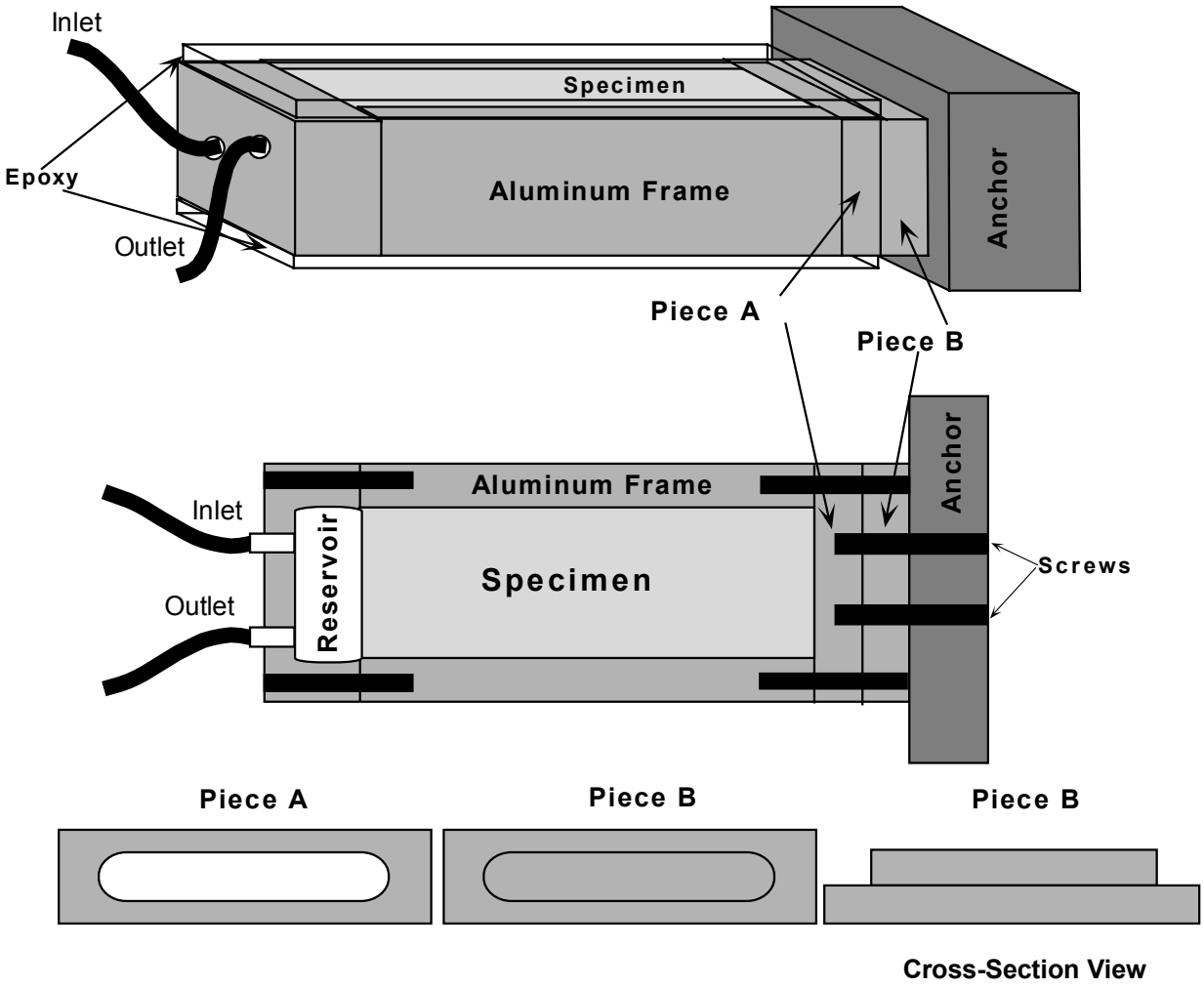

Figure 9: Schematic of a test cell showing oblique and side views. Pieces A and B comprise the bottom aluminum bar on the test cell. Piece A, with its open center is epoxied directly onto the sample. This end remains open during the saturation period. Piece B fits into the open slot of piece A. When inserted with plumber's putty the end now becomes a no-flux boundary.

very low conductivity material) along the end of the sample, in contact with the area where the two pieces join, a no-flux boundary was created.

Once the aluminum bars were constructed, the frame and samples were encased in epoxy. The epoxy was used to form no flux boundaries along the faces and edges of the sample. A high viscosity epoxy was used to minimize imbibition into the rock. One drawback of using the high viscosity epoxy was that air bubbles formed in the epoxy. After putting epoxy on the first face

of sample KB1am-1 it was found that more epoxy than desired entered the fracture. Therefore, on the second face a piece of clear contact paper was sealed over the fracture prior to sealing with epoxy.

2.5 Tracer Solution

Critical to the imaging process is the selection of a tracer that is "visible" to X-ray imaging. In previous studies utilizing X-ray absorption imaging, iodine has been used because it is geochemically conservative and it has favorable X-ray absorption characteristics [*Tidwell et al.*, 2000]. Iodine is assumed to mostly be in the form of the iodide ion.

Ten-weight-percent potassium iodide (KI) was used as the tracer solution. Assuming that the volume of the solution did not change with the addition of the KI, 10 weight percent converts to 100,000 mg/L KI and 76,300 mg/L I^-. Tap water was used as the tracer solution because the chemistry of the tap water was similar to the chemistry of the groundwater where the samples were obtained (see Appendix A for sample water chemistry of Albuquerque, New Mexico municipal water and water from the Kamaishi mine).

Because the samples were saturated in a vacuum chamber (see Section 2.6) some evaporation of the solution took place during the saturating process. Thus, there was some variation in tracer concentration over the saturation period. The density of the solution was measured periodically while the samples were being saturated in order to monitor the evaporation. In addition, 10 weight percent KI solution was added to the container holding the samples periodically during the saturation process.

2.6 Sample Saturation

After the samples were epoxied in their aluminum frame they were ready for saturating. The samples were weighed dry then placed in a vacuum chamber. Once in the chamber the air was removed from the chamber and carbon dioxide (CO_2) emplaced. The air in the chamber was replaced with CO_2, which dissolves more easily in water than air, to minimize the possibility of entrapped air in the sample. The CO_2 was evacuated and refilled into the chamber three times and then was allowed to sit. After sitting in the CO_2 filled chamber for approximately 2.5 hours, the CO_2 was again removed creating a vacuum in the chamber. With the vacuum, the container holding the samples was filled with the tracer solution. Samples were saturated under a vacuum in the tracer solution from April 2, 1999 – May 21, 1999, except for the period between April 20

- April 29 when the samples were left in the tracer solution under ambient conditions. During this entire time period the samples were weighed periodically.

The change in mass for each sample as it saturated is shown in Figure 10. In calculating the change in mass the estimated mass of tracer in the reservoir was taken into account. The estimation of the mass in the reservoir is further discussed in Section 3.3. Ideally one saturates the sample until the change in mass approaches zero. Examination of Figure 10 shows that while the rate of change in mass decreased over the time of the saturation period, there is still an increasing trend in change in mass at the end of the saturation period. The saturation process was very slow and there were time constraints for completing the experiments, therefore, it was decided that the samples were sufficiently saturated after 49 days.

2.7 Diffusion Experiment

Once saturated the test cells were mounted on a steel frame (Figure 11) and the diffusion experiment was ready to begin. The test cells were mounted to provide a consistent position of the samples from X-ray to X-ray shot. The test cells were arranged so that the reservoirs were on top of the rock sample. This position was chosen so that the less dense fluid that circulated through the reservoir was above the denser tracer solution used to saturate the rock sample. Therefore, mixing due to density differences was not expected. A fixed density wedge was also mounted to the frame to provide information that is constant in every image. The wedge was composed of 10% by weight KI solution in epoxy. The absorption of the X-rays increases as this thickness of the wedge increases. Because data from multiple images were required to calculate the relative concentration, total mass, and porosity at a given point, care in registering images

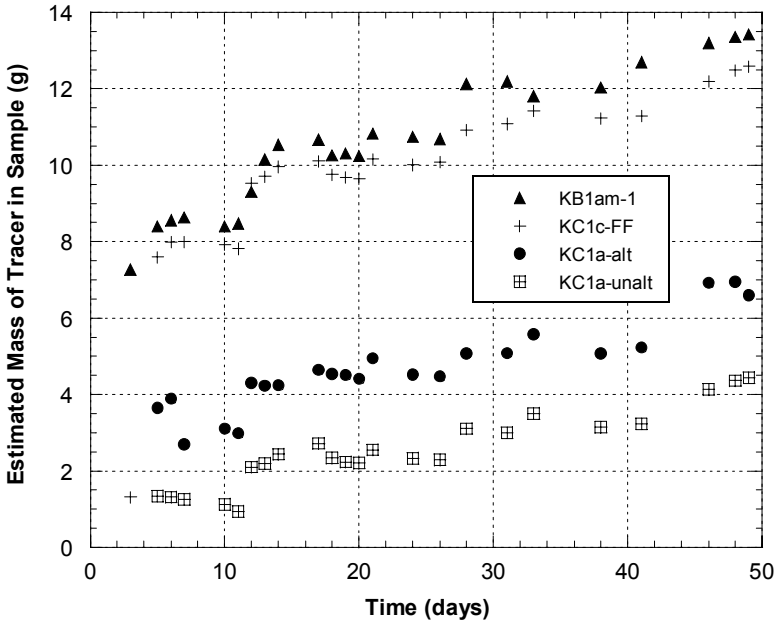

Figure 10: Change in mass in individual samples over the saturation time period.

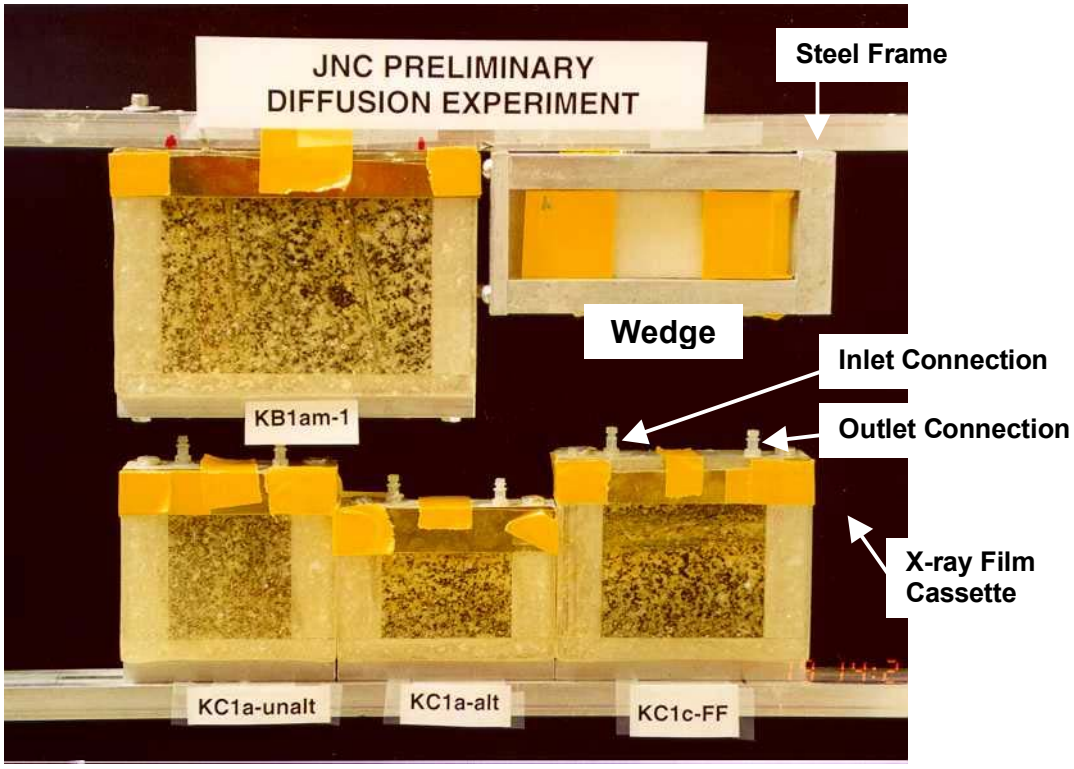

Figure 11: Photograph of test cells mounted on steel frame and in position for X-ray imaging.

was required. To aid in this process, lead reference marks were strategically affixed to the test system.

A schematic of the test system used in the diffusion experiments is shown in Figure 12. The primary components included the sample test cells, the fixed-density wedge, and the fluid delivery system. A constant-tracer-concentration-boundary condition was achieved by circulating fluid (tap water) through the reservoir. Note that the samples were originally saturated with a KI tracer (C = Co) and the concentration boundary condition was C = 0. Therefore, the experiment visualized diffusion out of the samples. The experiments commenced with the circulation of clean, tap water. The water circulated from the upstream reservoir to each individual sample reservoir and out to four separate downstream reservoirs.

The experiments started on May 25, 1999. X-ray images were taken periodically throughout the 202-day duration of the experiment (see asterisks in Figure 13). Note that on May 25, 6 images were taken of samples KB1am-1 and KC1c-FF and 4 images were taken of KC1a-alt and KC1a-unalt. On May 26, 1999 2 images were taken of all the samples. Subsequently, only one image was collected on the specified dates.

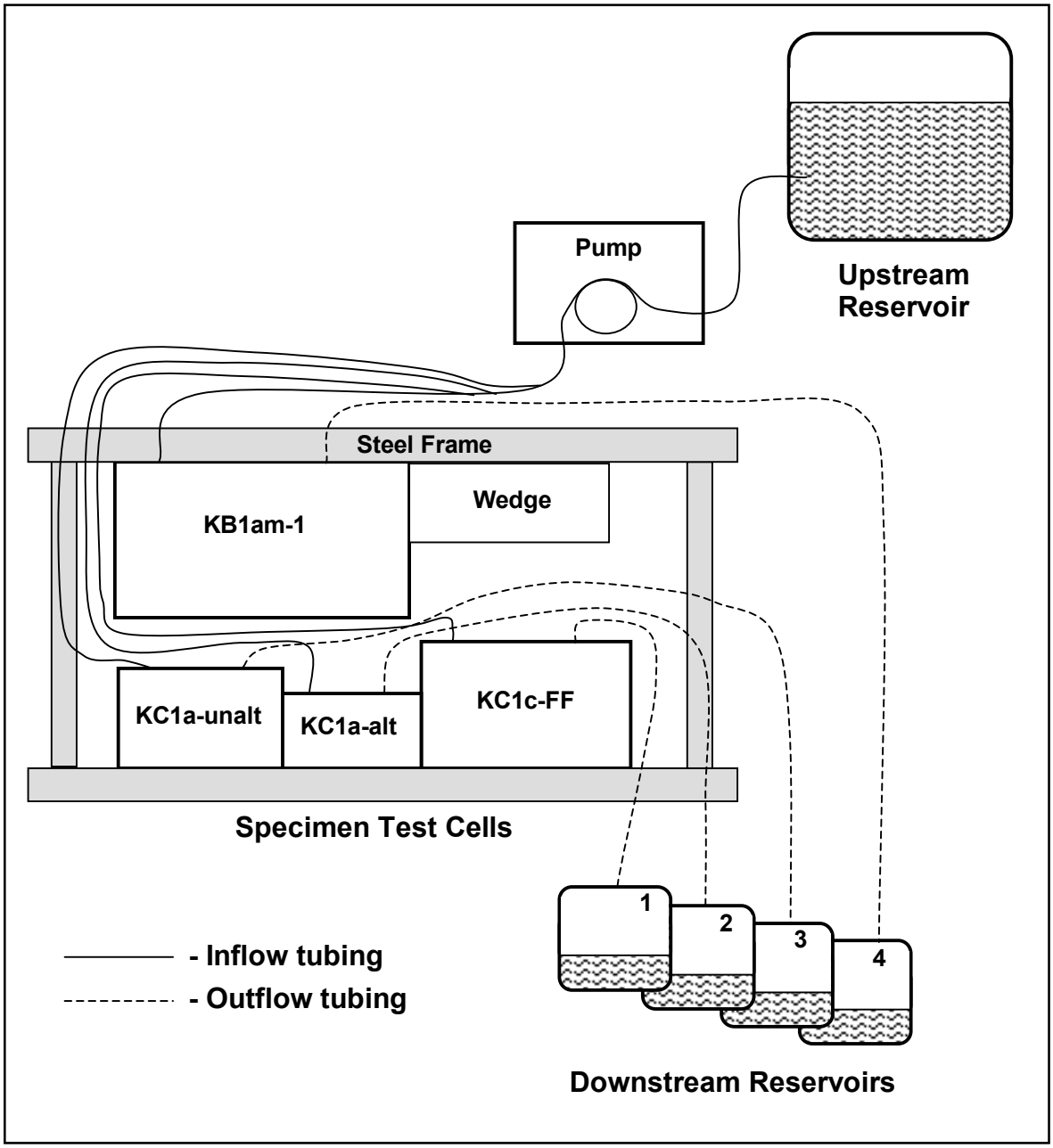

Figure 12: Schematic of experimental system.

Flow rates were maintained at approximately 1 ml/min until June 16, 1999 when it was decreased to approximately 0.5 ml/min. The pump ran continuously for 10 days. After mass out of the samples was thought to have decreased significantly the pump was turned off periodically. Table 2 shows the pumping schedule throughout the time period of the experiment. Flow rates through the reservoir were low enough to avoid positive fluid pressures in the reservoir. The mass of fluid in the downstream reservoirs was monitored gravimetrically in order to check pumping rates.

May 1999

Su	M	T	W	Th	F	S
						1
2	3	4	5	6	7	8
9	10	11	12	13	14	15
16	17	18	19	20	21	22
23	24	25 *	26 *	27 *	28 *	29
30	31 *					

June 1999

Su	M	T	W	Th	F	S
		1 *	2	3 *	4 *	5
6	7 *	8	9 *	10	11 *	12
13	14 *	15 ♦	16 *	17	18 *	19
20	21 *	22	23 *	24	25 *	26
27	28 *	29	30 *			

July 1999

Su	M	T	W	Th	F	S
				1	2 *	3
4	5	6 *	7	8 *	9	10
11	12 *	13 ♦	14 50	15 *	16 ♦	17
18	19 *	20	21	22	23 *	24
26	27	28	29 *	30	31	

August 1999

Su	M	T	W	Th	F	S
1	2 *	3	4	5	6	7
8	9 *	10	11	12	13	14
15	16 *	17	18	19 *	20	21
22	23	24	25 *	26	27	28
29	30	31 *				

September 1999

Su	M	T	W	Th	F	S
			1	2 100	3	4
5	6	7 *	8	9	10	11
12	13	14 *	15	16	17	18
19	20	21	22	23 *	24	25
26	27	28	29 *	30		

October 1999

Su	M	T	W	Th	F	S
					1	2
3	4	5	6	7	8	9
10	11	12	13 *	14	15	16
17	18	19	20	21	22 150	23
24	25	26	27 *	28	29	30
31						

November 1999

Su	M	T	W	Th	F	S
	1	2	3	4	5	6
7	8	9	10 *	11	12	13
14	15	16	17	18	19	20
21	22	23	24 *	25	26	27
28	29	30				

December 1999

Su	M	T	W	Th	F	S
			1	2	3	4
5	6	7	8	9	10	11 200
12	13 *	14	15	16	17	18
19	20	21	22	23	24	25
26	27	28	29	30	31	

Figure 13: X-ray schedule. Bold boxes on May 25 and December 13 mark the start and end of the experiment. The small numbers in the lower portion of some of the boxes mark the number of days the experiment has been running in 50-day increments. Asterisks (*) mark dates when x-ray images were taken. Diamonds (♦) mark dates when leaks were noted.

2.8 X-Ray Absorption Imaging

The central process to the experiments was the acquisition of X-ray images at selected time intervals throughout the test to visualize and quantify the diffusion process such as was used by *Tidwell et al.* [2000]. High-resolution, X-ray absorption images were acquired by directing a beam of X rays at the face of the test cells while recording the transmitted X rays on film secured in a cassette behind the test system. The X-ray source was located a sufficient distance from the film (approximately 2.8 m) to expose the entire film while minimizing parallax. X-ray source parameters used in imaging were tuned to the absorption characteristics of the tracer. A source

Table 2: Pumping schedule during the duration of the experiment

Date Started	Actual Pump Rate (ml/min)[1]	Effective Pump Rate (ml/min)[2]	Hours Pump on Per Day	Minimum reservoirs volumes purged per day
5/25/99	1	1	24	82
6/4/99	1	0.25	6	20
6/17/99	0.5	0.25	12	20
7/8/99	0.5	0.2	9	15
7/22/99	0.5	0.1	5	8
9/20/99	0.5	0.04	2	3

1 – Actual rate pumping.
2 - Effective pump rate as if the pump were running continuously.

intensity of 60 kV at 27 mA was used. The accompanying exposure time was set to maximize image contrast, which is a function of sample thickness and tracer concentration. Exposure time was determined by trial-and-error to be 17 minutes for samples KC1a-alt and KC1a-unalt and 13 minutes for KB1am-1 and KC1c-FF. The exposed X-ray film was developed after each shot and was then ready for digitizing.

2.9 Digitizing of X-Ray Film

Digitizing of the X-ray film is necessary to quantify the information from the experiments, namely the spatial variation in mass of solute in the samples as a function of time. The amount of X rays transmitted through the sample is, in part, dependent on the solute mass. The digitizing process produces gray-level light-intensity values at a pixel scale. The more X rays that are transmitted, the lighter the X-ray film, and therefore the higher the gray-level intensity recorded when digitizing the film. Digitizing was accomplished by placing the exposed X-ray film in front of a diffused bank of high-frequency (60 MHz), high-output fluorescent lights. A computer-controlled feedback loop was used to maintain consistent light intensity during imaging. Variation in the transmitted light intensity field was recorded by means of a charge-coupled device (CCD) camera focused on the front of the X-ray film. The CCD camera output was digitized into an array of at least 1024 x 1024 points, with each point assigned a gray level value between zero and 4095 according to the transmitted light intensity. The array size of the camera and the size of the test system determine the spatial resolution of the acquired image. For this experiment each pixel measured approximately 0.3 mm on a side. To obtain gray-level values for one piece of film, 50 images were acquired by the CCD camera and averaged. This averaging was done to reduce the random error produced by CCD signal noise [*Detwiler et al.*, 1999].

X-ray film taken of samples KC1c-FF and KB1am-1 was digitized at two different times. A group of film was digitized before the experiment was finished (early images). After the experiment was completed the late-time images were digitized along with some of the earlier images. The dry and saturated images were digitized both times. X-ray film taken of samples KC1c-alt and KC1c-unalt was digitized all at one time after the completion of the experiment.

2.10 Analysis of Outflow Solution

As shown in Figure 12, samples were collected from the outflow solution. The sample bottles were changed each time an X-ray image was collected. Bottles were weighed before and after being attached to the experimental system so that the mass of the sample was known. These samples were then analyzed for iodide concentration. Based on the mass and concentration information, the mass of iodide that diffused out of each sample was estimated. The initial mass of iodide in each sample was estimated from the initial concentration of the tracer and the porosity and volume of each sample. Based on these estimates, the mass in the sample at specific times as reported in Sections 4.1 and 4.3.4 were estimated.

Iodide analyses were performed at the Harry Reid Center at the University of Nevada, Las Vegas. The analyses were conducted using a high performance liquid chromatograph (HPLC) consisting of a SpectraSYSTEM P4000 gradient pump, a SpectraSYSTEM AS1000 autosampler, and SpectraSYSTEM UV1000 detector. A SUPELCOSIL^{TM} LC-ABZ Plus column (15 cm x 4.6 mm) with a 5-μm particle size (Supelco, Chromatographic Products, Bellefonte, PA) was used for all analyses. The mobile phase consisted of potassium phosphate buffer (0.05 M KH_2PO_4 adjusted to a pH of 2.7 with H_3PO_4) and either methanol (HPLC Grade, Burdick & Jackson) or acetonitrile with a flowrate of 1mL/minute, an injection volume of 20μL, and a detection wavelength of 230nm. The detection limit of the analyses was 0.005 mg/L.

2.11 Potential Sources of Error

Sources of error can be divided into error associated with running the experiment and image analysis error. Experimental error include errors associated with not completely saturating the samples, sample volume measurements, leaks from the system, and movement of the X-ray head.

As discussed in Section 2.6, there is evidence that the samples were not completely saturated prior to starting the diffusion experiment. The total mass of tracer in the sample is relevant for the estimate of bulk porosity of each sample (see Section 3.3). As the bulk porosity estimates were in the expected range based on previous measurements (Section 4.2), the samples were thought to be saturated sufficiently. Errors in the measurement of bulk porosity will not effect the relative concentration distributions and will only have a minimal effect (if any at all) on the relative mass and therefore diffusion coefficient estimates (Section 3.4).

There are also potential errors in the calculation of the total volume of the samples. The samples were assumed to be rectangular blocks. This assumption is mostly valid because of the careful sample preparation. Several dimension measurements were taken at different locations along the sample and the measurements were consistent. However, it is possible that there was minimal chipping along the edges of the sample. Thus the assumption of rectangular blocks leads to an overestimate of the sample volume. This error only effects the porosity estimates. As stated in the previous paragraph, the porosity measurements were determined to be reasonable and do not have a strong effect on the estimations of diffusion coefficients.

Another source of experimental error is leaks from the system. While running the experiments, yellow staining from the KI solution was noted in the test cells. The staining is due to leaks

between the sample, aluminum bars and epoxy indicating there was an error in the no-flow boundary assumptions. At certain times leaks were noted such that solution was actually dripping from the epoxy-aluminum contacts in the test cells. When these leaks were noted additional sealant was put on the test cells to stop the leaks. The dates of leaks were also noted so that they could be compared with the analyses to see if large drops in concentrations in the test cells coincided with the dates of the leaks (see ♦ in Figure 13). To evaluate the effects of the leaks, comparisons were made between the information obtained from the X-ray data (which could potentially overestimate mass loss due to diffusion) and information obtained from the recovered mass in the outflow solution (which could potentially underestimate mass loss due to diffusion) (see Section 4.3.4).

Movement of the X-ray head during the course of the experiment could also be a source of experimental error. As other experiments were run at the same time, the X-ray head had to be moved in order to take images of these other experiments. Each time images were taken for these experiments care was taken to move the X-ray head back to the original position so that the intensity of the images were consistent. On three dates (June 6, June 11, and June 14), the X-ray head was clearly not aligned correctly and these images were not analyzed. On the other dates, and effects in change of X-ray head location were thought to be minimal. Dates of when the X-ray head had to be re-aligned were noted. Errors from X-ray head movement can be partially corrected with the wedge analyses (Section 3.1). The wedge error analyses (Section 3.1 and 4.3.1) captures this error along with others discussed below.

Potential sources of image-analyses errors include image registration, CCD camera noise, and variations in the light-source intensity, X-ray source intensity, and the film developing process. To assist with film registration lead reference points were affixed to each rock sample. Image registration is accomplished manually, with the assistance of a computer program that minimizes the least-squared difference in distance of these markers. This process allows for the registration of the images within less than $1/10^{th}$ of a pixel (in this case, less than 0.03 mm). As described in Section 3.1, the epoxy wedge was used to correct for temporal variations in the light source intensity and film developing variations. Evaluations of the errors have shown that the errors can be reduced to 3% or less (Tidwell, personal communications). This result is consistent with what errors calculated for the experiments reported here (see Section 4.3.1).

3 EXPLANATION OF IMAGE ANALYSES

The steps taken in analyzing the X-ray absorption imaging data are presented in this section. Section 3.1 describes how the constant density wedge is used to adjust the gray-level intensities in the film to correct for variations in the source intensity and variations in film quality. It also describes how the gray-level information on the wedge is used to calculate errors in the gray-level adjustment. Section 3.2 describes how detection limits of the X-ray absorption imaging technique as employed in this study are evaluated. Sections 3.3 and 3.4 describe how pixel-scale porosity, relative concentration and relative mass are calculated from the gray-level light-intensity information. Finally, Section 3.5 describes how diffusion coefficients were estimated.

3.1 Wedge Error Analysis

As mentioned in Section 2.7, an epoxy wedge was placed on the frame shown in Figures 11 and 12 along with the samples. Therefore, each time an X-ray image was taken, the wedge was imaged. The images of the wedge were then used to correct for variations in the source intensity and variations in film and developing fluid quality.

For each digitized image, the gray-level intensity versus location along the wedge was plotted along the same transect through the wedge. A polynomial function was fit to the wedge data. One curve was chosen as the reference and all other wedge intensity data were mapped back to the reference. Once the reference mapping has taken place, the image gray-level intensities of the entire digitized film (including the samples of interest) were adjusted according to the mapping. The polynomial was thus used to adjust the gray-level intensities so that the gray-levels of the images of the wedge will be approximately the same for all of the images.

By comparing the gray-level intensity of the transect along the wedge of the gray-level adjusted image to that of the reference image, an error analyses can be made:

$$Error = \frac{abs\left(GLI_{ref} - GLI_{image}\right)}{GLI_{ref}} \tag{1}$$

where GLI_{ref} is the gray-level intensity of the reference image and GLI_{image} is the gray level intensity of the gray-level adjusted image.

3.2 Evaluation of Detection Limits

As mentioned in Section 2.11, there are many sources of error associated with the image analyses. Error due to these variations is corrected to some extent and evaluated by the wedge analysis described in Section 3.1. There are also uncontrollable errors such as variation in scattering of X-rays as they hit the test cells and different minerals within the sample. If the variability in gray-level light intensity due to this uncontrollable and uncorrectable error is large

relative to differences in gray-level light intensity between different images of interest, then the technique used in these experiments is not appropriate. For this reason, these uncontrollable and uncorrectable errors, herein referred to as detection limits, were quantified and compared to calculations made using the gray-level light intensity data.

The detection limit is defined as the difference between the average gray-level light intensity of the same sample or region within a sample of two different images taken under the same conditions. In this case images of the samples saturated with iodine were used. For example, the detection limit of the altered region of sample KC1a-alt was determined by 1) calculating the average gray-level light intensity for the altered region of the sample from one sheet of digitized film taken when the sample was saturated with KI, 2) do the same thing from a second sheet of digitized film taken at a different time, 3) calculating the difference between the two average gray-level light intensity values. This method might slightly underestimate the error because the amount of X-ray scattering is also dependent on the amount of tracer in the sample, which changes with time. The detection limit was compared to the difference between the average gray-level light intensity of each individual image taken as a function of time and the image of the dry sample. In doing the detection-limit analyses, the different regions of interest (recrystallized fracture-filling material, gouge-filled fractures, altered and unaltered matrix) were analyzed separately. The whole samples were also examined. As stated in Section 2.9, the images of KB1am-1 and KC1c-FF (and their associated regions of interest) were digitized at two different times. Therefore, early-time, and late-time images are differentiated. Results of this detection-limit analyses are presented in Section 4.3.2.

3.3 Porosity Estimates

The porosity ($\phi_{i,j}$) at each pixel is determined from the X-ray images taken of the tracerless (I_d) and tracer-saturated (I_s) samples. The natural log transformed images are subtracted and then normalized by the mean value and scaled by the bulk porosity:

$$\phi_{i,j} = \frac{\ln(I_s)_{i,j} - \ln(I_d)_{i,j}}{E\left[\ln(I_s)_{i,j} - \ln(I_d)_{i,j}\right]} \phi_{bulk} \frac{z_{i,j}}{z_{avg}} \tag{2}$$

where $E[\ln(I_s)_{i,j} - \ln(I_d)_{i,j}]$ is the average difference between the tracer saturated and tracerless images, ϕ_{bulk} is the bulk porosity of the rock slab, $z_{i,j}$ is the thickness of the slab at point i,j, and z_{avg} is the average thickness of the rock slab. As the samples were all ground to have an even thickness, the $z_{i,j}/z_{avg}$ term drops out of the equation.

The bulk porosity was estimated by calculating the change in mass between the dry samples and saturated sample as follows:

$$\phi_{bulk} = \frac{\left(M_{sat} - M_{dry} - M_{Res}\right)}{\left(\rho_{tracer} V\right)} \tag{3}$$

where M_{sat} is the mass of the saturated sample, M_{dry} is the mass of the dry sample, M_{Res} is the mass of the tracer in the reservoir, ρ_{tracer} is the density of the tracer and V is the volume of the sample. M_{sat} and M_{dry} are measured directly. Two methods were used to calculate M_{Res}: 1) calculating the difference in the mass of the sample with the reservoir full and the reservoir empty, and 2) calculating the mass based on the volume of the reservoir (estimated from the specifications for milling) and the density of the tracer. The density of the tracer was measured periodically throughout the saturation process. The volume of the sample was calculated based on the measurements of the dimensions of the sample prior to putting the sample in the test cell (see Table 1). The minimum porosity was calculated by assuming the maximum tracer density and the maximum mass of tracer in the reservoir. Conversely, the maximum value of the porosity was calculated by assuming the minimum tracer density and the minimum mass of tracer in the reservoir. The expected porosity value was calculated using the measured tracer density (and linearly extrapolating between points when measurements were not made) and the expected volume of tracer in the reservoir (using the second method as described above). Results of the porosity calculations are shown in Sections 4.2 and 4.3.3.

3.4 C/C_o and M/M_o Estimates

Relative concentration is calculated from the adjusted gray-level images by applying linear absorption theory [*Tidwell and Glass*, 1994]. Specifically, at each point or pixel in the image domain the following equation is applied:

$$\frac{C}{C_o} = \frac{\ln(I) - \ln(I_d)}{\ln(I_s) - \ln(I_d)} \tag{4}$$

where I is the transmitted light intensity at a fixed point, I_s is the transmitted light intensity at the same point on the image for the fully tracer-saturated condition (image $C/C_o = 1$), and I_d is the transmitted light intensity at the same point on the image before the sample has been saturated with tracer, the dry image, (image $C/C_o = 0$).

To assist in the analyses, the normalized cumulative mass (M/M_o) for the area of the gouge-filled fractures in KB1am-1, the fracture filling material in KC1c-FF, the altered matrix in sample KC1a-alt, and the entire samples for all four samples was calculated as follows:

$$\left(\frac{M}{M_o}\right) = \frac{\sum_{i=1}^{N}\left(\frac{C}{C_o}\right)_i z_i \phi_i}{\sum_{i=1}^{N} z_i \phi_i} \tag{5}$$

where M is the mass of tracer in the area at the time the X-ray image was taken and M_o is the corresponding quantity when the sample is saturated with tracer, z_i is the thickness of the slab at a given pixel, ϕ_i is the corresponding porosity and N is the number of pixels in the area. The results are the relative concentration and relative mass calculations are presented in Section 4.3.4.

3.5 Diffusion Coefficient Estimates

Two methods were used to estimate the diffusion coefficients for different portions of the samples: an analytical method and a numerical (semi-analytical) method employing multiple rates of mass transfer. The regions of interest (gouge-filled fractures, recrystallized fracture-filling material and altered matrix) were analyzed using both methods. Relative mass as a function of time was calculated for each region, as described in Section 3.4, and used to calculate the diffusion coefficient. The results of the diffusion coefficient estimates are shown in Section 4.4.

3.5.1 Analytical Solution

The configuration of a constant tracer concentration boundary condition along one edge of the test sample while the other edges and faces are maintained as zero flux boundaries allows direct comparison with analytical solutions for 1-D diffusion in a finite slab. According to *Crank* [1975] the relative concentration is a function of position and time $C/C_o(x,t)$ is given by

$$\frac{C}{C_o}(x,t) = 1 - \frac{4}{\pi}\sum_{n=0}^{\infty}\frac{(-1)^n}{2n+1}\exp\left[\frac{-D_e(2n+1)^2\pi^2 t}{4l^2}\right]\cos\left[\frac{(2n+1)\pi x}{2l}\right] \tag{6}$$

where D_e is the diffusion coefficient, l is the slab length, and n is a summation index. Similarly consider M the total mass of tracer in the sample at time t and M_o the corresponding quantity when the sample is saturated, their ratio is given by:

$$\frac{M}{M_o} = 1 - \sum_{n=0}^{\infty}\frac{8}{(2n+1)^2\pi^2}\exp\left[\frac{-D_e(2n+1)^2\pi^2 t}{4l^2}\right] \tag{7}$$

Important assumptions made in these solutions are that the diffusion coefficient is constant (i.e., independent of solute concentration), the porous medium is homogeneous, the tracer is conservative and the boundary conditions are constant throughout the test.

Inversion and truncation of Equation 7 provides a direct means of calculating D_e from the M/M_o profile. *Crank* [1975] gives the relation:

$$D_e = \frac{0.196l^2}{t_{0.5}} \tag{8}$$

where $t_{0.5}$ is the time for which $M/M_o = 0.5$. The diffusion coefficient, D_e is defined as

$$D_e = D_o \tau \tag{9}$$

where D_o is the free water diffusion coefficient and τ is the tortuosity. The error caused by the truncation is reported to be approximately 0.001 percent.

Equations 6 - 8 serve as the basis for analyzing the matrix diffusion. Specifically, the relative concentration $C/C_o(x,t)$ and the mass removal M/M_o as measured by X-ray imaging can be compared directly to Equations 6 and 7 to assess whether matrix diffusion in the samples follows a constant rate. Equation 8 was used to calculate the effective diffusion rate assuming uniform diffusion.

3.5.2 Multirate Modeling

The data analysis methods of *Haggerty and Gorelick* [1998] were also used to evaluate whether multiple rates of diffusion are present during the course of the experiments. To understand the multirate model of mass transfer, one can consider a system as having a distribution of diffusion rates. The scale (both time and length) of the system controls which diffusion rates are important. At large scales, for example, features contributing to fast diffusion rates may become saturated with solute and no longer contribute to the diffusive response of the system. Also at larger scales, more surface area becomes accessible for diffusion. A model of multirate diffusion has been shown to be important in the Culebra dolomite at the Waste Isolation Pilot Plant (WIPP) site, the U. S. Department of Energy's deep geologic repository for transuranic nuclear waste site in New Mexico [*Haggerty et al.*, 2001]. The multirate model also has potential implications for Performance Assessment (PA) calculations [*McKenna et al.*, 2001]. A conventional model of mass transfer with only a single-rate coefficient may be an adequate conceptualization only if the time and spatial scale of the experiment being modeled and the total system being assessed are the same. At the laboratory and field scale it may be possible to determine an adequate integrated single-rate diffusion coefficient. However, such measurements are often not possible at the PA scale. To more appropriately perform PA calculations one must address the scaling issues that influence the mass transfer rate coefficients. One approach is to use a distribution of rate coefficients or calculating an integrated single-rate coefficient that accounts for the multiple rates of diffusion that are appropriate at the PA scale [*McKenna et al.*, 2001].

The curve-matching and Laplace transform methods described by *Haggerty and Gorelick* [1998] were used to calculate the distributional properties of the diffusion coefficients (i.e., mean and variance of a log-normal distribution). *Fleming* [1999] and *Fleming and Haggerty* [2001] developed a code specifically to estimate both multirate and single-rate parameters from experiments with this specific set-up (referred to as static diffusion experiments). The approach for this analysis provides estimates of μ_d (the mean of the natural log distribution of D_e), and σ_d (the standard deviation of natural log distribution of D_e, calculated for multirate diffusion only). The assumed multirate distribution of diffusion coefficients is lognormal. The correct distribution for the materials in these experiments is currently unknown.

The code estimates μ_d and σ_d by normal inversion. The code iteratively simulates the experiment and compares the log-space simulation data to the log-space observed data (M/Mo versus time). Root mean square error (RMSE) was used as a measure of fit, as log-transformed data shows a greater sensitivity to the late-time, low mass ratios at which multirate effects are greatest. The parameter estimation statistics have been provided for the multirate and single-rate interpretations. This information is a useful statistical estimate of the precision of the modeling results, and is the primary advantage of using formal parameter estimation techniques as opposed to conventional manual calibration of the model to the data. The 95% confidence intervals presented in Section 4.4 represents ± 2 standard deviations about the best-fit value of each parameter.

4 RESULTS

This section describes the results of the experiment analyses. Included are the results of analyzing the outflow solution for iodide (Section 4.1) and calculations of bulk porosity values for each sample (Section 4.2). The X-ray image analyses include evaluation of errors as determined by the wedge analyses (Section 4.3.1), detection limits (Section 4.3.2), calculations of pixel-scale porosity (Section 4.3.3) and relative concentration (Section 4.3.4). In addition, the relative mass estimates based on the X-ray data are presented and compared to relative mass estimates based on the outflow solution data (Section 4.3.4). Finally, diffusion coefficient estimates are presented and discussed (Section 4.4).

4.1 Out-Flow Solution Analyses

The concentrations of iodide measured in the outflow solution are presented in Appendix B. Calculations used to estimate iodide mass for each sample presented in Section 4.3.4 are included in Appendix C. Based on blind duplicates, the repeatability of iodide measurements was within 5% with the exception of two samples of concentrations less than 0.04 mg/L. The precision of the analyses was also within 5% for standards with concentrations of 0.25 mg/L and above, within 7% for concentrations of 0.05 mg/L and 2-14% for standards with concentrations of 0.025 mg/L. The lower repeatability and precision for the lower concentrations should not have much impact on the mass estimates, as there is such a low iodide mass in those samples.

4.2 Bulk Porosity Calculations

The bulk porosity estimates are plotted as a function of time during the saturation period in Figure 14. As the samples were still gaining mass during at the end of the saturation period, it is expected that the porosity estimates were still increasing. The error associated with not fully saturating the samples is discussed in Section 2.11. The maximum weight gain over the 49-day saturation period was used to calculate the porosity values as described in Section 3.3 (Table 3).

Table 3: Porosity estimates for each sample

Sample	Description	Expected Porosity	Minimum Porosity	Maximum Porosity	Porosity reported in *Ota et al.* [1998]
KB1am-1	Fractured sample	3.3%	3.0%	3.6%	---
KC1c-FF	Fracture-Filling	6.9%	6.3%	7.6%	5.6% – 8.6%
KC1a-alt	Altered matrix	6.6%	5.9%	7.6%	2.2% – 3.2%
KC1a-unalt	Unaltered matrix	3.1%	2.6%	3.6%	1.1% – 2.3%

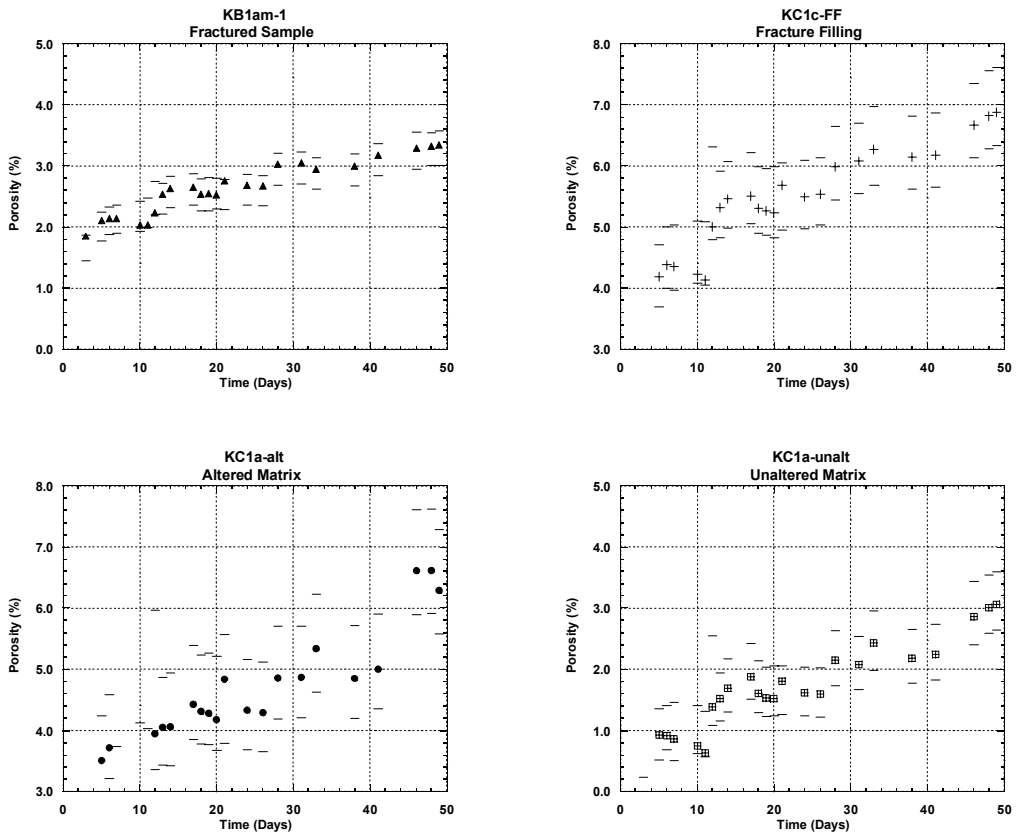

Figure 14: Estimated bulk porosity (with associated error shown as bars) of each sample as a function of time during the saturation period.

Porosity estimates of KC1c-FF and KC1a-unalt are in the range and slightly above of what was reported by *Ota et al.* [1998], respectively. The bulk porosity of sample KB1am-1 is also just slightly above what was reported for the unaltered matrix porosity by *Ota et al*. [1998]. This value is logical since the sample is largely composed of unaltered matrix with some higher porosity regions. For samples KB1am –1, KC1c-FF, and KC1a-unalt the expected porosity was used for the image analyses calculations to calculate the porosity distributions.

It can be seen that the porosity estimates for the KC1a-alt are significantly higher than that reported in *Ota et al.* [1998]. Explanations of the discrepancies could be sample damage during shipping or sample preparation or potential void space between the sample and the epoxy. The discrepancy might also be due to differences in measuring techniques. A smaller sample was measured by *Ota et al.* [1998] that might not have captured the range in porosity values in sample KC1a-alt. Based on the uncertainty in the bulk porosity of sample KC1a-alt, two values were used in calculating the porosity distribution: 6.6% and 3.2%.

4.3 Image Analysis

Error analysis and evaluation of detection limits are presented to determine the adequacy of the X-ray absorption imaging for these experiments. Results focusing on porosity, C/Co, M/Mo distributions and diffusion coefficient estimates for the gouge-filled fractures, recrystallized fracture-filling material and altered matrix are then presented.

4.3.1 Wedge Error Analysis

Figure 15 presents the average, minimum and maximum error for all of the images based on the wedge error analyses (Section 3.1). Examination of Figure 15 shows that the maximum error does not exceed 5%. It can also be generalized that on average, the errors are less than 2% for most of the images. As noted in Section 2.8, samples KC1a-alt and KC1a-unalt were exposed to X rays for 17 minutes where as samples KC1c-FF and KB1am-1 were exposed for only 13 minutes. Therefore, separate film was digitized for the two groups of samples. In addition, the film for samples KC1c-FF and KB1am-1 was digitized at two different times. A group of film was digitized before the experiment was finished (early images) and after the experiment was completed the late-time images were digitized along with some of the earlier images for comparison. The dry and saturated images were digitized at both times.

4.3.2 Evaluation of Detection Limits

Figure 16 shows how close the individual images approach the detection limit, as defined in Section 3.2, as the tracer diffuses out of the samples. In each graph the following values are plotted as a function of time:

$$\frac{GLI_{image}(t) - GLI_{dry}}{\text{Detection Limit}} \tag{10}$$

Thus, a value of 1 indicates the detection limit. Data are presented for the whole sample and the specific regions of interest (gouge-filled fractures (Figure 16a), recrystallized fracture-filling material (Figure 16b), altered matrix (Figure 16c), and unaltered matrix (Figure 16d)).

The farther from the detection limit, the more reliable the data. For the gouge-filled fractures and the recrystallized fracture there is a sufficient difference between the detection limit and the time-dependent data (at least almost an order of magnitude) such that all of the data for these regions are meaningful. However the time-dependent data for both the whole sample and altered-matrix region of KC1a-alt and the whole sample of KC1c-FF does approach the detection limit. Based this information, data from the altered matrix obtained 160 days after the start of the experiment, and possibly even earlier is suspect. These data were therefore not used when calculating diffusion coefficients.

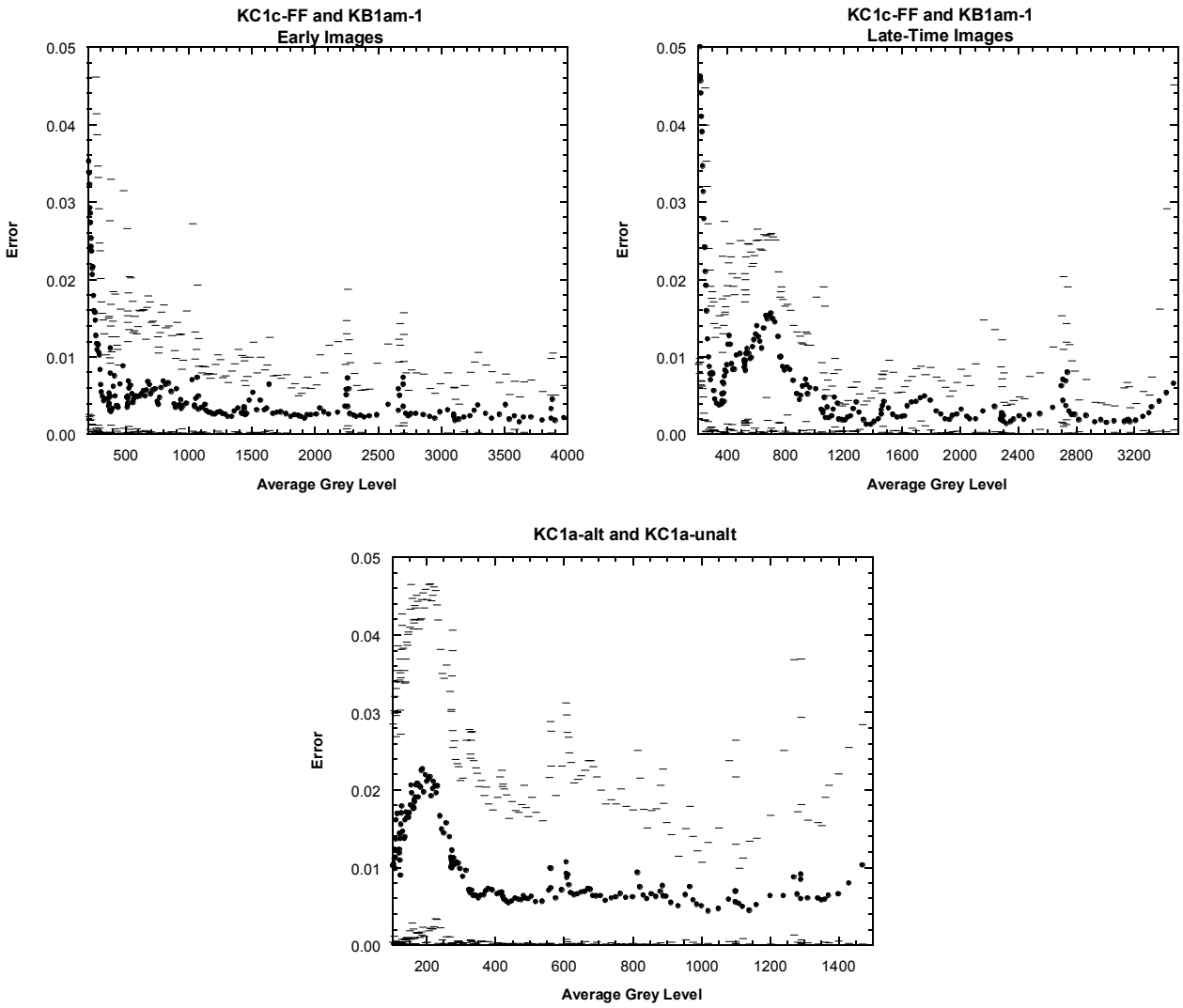

Figure 15: Results of error analysis using the data from the fixed density epoxy wedge. Maximum error does not exceed 5% and on average errors are better than 2%. Filled circles represent mean error of all images and lines represent minimum and maximum error.

The detection limit analyses for the unaltered matrix is quite different than for the other samples. There is a greater amount of scatter in the data and a time-dependent trend is not evident. This scattering and lack of a great enough contrast between the dry and saturated image leads to the conclusions that there is not enough pore-space, and therefore not enough tracer in the sample to make analyses of these images meaningful. Based on this analysis, it appears that the X-ray absorption imaging technique as performed in this experiment only works for regions with average porosity values above 3 – 4%.

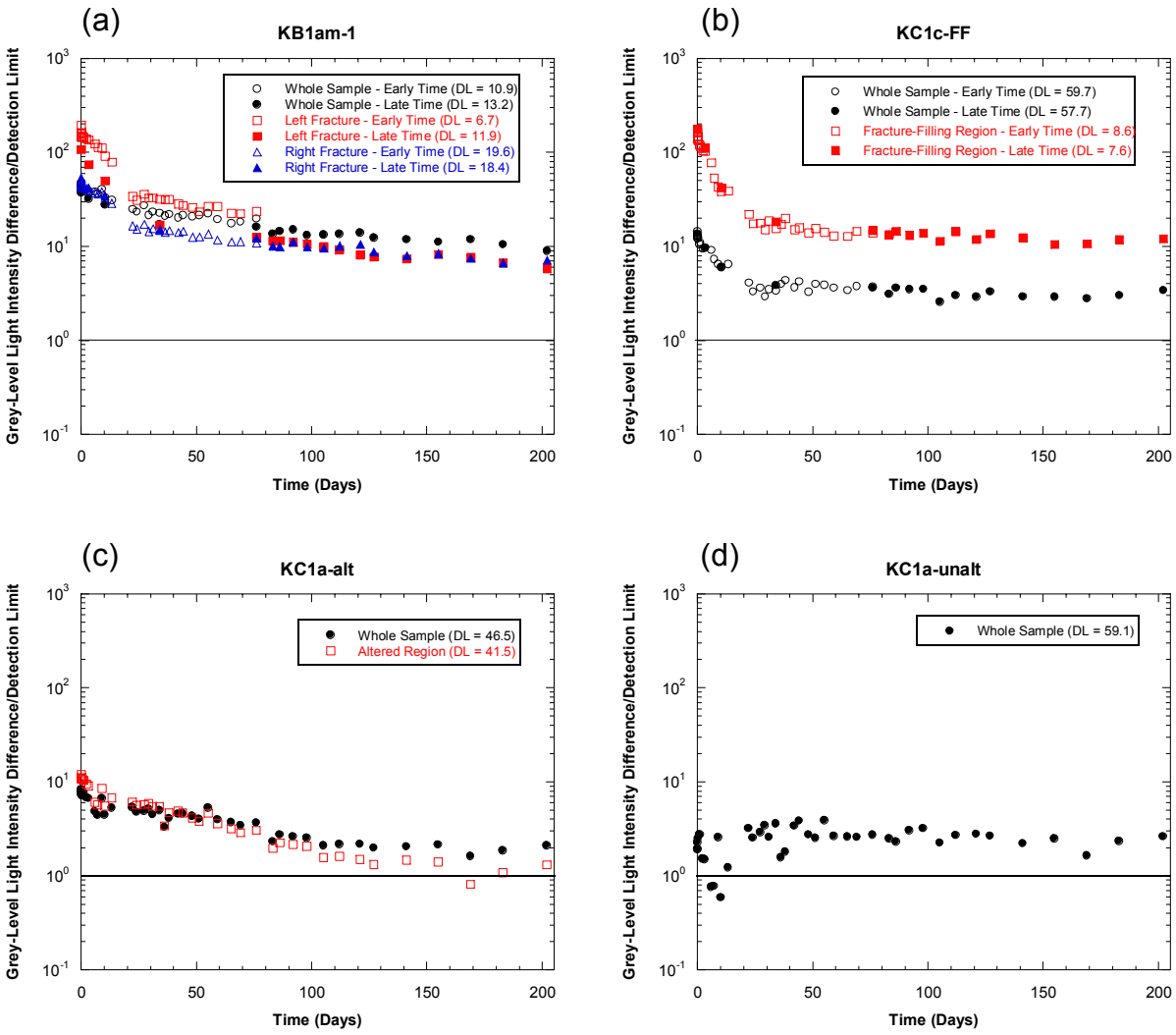

Figure 16: Evaluation of detection limits for whole samples and regions of interest (gouge-filled fractures, recrystallized fracture-filling material and altered matrix). Note the sample KC1a-unalt, which has an average porosity of 3.1% is below the detection limit of the technique. The similarity of the gray-level light intensity differences between the time-dependent images and the dry sample images indicates that the imaging of the whole samples are dominated by the high-porosity regions of interest.

Note that the slopes of the data for the regions of interest are generally slightly steeper than the equivalent slope for the whole sample. This observation is not surprising as the diffusion rates should be faster in the regions of interest and therefore mass loss as a function of time is expected to be greater. What is surprising is that the slopes of the whole samples and the regions of interest are so close to each other. This similarity in slopes implies that diffusion in the higher-porosity regions of interest dominate what is observed in diffusion over the whole sample with the X-ray absorption imaging technique as applied to these experiments.

4.3.3 Porosity Estimates

Porosity distributions of the four samples are presented in Figure 17. A range of 0 – 25% was used to emphasize the high porosity areas, specifically the gouge-filled fractures and the recrystalized fracture-filling material. When the bulk porosity of 6.6% is used to calculate the porosity distribution of KC1a-alt (Figure17d) an area of high porosity is seen in the upper right-hand portion of the sample. This area is thought to be unrealistically high based on other porosity measurements of the altered matrix. As discussed in Section 3.3, it is possible that there is an error in the bulk porosity measurement. If a bulk porosity value of 3.2% [*Ota et al*., 1998] is used, then the porosity distribution of the sample (Figure 17e) seems more realistic. Therefore, a bulk porosity of 3.2% was used in the other image analyses calculations. Examination of the photographs of the sample (e.g. Figure 7) does not give any indication of a higher porosity area in the regions shown in Figure 17d and e. Further examination of the sample is necessary to determine why this higher porosity region exists.

The partially gouge filled fractures showed a range in porosity of 7-21% with an average value of 13% in the left-hand fracture and 9% in the right-hand fracture (Figure 17a). The recrystalized fracture fillings showed a porosity range of 5-24% with an average value of 13% (Figure 17b) and the altered matrix showed porosity ranging from 3-12% (assuming a bulk porosity of 3.2% for the whole sample) with an average porosity of 4% (Figure 17e). The reason why the recrystalized fracture fillings showed higher porosity than the partially gouge filled fracture is not clear. One possible explanation is that these porosity values are calculated over the integrated sample thickness. The partially gouge-filled fractures are rather narrow in width and the fracture plane is not perfectly parallel to the X-ray beam. Thus some matrix could be included in the integration over the thickness of the sample. It is also possible that there was some sample damage to the recrystallized fracture-filling material during shipping and sample preparation leading to some inappropriately high-porosity fractures in the sample (see Figure 6b).

The unaltered matrix generally had porosity values less than 3 to 4%. The healed fractures shown in Figures 5 and 8 are not evident in the porosity image (Figure 13a and c), indicating that they have properties close to that of the unaltered matrix. It is also possible that, as with the gouge-filled fractures, the healed fractures are thin and not perfectly aligned with the x-ray beam and are thus averaged with the matrix material.

4.3.4 C/Co and M/Mo Estimates

C/C_o distributions at various times in the gouge-filled fractures in sample KB1am-1 are shown in Figures 18. It can be seen that the iodide concentration is clearly decreasing in the gouge-filled fractures. In addition, the rates at which they are decreasing is different for the two fractures (note that the same times are shown for both fractures). The fractures themselves are clearly heterogeneous with areas where concentrations decrease faster than other areas. Evidence of three-dimensional diffusion can also be seen in the fracture on the left side of KB1am-1 as low-concentration bullets appear at time = 7.27 and 10.2 days. The fracture-filling material also shows heterogeneous behavior as the concentrations decrease non-uniformly in the material through time (Figure 19).

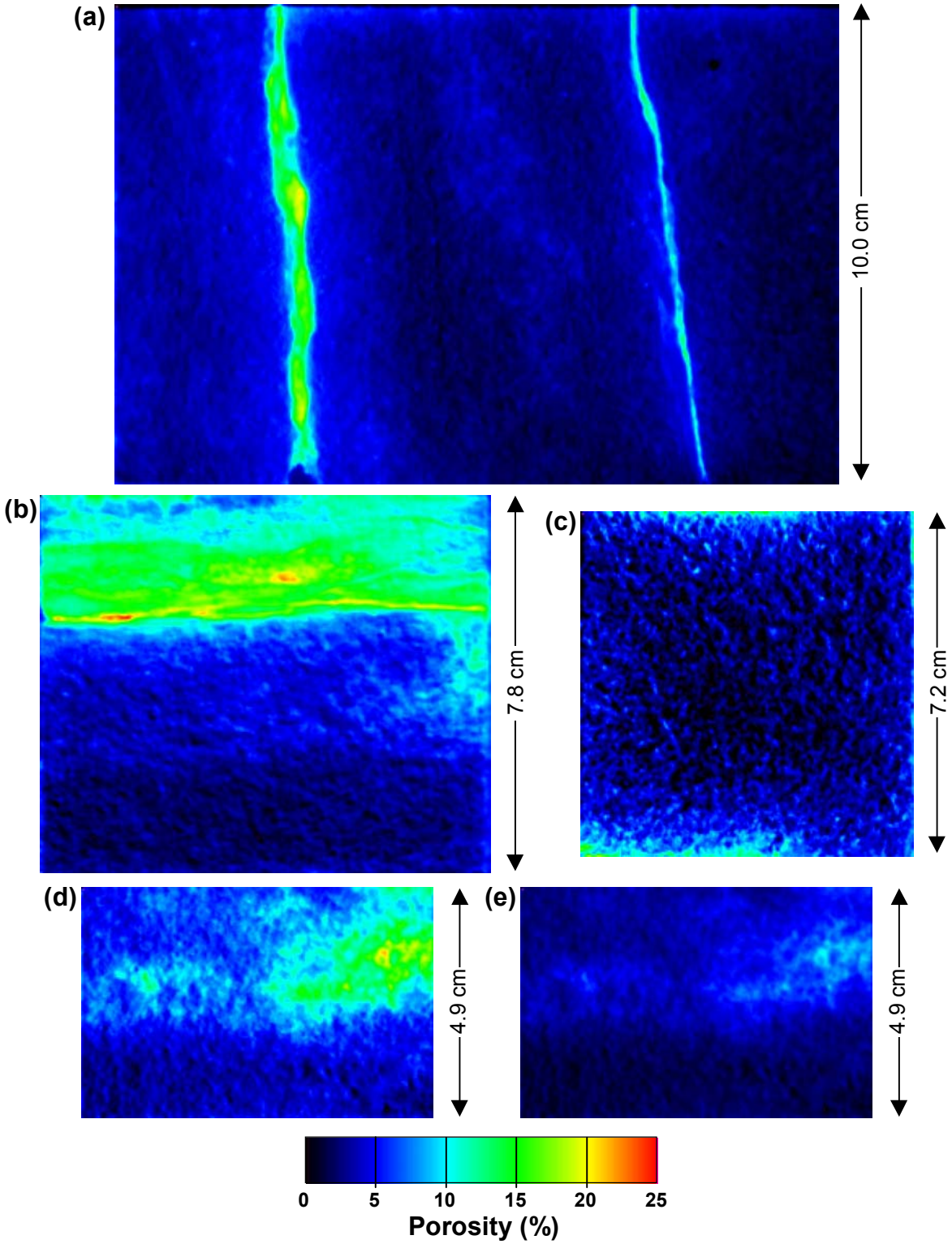

Figure 17: Porosity distribution for each samples KB1am –1 (sample with gouge-filled fractures) (a), KC1c-FF (sample with recrystallized fracture-filling material) (b), KC1a-unalt (sample with unaltered matrix) (c), and KC1a-alt (sampled with altered matrix) (d and e). The mean porosity is set to 6.6% and 3.2% for the images shown in (d) and (e), respectively. Note the range of porosity values shown in each image is 0 – 25%.

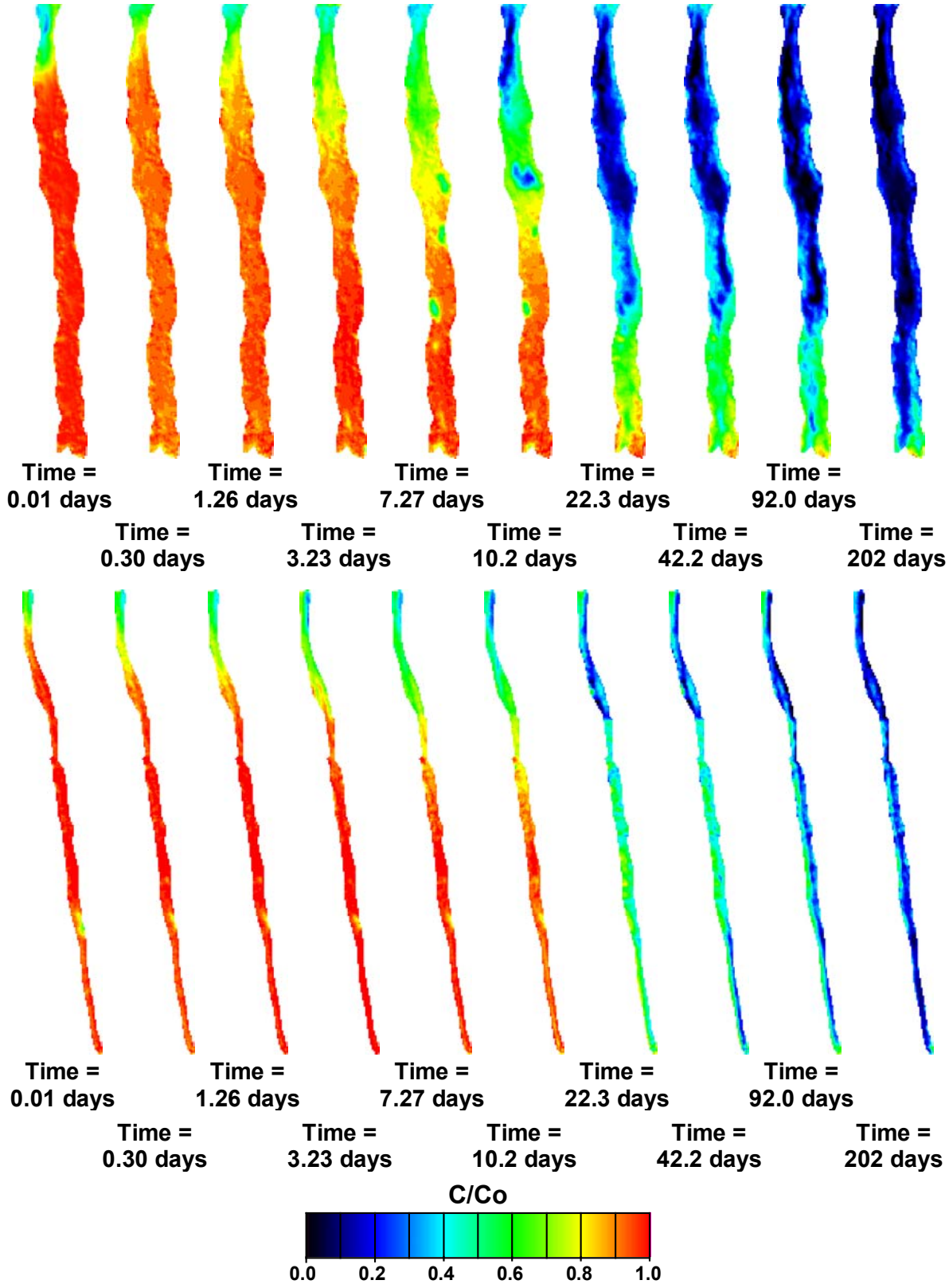

Figure 18: C/Co images of the fractures on the left (top) and right (bottom) side of sample KB1am-1. Observe diffusion out of the samples in the upward direction as a function of time. For scale, each fracture is approximately 10 cm long. Pixel size is approximately 0.3 mm on a side.

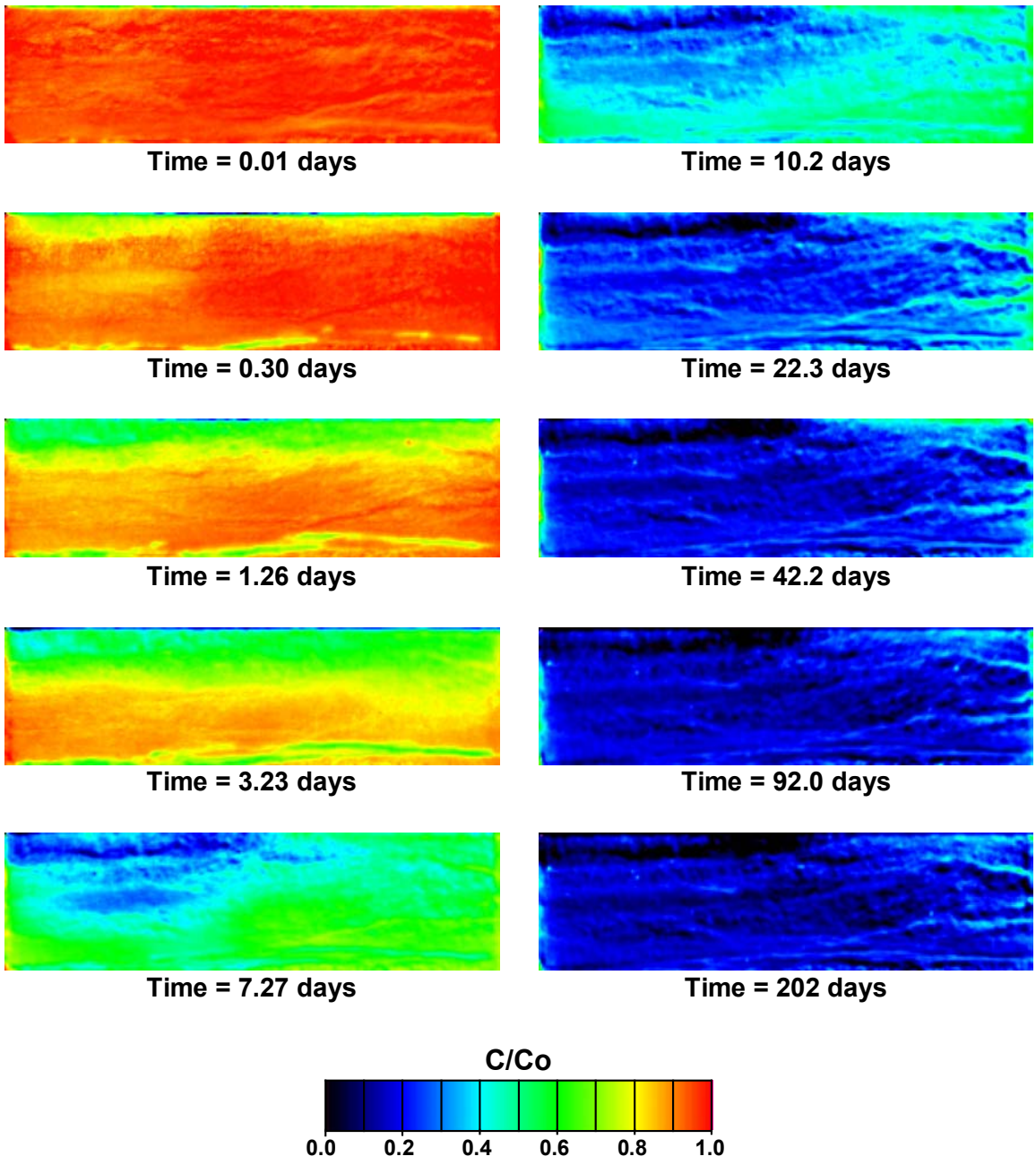

Figure 19: C/Co images of the recrystallized fracture-filling material in sample KC1c-FF. Observe diffusion out of the samples in the upward direction as a function of time. The region shown is approximately 9.4 X 2.6 cm. Pixel size is approximately 0.3 mm on a side.

Concentration distributions through time are also shown for the altered matrix (Figure 20). There appears to be more scatter or noise in these concentration distributions, though the concentrations are clearly decreasing over the time of the experiment. Because there is a smaller difference in contrast between the saturated and dry images in the matrix area, noise in the imaging technique becomes more apparent. It is of interest to note that the high-porosity region

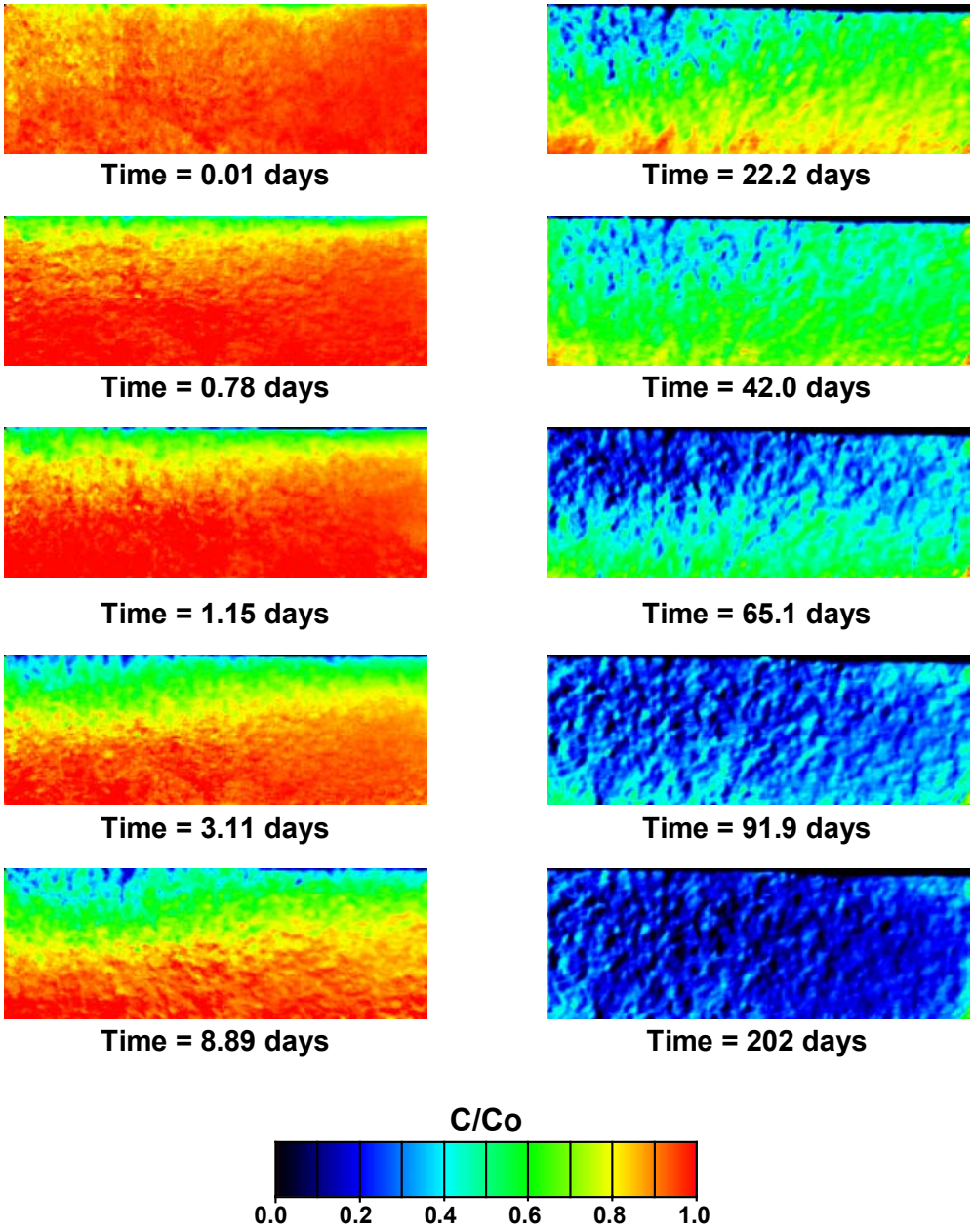

Figure 20: C/Co images of the altered matrix portion of sample KC1a-alt. Observe diffusion out of the samples in the upward direction as a function of time. The region shown is approximately 7.3 X 2.6 cm. Pixel size is approximately 0.3 mm on a side.

evident in Figure 17d and e does not seem to affect the C/Co distributions. In fact, diffusion appears to be faster on the left-side of the sample, away from the high-porosity region.

Relative mass estimates for the entire samples and regions of interest are presented in Figure 21. As a check of the image analyses technique, the relative-mass estimates as calculated based on the analyses of the outflow solution (Sections 2.10 and 4.1) are also included. At very early

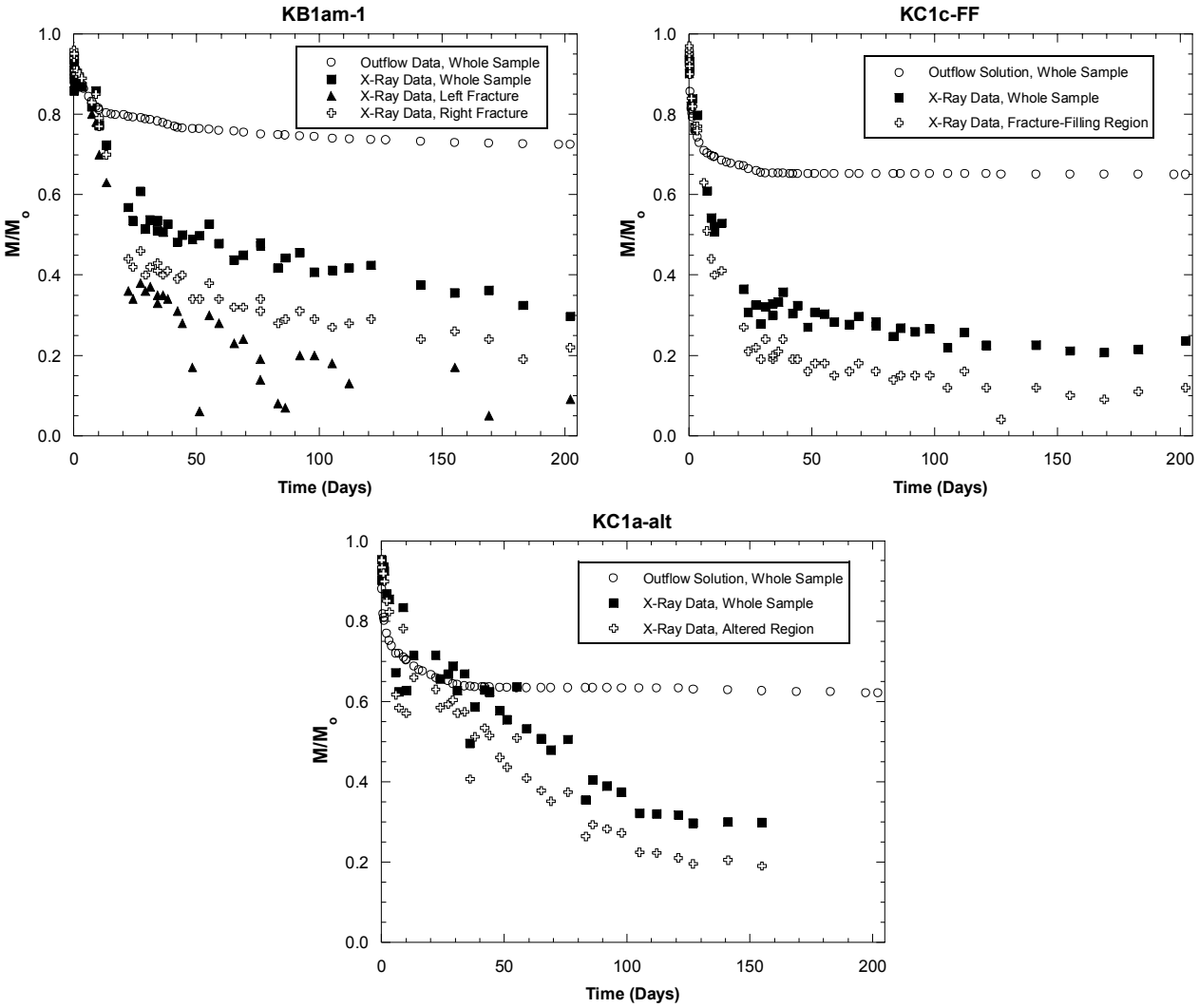

Figure 21: M/Mo calculated for the whole sample using the iodide concentration in the outflow solution and for the whole sample and regions of interest using the X-ray imaging data.

times, the correspondence of the two different estimate techniques (X-ray imaging and outflow solution) is very good, however at later times a discrepancy is clear.

There are two general explanations for the discrepancy between the X-ray and outflow solution data: 1) *mass loss* out of the system prior to entering the outflow solution bottles, 2) *mass redistribution* within in the sample from regions above to regions below the detection limit of the X-ray imaging analyses. It is difficult to determine the effect of each explanation on the results. Clearly, leaks were observed and did effect the results to a certain extent. However, examination of Figure 13 shows that the first leak was not detected until after day 21, well after the differences are noticed in the relative-mass curves for samples KB1am-1 and KC1c-FF. The observation of leaks does not preclude the possibility that there were leaks within the test cell (e.g. between the epoxy and the aluminum frame). It can be observed in Figure 21 that at early times the relative mass in the high-porosity regions decrease at a faster rate than that of the

whole sample. At later times, the rate of mass loss appears to be the same for both the high-porosity region and the whole sample. At these later times, the X-ray analysis is probably only capturing the mass loss from the high porosity regions even when examining the whole sample. This observation is consistent with the conclusions of the detection limit analyses (Section 4.3.2). No matter the explanation, diffusion is still the likely process causing the mass loss regardless of the boundary conditions. However, the effects on boundary conditions of mass loss due to leaks and mass redistribution need to be accounted for when analyzing the data.

Three other potential explanations that could contribute to the discrepancies between the X-ray and outflow-solution data are as follows: 1) outflow-solution iodide-concentration analytical error, 2) outflow solution concentrations falling below the detection limit of the analyses technique and 3) over-filling of outflow bottles at early times leading to loss of iodide mass in outflow-solution data. Based on the repeatability and precision of the analysis technique presented in Section 4.1 it is unlikely that errors from the analytical technique would have a large enough effect on mass calculations to account for the discrepancies observed in Figure 21. The large differences between the outflow-solution data and the X-ray data begin at approximately 12, 5, and 40 days for samples KB1am-1, KC1c-FF, and KC1a-alt, respectively. At these times, the concentrations measured in the outflow solution are still well above the detection limit, eliminating the second explanation. Spills from the outflow bottles were noted on day 0 and 1, well before the discrepancies are obvious. While the fluid most likely had a high iodide concentration, it is unlikely that this explanation can fully account the differences.

In summary, it is believed that the relative concentration and mass results of the X-ray imaging are only reliable for the high-porosity regions of interest. Based on the data discussed in Section 4.3.2 and these data, for regions with porosity less than approximately 3 - 4%, this technique does not produce adequate results. As all of the samples of this study contain some low-porosity regions, it is difficult to interpret the data for the entire sample. Therefore, only the data from the higher-porosity regions of interest are analyzed to calculate diffusion coefficients. Because of the potential impacts of the leaks observed during the experiment and the uncertainty in diffusion rates in the low-porosity areas, the boundary conditions of the system need to be carefully evaluated when analyzing the data.

4.4 Diffusion Coefficient Estimates

As stated in Section 3.5, two different methods were used to estimate the diffusion coefficients for the regions of interest (gouge-filled fractures, recrystallized fracture-filling material and altered matrix): an analytical method and a numerical method employing multiple rates of mass transfer. For both methods of analyses significant assumptions were made. Diffusion is assumed to be one-dimensional when in fact the materials are heterogeneous and diffusion paths could be tortuous. No-flow boundaries are assumed on all sides of the regions of interest, when in fact it is know that the analyzed areas are adjacent regions into which the tracer could diffuse and leaks were documented during the experiment. It is therefore assumed that diffusion into and out of the matrix surrounding the regions of interest is significantly slow compared to diffusion within the regions.

As the purpose of this study is to understand the differences in diffusion rates for the materials of interest in the Kurihashi granodiorite and the data from the lower-porosity regions in the samples are considered below the detection limits of this technique, diffusion coefficients were estimated using the X-ray data only for the gouge-filled fractures, the recrystallied fracture-filling material and the altered matrix. The diffusion coefficients were calculated using the relative mass data for the regions of interest (shown in Figure 21).

Single-rate, and multirate diffusion-coefficient values calculated using the methods described in Sections 3.5.1 and 3.5.2 are reported in Figures 22 and 23 and Table 4. Comparisons of the numerical calculations of relative mass curves to the experimental data are shown in Figure 24. Results are also compared to previous analyses reported in *Ota et al.* [1998].

Examination of Figures 22 and 23 show that different methods of calculating the diffusion coefficients provide consistent results for each of the materials. The largest variation in results are in the diffusion coefficients calculated for the recrystallized fracture-filling material in KC1c-FF. Examination of Figure 24 shows that the single-rate model could not provide a very good fit to the data and that this fit had the largest RMSE (Table 4). The diffusion coefficients calculated from through-diffusion experiments [*Ota et al.*, 1998] were consistently lower than those calculated using the X-ray absorption data.

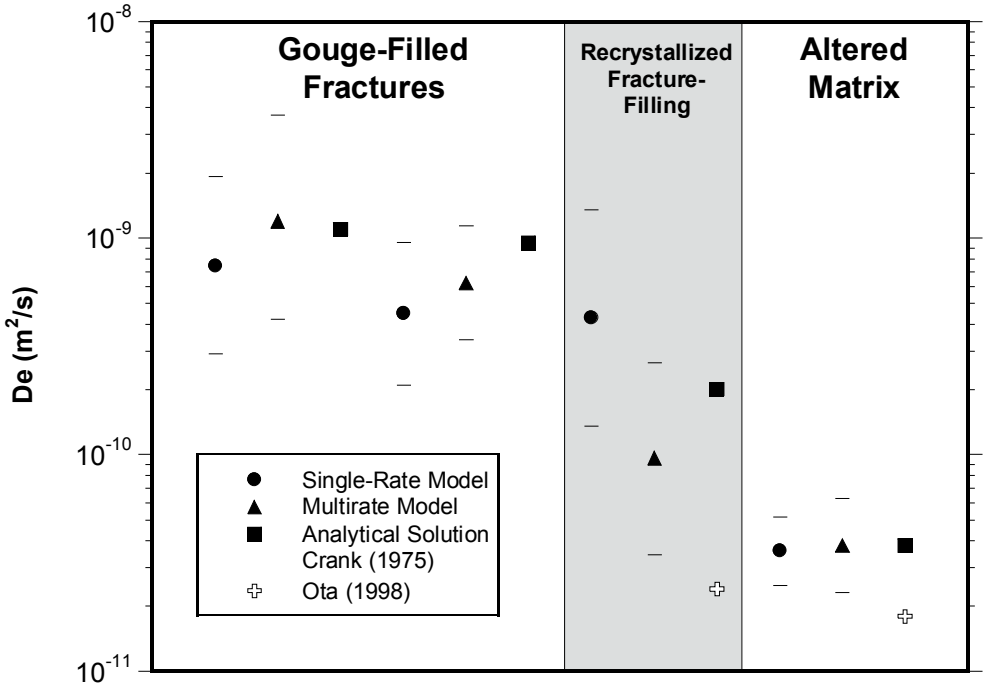

Figure 22: Effective diffusion coefficient estimates using a single-rate and multirate numerical model and an analytical solution [*Crank*, 1975]. Results are compared to those from through-diffusion experiments reported in *Ota et al.* [1998]. The geometric mean of multirate De is shown, the entire distribution is presented in Figure 23. The 95% confidence interval is shown for the numerical results with the bars.

Examination of Figure 22 and 23 also show that there are clear differences in the diffusion coefficients for the different materials. The diffusion coefficients calculated for the gouge filled fractures are almost one order of magnitude higher than that of the recrystallized fracture-filling material and over an order of magnitude higher than that of the altered matrix. The diffusion coefficients calculated for the recrystallized fracture-filling material are approximately one-half an order of magnitude higher than that of the altered matrix.

Based on the results of the multirate modeling, the diffusion coefficient distribution in the left-hand gouge-filled fracture and recrystallized fracture-filling material range over three-orders of magnitude (Table 4, Figure 23). Note, however, that the high end of calculated diffusion coefficient distribution for the gouge-filled fractures is above the aqueous diffusion coefficient. This means that 25% to 35% of the range is unrealistic. It is therefore likely that the recrystallized fracture-filling material is the most heterogeneous of all of the materials. The altered matrix appears to be the most homogeneous with a range less than two orders of magnitude.

Table 4: Diffusion coefficient estimates. D_e reported in m^2/s.

	KB1am-1 Left-Hand Fracture	KB1am-1 Right-Hand Fracture	KC1c-FF Recrystallized Fracture-Filling Material	KC1a-alt Altered Matrix
Crank [1975] Analytical Solution (m^2/s)	1.1×10^{-9}	9.5×10^{-10}	2.0×10^{-10}	3.8×10^{-11}
D_e Single Rate (m^2/s)	7.5×10^{-10}	4.5×10^{-10}	4.3×10^{-10}	3.6×10^{-11}
D_e Multirate (m^2/s)	1.2×10^{-9}	6.2×10^{-10}	9.6×10^{-11}	3.8×10^{-11}
Ota et al. [1998] (m^2/s)	---	---	2.4×10^{-11}	1.8×10^{-11}
σ_d Multirate	1.1	1.5	1.3	0.77
95% Confidence Range σ_d Multirate	0.9 - 1.4	1.1 - 1.8	1.3 - 1.3	0 - 2.9
RMSE Single Rate	3.1	1.8	4.0	0.8
RMSE Multirate	2.3	0.8	2.0	0.7

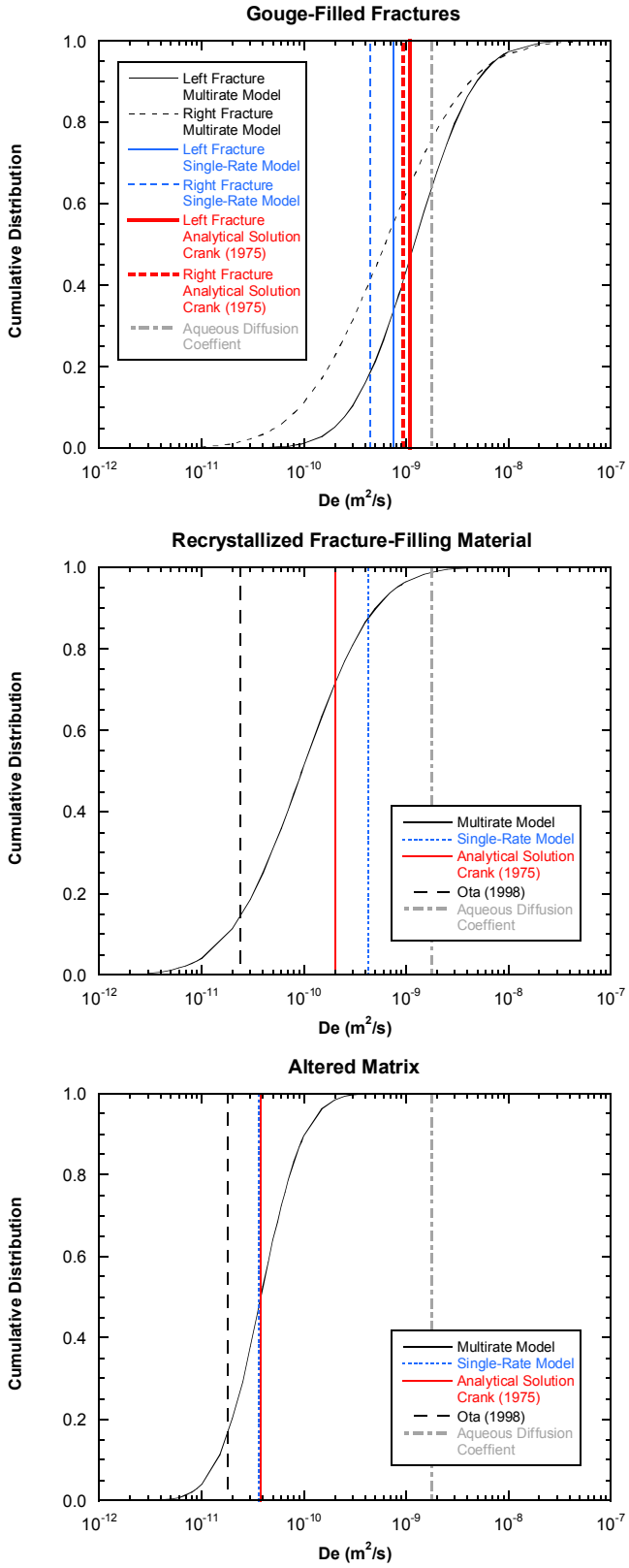

Figure 23: Comparison of multirate diffusion coefficient distributions to the single-rate estimates from the numerical model, Crank (1975) analytical solution and the through-diffusion experiments reported in Ota (1998) for the individual regions of interest.

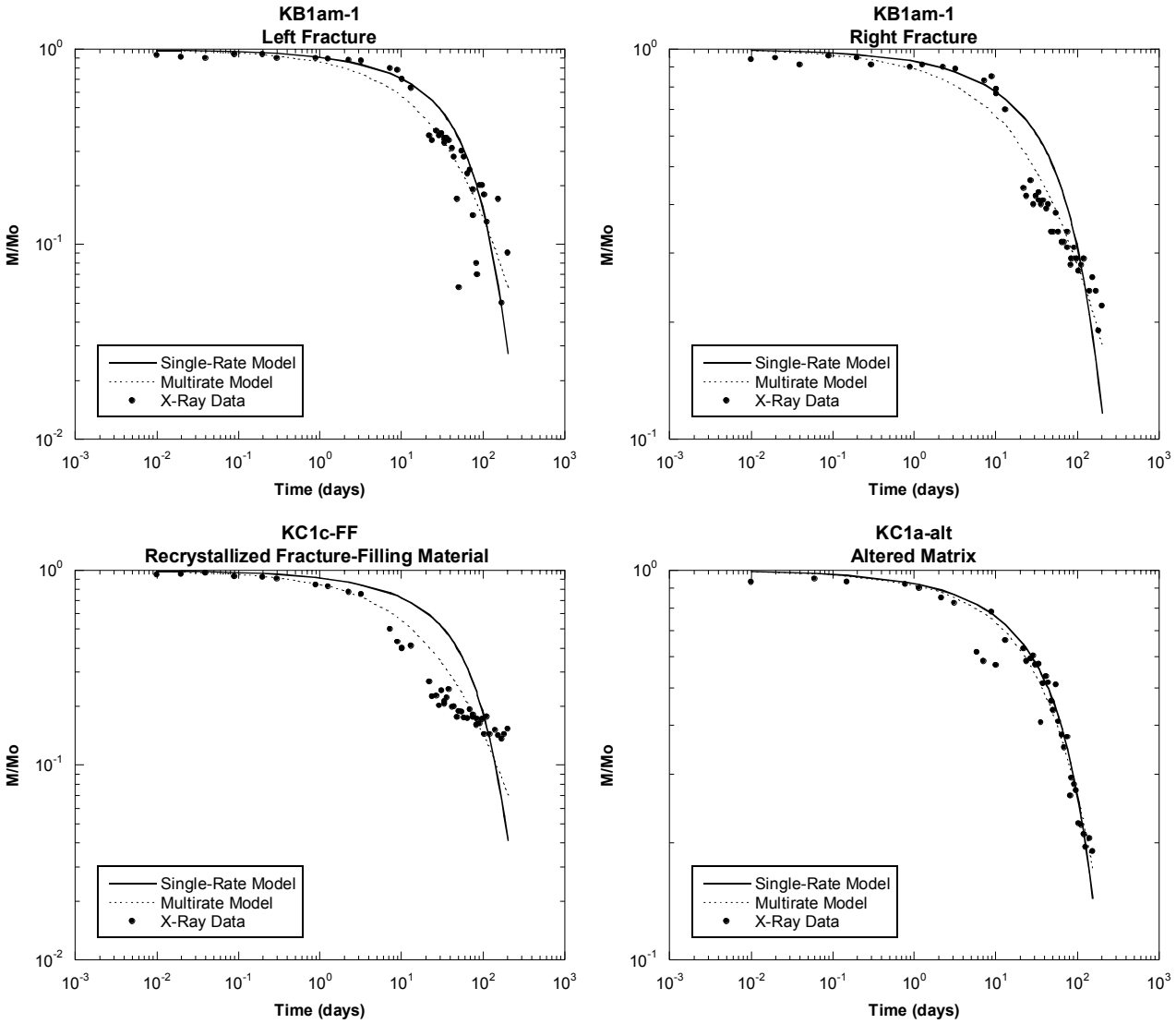

Figure 24: Comparison of results from both single-rate and multirate inverse numerical modeling to the X-ray absorption imaging data.

5 SUMMARY AND DISCUSSION

These experiments have demonstrated that diffusion can be an active process in the different environments of the Kurihashi granodiorite. Specifically, these experiments have provided the direct observation of diffusion in gouge-filled fractures, calcite-based recrystallized fracture-filling material and altered matrix. Analogous evidence of diffusion in the Culebra dolomite at the WIPP site, the U. S. Department of Energy's deep geologic repository for transuranic nuclear waste site in New Mexico, was important in convincing an independent oversight group (the Environmental Evaluation Group), the State of New Mexico's Attorney General's Office and the regulatory agency (the U. S. Environmental Protection Agency) that diffusion is a realistic retardation mechanism.

Qualitative visual examination of the relative concentration distributions of the regions of interest support different rates of diffusion in the different regions. Through X-ray absorption visualization techniques it is clear that the materials and diffusion rates are heterogeneous.

This analyses suggest that the X-ray absorption imaging technique, as employed in this experiment cannot be used quantitatively for regions where the porosity is less than 3% – 4%. It was therefore not possible to evaluate diffusion rates in the unaltered matrix. Based on the porosity images, it also appears that healed fractures have properties similar to that of the unaltered matrix.

For regions of porosity above the detection limit of 3% - 4% quantitative estimates of diffusion rates are possible. For the first time, estimates of diffusion coefficients for the fragile gouge-filled fractures could be made. Comparisons of diffusion rates in the different materials indicate that:

- diffusion rates in the gouge-filled fractures are almost one order of magnitude higher than that of the recrystallized fracture-filling material and over an order of magnitude higher than that of the altered matrix, and

- diffusion rates in the recrystallized fracture-filling material are approximately a factor of 5 higher than that of the altered matrix.

A consistent difference between diffusion rates as estimated by X-ray absorption imaging and through-diffusion experiments [*Ota et al.*, 1998] is apparent. There are several reasons why these experiments would lead to estimates of larger diffusion coefficients than other methods for measuring diffusion such as through-diffusion experiments: 1) X-ray absorption imaging can study more fragile fracture filling materials whereas through-diffusion experiments require a more solid sample to allow for sample fabrication, 2) through-diffusion experiments measure only that diffusion that is able to pass completely through the sample (i.e., connected porosity) where as the visualization technique measures diffusion in all regions, and 3) assumptions made in calculating diffusion coefficients based on the X-ray absorption imaging experimental data.

Modeling techniques are being developed and the X-ray data from the experiments presented in this report are being evaluated so the assumptions made in estimating diffusion coefficients are no longer necessary. The limiting assumptions of the modeling in this report are 1) one-dimensional diffusion when examination of relative concentration data clearly show three-dimensional diffusion could lead to an over estimate of diffusion coefficients, and 2) no interaction between the regions of interest and the adjacent matrix. Both of these assumptions could lead to an over estimate of diffusion coefficients. The new modeling technique will calculate heterogeneous diffusion-coefficients for any regions of interest at the pixel scale.

Finally, the results of these experiments are presently being used in performance assessment (PA)-scale calculations. The purpose of these calculations is to determine whether the flow wetted surface (FWS) can be legitimately increased due to diffusion in the fractures. These calculations will also be used to determine the effect of diffusion in the fractures and the potential increase in FWS on radionulclide releases at the PA scale. In addition, these calculations will evaluate the importance of multirate diffusion at the PA scale.

6 REFERENCES

Crank, J., The Mathematics of Diffusion, Clarendon Press, Oxford, 1975.

Detwiler, R. L., S. E. Pringle, and R. J. Glass, Measurement of fracture aperture fields using transmitted light: An evaluation of measurement errors and their influence on simulations of flow and transport through a single fracture, *Water Resour. Res.*, *35*(9), 2605-2617, 1999.

Fleming, S. W. and R. Haggerty, Modeling solute diffusion in the presence of pore-scale heterogeneity: method development and an application of the Culebra dolomite Member of the Rustler Formation, New Mexico, USA, , *J. Contam. Hydrol.*, *48*, 253-276, 2001.

Fleming, S. W., Single and multiple rates of nonequilibrium diffusive mass transfer at the laboratory, field and regional scales in the Culebra Member of the Rustler Formation, New Mexico, Master Thesis from Oregon State University, June, 1999.

Haggerty, R., S. W. Fleming, L. C. Meigs, and S. A. McKenna, Tracer tests in a fractured dolomite, 2. Analysis of mass transfer in single-well injection-withdrawal tests, *Water Resour. Res.*, *37*(5), 1129-1142, 2001.

Haggerty, R., S. M. Gorelick, Modeling mass transfer processes in soil column with pore-scale heterogeneity, *Soil Sci. Soc. Am. J.*, *62*, 62-74, 1998.

JNCa, H12: Project to Establish the Scientific and Technical Basis for HLW Disposal in Japan, Supporting Report 1, Geological Environment in Japan, *JNC TN1410 2000-002*, April 2000.

JNCb, H12: Project to Establish the Scientific and Technical Basis for HLW Disposal in Japan, Supporting Report 3, Safety Assessment of the Geological Disposal System, *JNC TN1410 2000-004*, April 2000.

McKenna, S. A., L. C. Meigs, and R. Haggerty, Tracer tests in a fractured dolomite, 3. Double porosity, multiple-rate mass transfer processes in convergent-flow tracer tests, *Water Resour. Res.*, *37*(5), 1143-1154, 2001.

Neretnieks, Diffusion in the rock matrix, an important factor in radionuclide retardation? *J. Geophys. Res., 85*(B8), 4379-4397, 1980.

Osawa, H., H. Sasamoto, T. Nohara, K. Ota, and Y Oshida, Development of a conceptual flow-path model of nuclide migration in crystalline rock – a case study at the Kamaishi in-situ test site, Japan, Mat. Res. Soc. Symp. Proc., *353*, 1267-1273, 1995.

Ota, K., Amano, K., and Ando, T., Brief overview of in situ contaminant retardation in fractured crystalline rock at the Kamaishi in situ test site, in Proceedings of an international workshop for the Kamaishi in situ experiments, Japan Nuclear Cycle Development Institute, August, 1998.

Tidwell, V. C., and R. J. Glass Jr., X ray and visible light transmission for laboratory measurement of two-dimensional saturation fields in thin-slab systems, *Water Resour. Res.*, *30*(11), 2873-2882, 1994.

Tidwell, V. C., L. C. Meigs, T. Christian-Frear, and C. M. Boney, Effects of spatially heterogeneous porosity on matrix diffusion as investigated by X-ray absorption imaging, *J. Contam. Hydrol.*, *42*, 285-302, 2000.

APPENDIX A: SAMPLE WATER CHEMISTRY OF ALBUQUERQUE, NEW MEXICO MUNICIPAL WATER AND WATER FROM THE KAMAISHI MINE

City of Albuquerque

1997 ANNUAL DRINKING WATER QUALITY SUMMARY

Daily, the Water Quality Unit responds to inquires about the water system and the water quality in Albuquerque. Here are answers to some commonly asked questions.

How does Albuquerque's water system work?
Ours is a "distributed" water system. So ne 91 wells in 25 wellfields are distributed over the Albuquerque Basin. Water from each well is pumped to a common wellfield collector line. Collector lines discharge to 42 storage reservoirs. Reservoirs are arranged throughout the City in trunks. Along a trunk, water from each reservoir is pumped to a higher elevation, then mixed with wellfield water already in the reservoir. Water is then gravity fed to the distribution system in lower elevation zones.

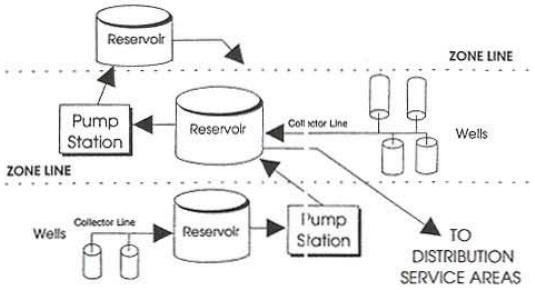

Which Well Supplies My Home?
The water in each reservoir is a blend of well waters. Each reservoir supplies a **distribution service area** within the distribution system. All distribution service areas are shown on the map on the following page.

How Is The Water Treated?
All water is treated with the disinfectant chlorine. In addition, fluoride is added to the water East of the Rio Grande. Water on the Westside contains adequate amounts of natural fluoride for prevention of tooth decay.

What is the Safe Drinking Water Act (SDWA)?
State and federal regulations require monitoring to determine compliance with maximum contaminant levels (MCLs). Maximum contaminant levels are the maximum permissible levels of any contaminant in drinking water.

Is Our Water Safe?
YES. Monitoring results for 1997 continue to meet all federal and state drinking water standards. The water quality monitoring program is designed not only to meet all requirements, but to provide additional assurance that your water is of the highest quality.

What Do We Test For?
Groundwater regulations require routine tests for some 83 contaminants. Our monitoring program tests for more than 100 contaminants at wells and reservoirs and at representative sample points throughout the water distribution system. Distribution system sample points are customer's water taps. Results of distribution monitoring is summarized for you on the following pages.

How Often Do We Test?
Samples are collected daily within the distribution system. Test samples are also collected monthly from wells and reservoirs. In 1997, more than 4,500 samples were collected representing more than 37,000 analytical results.

Who Analayzes the Samples?
All analyses are performed by certified laboratories. The New Mexico Department of Health Scientific Laboratory Division (SLD), the City of Albuquerque Public Works Water Quality Laboratory (WQL) and the New Mexico State University Soil, Water and Air Testing Laboratory.

What If a Contaminant Is Found?
No contaminant has ever been found in any reservoir at levels greater than regulations allow. If soil or groundwater contamination is reported in the vicinity of a well, monitoring frequency is increased. Please be assured that we are required to notify our customers if any standard is exceeded.

What Is Being Done To Protect and Maintain The Quality Of Groundwater?
The Ground-Water Protection Policy and Action Plan, or GPPAP, is a joint effort of the City of Albuquerque and Bernalillo County. The plan was adopted in 1993. Goals include finding and cleaning-up contaminated groundwater and promoting the coordinated protection and prudent use of the ground water resource throughout the region.

Should I Be Concerned About Lead?
Over the past six years, customers have collected samples for lead and copper analyses from taps throughout the City. Even in worse case scenario (homes built between 1982 and 1987) tap water was well below the action level for lead.

What About Arsenic?
Arsenic occurs naturally in varying amounts in groundwater throughout the Albuquerque Basin. Arsenic levels detected in monitoring at reservoirs and in the distribution system indicate that City water meets all current standards. Further information about arsenic can be obtained from the SDWA hotline at the number listed on the bottom of this page.

Why Is My Water Cloudy?
Water in the distribution system is under pressure. Air sometimes dissolves in the pressurized lines. At the faucet, the air gives water a "cloudy" or "milky" appearance. The quality of the water is not affected.

How Hard Is My Water?
Hardness occurs in varying concentrations throughout the water supply. Hardness ranges from soft to moderately hard dependent upon your location. Although there is no regulatory standard for hardness, levels are well under the EPA recommended range.

For further information on drinking water quality, contact the following:

City of Albuquerque
Water Quality Hotline: 857-8260

Bernalillo County
Environmental Health Department: 768-4390

New Mexico Environment Department
District 1: 841-9450

EPA Safe Drinking Water Act
SDWA Hotline: 1-800-426-4791

PUBLIC WORKS DEPARTMENT : WATER UTILITY DIVISION : WATER QUALITY UNIT

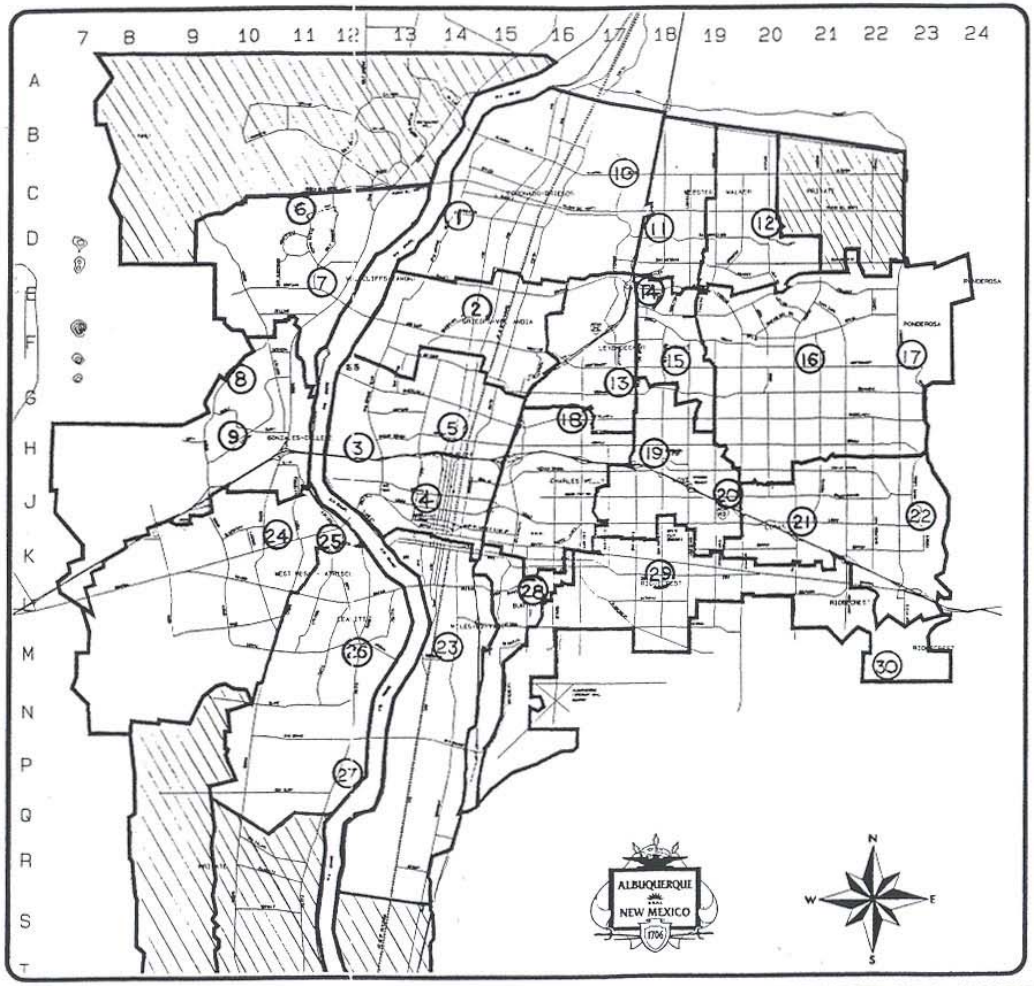

How To Use This Summary...

Use the map to locate your distribution service area as defined by the heavy black lines. Find the number of the nearest sample point.Use the tables on the next pages to find the results of testing for your sample point. Water quality components and their respective chemical abbreviations and units of measurement are listed across the top of the tables. Sample point numbers are listed in the column at the far left of the tables. Match the sample point row with the column components to find the minimum, average and maximum results for each component.

At the bottom of the table you will find the city-wide range of values, the limits of detection, and the EPA maximum contaminant level, action level, or recommended limit or range for each component.

PT No.	QUAD	NEAREST MAJOR INTERSECTION	GRID No.
1	NW	RIO GRANDE & RANCHITOS	D-14
2	NW	4TH ST. & MONTANO RD.	E-14
3	NW	I-40 & RIO GRANDE	H-12
4	NW	12TH & LOMAS	J-13
5	NW	MENAUL & 4TH ST.	H-14
6	NW	TAYLOR RANCH & CALLE NORTENA	D-11
7	NW	TAYLOR RANCH & MONTANO	E-11
8	NW	ST JOSEPHS & ATRISCO	G-10
9	NW	OURAY & UNSER	H-10
10	NE	WASHINGTON & ALAMEDA	C-17
11	NE	PASEO DEL NORTE & SAN PEDRO	D-18
12	NE	PASEO DEL NORTE & VENTURA	D-20
13	NE	SAN MATEO & MONTGOMERY	G-17
14	NE	ACADEMY & SAN MATEO	E-18
15	NE	MONTGOMERY & SAN PEDRO	F-18
16	NE	EUBANK & MONTGOMERY	F-21
17	NE	MONTGOMERY & TRAMWAY	F-22
18	NE	MENAUL & WASHINGTON	G-17
19	NE	MENAUL & SAN PEDRO	H-18
20	NE	CONSTITUTION & PENNSYLVANIA	J-19
21	NE	LOMAS & EUBANK	K-21
22	NE	TRAMWAY & LOMAS	J-23
23	SW	WOODWARD & 2ND. ST.	M-14
24	SW	CENTRAL & NORTH COORS	K-11
25	SW	CENTRAL & ATRISCO	K-12
26	SW	ISLETA & ARENAL	M-12
27	SW	ISLETA & RIO BRAVO	P-12
28	SE	YALE & STADIUM	L-15
29	SE	TRUMBULL & SAN PEDRO	L-18
30	SE	FOURHILLS	M-22

Flow Visualization and Processes Laboratory is located in Region 28

PUBLIC WORKS DEPARTMENT WATER UTILITY DIVISION WATER QUALITY UNIT

City of Albuquerque Public Works Department
.ic Water Distribution System 1997 Water Quality Summary

SAMPLE POINT NUMBER	INORGANICS																							
	ARSENIC As mg/l		BARIUM Ba mg/l		BORON B mg/l		CADMIUM Cd mg/l		CHROMIUM Cr mg/l		COPPER Cu mg/l		IRON Fe mg/l		LEAD Pb mg/l		SELENIUM Se mg/l		ZINC Zn mg/l		FLUORIDE F mg/l			NITRATE + NITRITE NO3+NO2 mg/l as N	
	MEAN	MAX	MEAN	MAX	MEAN	MAX	MEAN	MAX	MEAN	MAX	MEAN	MAX	MEAN	MAX	MEAN	MAX	MEAN	MAX	MEAN	MAX	MIN	MEAN	MAX	MEAN	MAX
1	0.008	0.008	0.056	0.061	0.107	0.123	ND	ND	0.002	0.003	0.006	0.008	0.012	0.018	0.002	0.002	ND	ND	0.008	0.011	0.9	1.0	1.1	ND	ND
2	0.008	0.009	0.082	0.092	0.115	0.199	ND	ND	0.003	0.005	0.010	0.013	0.011	0.013	0.002	0.002	ND	ND	0.047	0.069	0.9	1.0	1.1	0.2	0.6
3	0.009	0.011	0.055	0.065	0.123	0.152	ND	ND	0.003	0.007	0.014	0.030	0.010	0.011	0.002	0.002	ND	ND	0.011	0.027	0.9	1.0	1.2	0.1	0.2
4	0.010	0.011	0.081	0.090	0.137	0.161	0.002	0.002	0.004	0.009	0.006	0.009	0.221	0.442	0.002	0.002	ND	ND	0.087	0.141	0.9	1.0	1.2	0.3	0.5
5	0.009	0.012	0.059	0.082	0.142	0.174	0.002	0.002	0.004	0.007	0.012	0.018	0.012	0.016	ND	ND	ND	ND	0.069	0.151	0.9	1.0	1.1	0.1	0.3
6	0.014	0.016	0.055	0.059	0.171	0.193	ND	ND	0.005	0.009	0.005	0.006	ND	ND	ND	ND	ND	ND	ND	ND	0.9	1.0	1.1	1.7	1.9
7	0.014	0.016	0.055	0.060	0.171	0.205	ND	ND	0.005	0.006	0.014	0.018	ND	ND	ND	ND	ND	ND	0.006	0.009	0.9	1.0	1.1	1.8	2.0
8	0.015	0.015	0.054	0.056	0.169	0.180	ND	ND	0.005	0.008	0.005	0.006	ND	ND	ND	ND	0.002	0.002	ND	ND	0.8	1.0	1.1	1.3	1.7
9	0.019	0.022	0.045	0.054	0.174	0.176	ND	ND	0.005	0.010	0.006	0.009	ND	ND	ND	ND	0.002	0.003	0.032	0.113	0.8	1.0	1.2	1.3	1.5
10	0.018	0.022	0.083	0.099	0.152	0.184	ND	ND	0.003	0.005	0.017	0.053	0.010	0.011	ND	ND	ND	ND	0.023	0.051	0.8	0.9	1.0	0.2	0.4
11	0.029	0.035	0.086	0.103	0.156	0.168	ND	ND	0.002	0.003	0.028	0.061	0.013	0.016	0.002	0.003	ND	ND	0.103	0.120	0.8	0.9	0.9	0.2	0.2
12	0.020	0.031	0.133	0.170	0.130	0.135	ND	ND	0.002	0.003	0.026	0.032	0.090	0.331	0.002	0.003	ND	ND	0.032	0.111	0.7	0.9	1.1	0.2	0.5
13	0.006	0.008	0.093	0.101	0.068	0.087	ND	ND	0.003	0.005	0.006	0.008	ND	ND	ND	ND	ND	ND	0.007	0.012	0.7	0.9	1.0	0.4	0.7
14	0.019	0.036	0.095	0.123	0.141	0.193	ND	ND	0.003	0.005	0.017	0.025	0.011	0.012	ND	ND	ND	ND	0.008	0.021	0.9	1.0	1.0	0.3	0.5
15	0.006	0.008	0.095	0.110	0.093	0.132	ND	ND	0.003	0.005	0.021	0.035	0.011	0.015	ND	ND	ND	ND	0.014	0.022	0.9	1.0	1.0	0.4	0.5
16	0.017	0.024	0.157	0.168	0.160	0.198	0.002	0.002	ND	ND	0.060	0.081	0.012	0.017	0.003	0.004	ND	ND	0.008	0.013	1.0	1.0	1.1	0.2	0.3
17	0.012	0.016	0.142	0.153	0.115	0.143	ND	ND	0.003	0.005	0.009	0.012	0.011	0.013	ND	ND	ND	ND	0.007	0.010	0.9	1.0	1.1	0.2	0.3
18	0.006	0.007	0.095	0.116	0.091	0.124	ND	ND	0.003	0.004	0.005	0.006	ND	ND	ND	ND	ND	ND	0.020	0.032	0.9	1.0	1.1	0.3	0.5
19	0.003	0.006	0.118	0.127	0.068	0.079	ND	ND	0.002	0.003	0.005	0.006	ND	ND	ND	ND	ND	ND	0.040	0.071	0.5	0.9	1.2	0.4	0.5
20	0.002	0.003	0.146	0.161	0.084	0.102	ND	ND	0.002	0.003	0.011	0.018	ND	ND	ND	ND	0.002	0.003	0.007	0.010	0.5	0.7	1.2	0.2	0.3
21	0.003	0.004	0.136	0.154	0.081	0.096	ND	ND	0.003	0.003	0.007	0.011	0.014	0.021	ND	ND	0.002	0.003	0.018	0.023	0.8	0.9	1.0	0.5	0.9
22	0.002	0.004	0.123	0.145	0.071	0.095	ND	ND	0.002	0.003	0.025	0.035	0.033	0.104	ND	ND	ND	ND	0.013	0.033	0.8	1.0	1.1	0.7	1.0
23	0.022	0.029	0.080	0.100	0.173	0.215	ND	ND	0.003	0.004	0.012	0.033	0.061	0.214	ND	ND	ND	ND	0.013	0.033	0.9	1.1	1.2	0.4	0.4
24	0.022	0.025	0.032	0.043	0.212	0.241	ND	ND	0.009	0.012	0.005	0.006	0.013	0.023	ND	ND	0.002	0.002	0.006	0.007	1.0	1.1	1.1	1.2	1.6
25	0.014	0.016	0.031	0.038	0.243	0.258	ND	ND	0.011	0.014	0.008	0.012	ND	ND	ND	ND	ND	ND	0.005	0.006	0.8	0.9	0.9	0.7	0.8
26	0.030	0.040	0.016	0.025	0.275	0.337	ND	ND	0.014	0.017	0.008	0.014	ND	ND	ND	ND	0.003	0.003	0.007	0.010	1.0	1.1	1.3	1.6	1.8
27	0.031	0.037	0.012	0.022	0.281	0.313	ND	ND	0.015	0.019	0.005	0.006	0.010	0.011	ND	ND	0.002	0.003	0.006	0.008	1.0	1.1	1.2	1.6	1.8
28	0.011	0.012	0.113	0.121	0.124	0.129	ND	ND	0.002	0.003	0.119	0.172	0.190	0.315	0.002	0.002	ND	ND	0.077	0.125	0.7	1.0	1.2	0.2	0.4
29	0.005	0.007	0.138	0.162	0.084	0.096	ND	ND	0.002	0.003	0.013	0.020	0.100	0.323	0.003	0.006	ND	ND	0.101	0.173	0.7	0.9	1.0	0.3	0.5
30	0.003	0.004	0.154	0.167	0.076	0.091	ND	ND	0.002	0.003	0.014	0.024	0.011	0.012	ND	ND	ND	ND	0.006	0.009	0.7	0.9	1.1	0.4	0.5
CITY-WIDE VALUES	0.013	0.040	0.087	0.170	0.140	0.337	0.002	0.002	0.004	0.019	0.017	0.172	0.029	0.442	0.002	0.006	0.002	0.003	0.026	0.173	0.5	1.0	1.3	0.6	2.0
LIMIT OF DETECTION	0.002		0.002		0.05		0.002		0.002		0.005		0.010		0.002		0.050		0.005		0.1			0.1	
RECOMMENDED LIMIT/ RANGE MCL or *ACTION LEVEL*	0.05		2		N/A		0.005		0.1		*1.3*		N/A		*0.015*		0.050		N/A		4.0			10	

mg/l=milligrams per liter; ug/l=micrograms per liter; MIN=minimum; MEAN=average; MAX=maximum; MCL= Maximum Contaminant Level; Limit of Detection=lowest reliable measurement; ND=not detected; N/A=not applicable; ≥=less than or equal to

City of Albuquerque Public Works Department
ic Water Distribution System 1997 Water Quality Summary

GENERAL CHEMISTRY

SAMPLE POINT NUMBER	ALKALINITY mg/l as CaCO3		BICARBONATE HCO3 mg/l as CaCO3		CALCIUM Ca mg/l		CHLORIDE CL mg/l		HARDNESS grains/gallon as CaCO3		MAGNESIUM Mg mg/l		POTASSIUM K mg/l		SILICA Si-SiO2 mg/l as SiO2		SODIUM Na mg/l		SULFATE SO4 mg/l		TOTAL DISSOLVED SOLIDS mg/l	
	MEAN	MAX	MEAN	MAX	MEAN	MAX	MEAN	MAX	MEAN	MAX	MEAN	MAX	MEAN	MAX	MEAN	MAX	MEAN	MAX	MEAN	MAX	MEAN	MAX
1	136	139	136	138	35	40	12	13	7	7	8	10	8	8	67	71	46	50	75	81	334	368
2	126	139	125	138	39	45	13	14	8	8	7	8	6	7	56	64	35	48	66	78	299	332
3	137	139	136	138	35	37	15	21	7	7	7	8	7	8	65	69	49	54	78	84	343	348
4	127	141	126	141	38	43	22	29	8	8	8	9	7	7	65	73	41	52	69	90	325	356
5	136	140	135	139	35	39	15	22	7	8	7	8	8	8	67	69	52	58	78	86	338	348
6	125	131	124	129	18	19	9	9	4	4	4	4	6	7	68	71	57	61	52	59	291	308
7	124	126	123	125	18	19	9	10	4	4	4	4	6	7	68	72	56	58	51	57	282	288
8	129	132	127	130	18	19	9	10	4	4	4	4	6	7	68	71	60	64	57	61	305	308
9	133	142	131	139	15	18	10	12	3	5	3	4	6	6	60	67	68	81	64	73	308	324
10	132	139	130	138	33	46	34	43	7	9	7	8	5	6	52	60	49	57	47	49	299	340
11	133	135	131	134	33	36	40	44	7	8	6	8	5	7	56	63	51	57	38	39	312	368
12	125	129	125	128	49	53	71	81	8	9	4	5	4	4	36	38	51	60	33	35	329	372
13	117	130	117	128	43	49	14	16	8	9	5	6	3	5	41	54	27	38	55	63	276	336
14	125	132	124	131	41	52	32	43	7	8	6	6	4	7	48	61	44	68	42	49	291	328
15	121	126	120	126	45	50	17	27	7	8	5	5	3	3	37	41	28	32	41	45	259	288
16	126	129	126	129	50	52	63	74	8	10	5	5	4	5	38	40	48	57	34	38	321	340
17	124	128	124	127	48	51	52	65	9	9	5	5	3	4	36	38	39	42	35	39	302	332
18	120	134	119	132	40	47	15	19	7	8	6	6	4	6	44	59	33	44	56	72	264	288
19	116	121	114	119	39	45	17	20	7	8	4	5	3	3	34	37	27	29	38	45	235	248
20	119	120	118	119	42	45	29	42	7	8	4	5	3	3	35	41	32	34	34	37	266	288
21	120	123	119	123	40	44	24	30	7	8	4	5	3	4	38	42	33	37	42	48	260	292
22	124	129	123	127	41	47	22	32	7	8	5	5	3	3	33	36	33	36	41	46	253	280
23	114	120	113	118	31	36	26	35	6	6	7	7	7	8	70	80	48	57	55	70	313	320
24	136	141	134	139	16	18	13	14	4	4	3	4	5	6	56	65	81	88	73	79	327	342
25	135	139	133	138	23	25	17	17	5	6	5	5	5	6	57	65	82	86	98	103	381	432
26	140	144	135	138	9	12	18	25	2	3	2	2	2	3	43	53	114	148	99	115	386	408
27	141	144	135	138	8	10	23	26	2	2	1	2	2	2	43	48	118	126	104	116	390	428
28	110	111	109	110	36	38	36	39	7	7	7	8	6	6	61	67	35	37	36	41	285	304
29	113	115	112	113	40	42	34	36	8	8	6	6	4	4	40	45	30	33	31	34	255	264
30	112	115	112	114	41	43	33	35	8	10	5	6	3	4	37	40	29	30	31	33	252	256
CITY-WIDE VALUES	126	144	124	141	33	53	25	81	6	10	5	10	5	8	51	80	50	148	55	116	303	432
LIMIT OF DETECTION	10		1		0.05		4		1		0.01		1		0.5		0.05		7		1	
RECOMMENDED LIMIT/ RANGE **MCL** or *ACTION LEVEL*	30-500		N/A		200		250		15		125		1000		N/A		200		250		500	

mg/l=milligrams per liter; ug/l=micrograms per liter; MIN=minimum; MEAN=average; MAX=maximum; MCL= Maximum Contaminant Level; Limit of Detection=lowest reliable measurement; ND=not detected; N/A=not applicable; ≤=less than or equal to

City of Albuquerque Public Works Department
ic Water Distribution System 1997 Water Quality Summary

SAMPLE POINT NUMBER	GENERAL CHEMISTRY												ORGANICS	
	FREE CHLORINE RESIDUAL mg/l			CONDUCTANCE micromhos/cm			pH Field pH Standard Units			TEMPERATURE Field Temperature Fahrenheit			TOTAL TRIHALOMETHANES ug/L	
	MIN	MEAN	MAX	MIN	MEAN	MAX	MIN	MEAN	MAX	MIN	MEAN	MAX	MEAN	MAX
1	0.5	0.6	0.8	424	460	477	7.51	7.65	7.83	49	64	70	11.1	12.3
2	0.4	0.5	0.6	373	420	462	7.44	7.49	7.56	53	63	78	10.5	13.8
3	0.5	0.6	0.6	407	454	501	7.51	7.58	7.74	56	68	83	15.1	22.2
4	0.5	0.6	0.6	375	436	501	7.47	7.61	7.67	57	67	79	14.2	24.1
5	0.5	0.6	0.7	405	457	496	7.33	7.46	7.62	61	67	75	9.6	11.8
6	0.7	0.8	0.9	392	398	407	7.74	7.89	8.12	50	72	86	0.5	2.0
7	0.8	0.8	0.8	387	390	395	7.66	7.93	8.10	68	73	80	0.0	0.0
8	0.6	0.8	0.9	383	401	419	7.69	7.90	8.05	61	71	80	6.3	23.7
9	0.6	0.7	0.8	414	435	460	8.02	8.12	8.34	54	69	81	0.9	2.4
10	0.6	0.6	0.7	360	460	497	7.66	7.86	8.03	53	63	74	5.9	7.3
11	0.5	0.7	0.8	430	461	474	7.59	7.68	7.86	58	67	76	5.1	7.7
12	0.6	0.7	0.8	452	539	577	7.34	7.49	7.69	59	66	76	0.9	2.6
13	0.5	0.6	0.6	333	390	421	7.41	7.48	7.57	59	68	75	4.9	8.5
14	0.6	0.7	0.8	370	429	466	7.45	7.59	7.69	56	65	75	6.1	9.7
15	0.4	0.6	0.7	349	373	415	7.30	7.54	7.73	61	69	78	2.9	4.4
16	0.4	0.6	0.8	455	524	575	7.42	7.49	7.58	71	72	74	2.1	7.2
17	0.6	0.7	0.8	461	483	519	7.46	7.56	7.76	53	68	79	5.8	10.8
18	0.5	0.5	0.6	365	406	446	7.15	7.48	7.83	60	67	76	5.8	8.0
19	0.6	0.7	0.7	319	347	359	7.53	7.63	7.69	58	67	72	3.5	7.4
20	0.6	0.7	0.7	345	391	437	7.32	7.56	7.81	64	68	72	4.0	9.3
21	0.6	0.7	0.7	370	395	432	7.43	7.59	7.85	46	62	75	6.4	8.6
22	0.7	0.8	0.8	349	369	400	7.61	7.72	7.90	53	67	78	3.3	4.4
23	0.6	0.6	0.7	423	444	455	7.48	7.75	7.86	53	66	81	7.2	10.1
24	0.7	0.8	0.9	438	468	481	8.07	8.25	8.51	68	75	80	5.3	7.7
25	0.6	0.7	0.8	477	514	539	7.54	7.85	8.09	59	73	79	16.7	18.9
26	0.5	0.7	0.8	456	508	616	7.94	8.42	8.61	59	69	80	8.6	16.7
27	0.7	0.7	0.8	422	539	587	8.42	8.60	8.68	55	72	83	7.6	14.0
28	0.3	0.4	0.6	410	413	418	7.56	7.62	7.68	54	63	76	1.9	4.4
29	0.3	0.6	0.8	385	394	402	7.53	7.67	7.84	56	68	80	4.9	9.8
30	0.8	0.9	0.9	372	391	403	7.44	7.62	7.78	55	66	80	2.2	3.5
CITY-WIDE VALUES	0.3	0.7	0.9	319	436	616	7.15	7.73	8.68	46	68	86	6.0	24.1
LIMIT OF DETECTION		0.1			N/A			0.1			N/A		0.5	
RECOMMENDED LIMIT/ RANGE MCL or *ACTION LEVEL*		≥ 0.3			1000			N/A			N/A		100.0	

MONITORING ALSO INCLUDES . . .

VOLATILE ORGANIC COMPOUNDS : DETECTED ONLY AT SAMPLE POINT 30

SAMPLE POINT NUMBER	Xylenes (total) ug/l MEAN	MAX
30	ND	0.9
LIMIT OF DETECTION	0.5	
MCL	10,000	

OTHER VOLATILE ORGANIC COMPOUNDS and MCLs (ug/l) collected quarterly: NO DETECTION

Vinyl chloride (2 ug/l)	para-Dichlorobenzene (75 ug/l)	o-Dichlorobenzene (600 ug/l)
Benzene (5 ug/l)	1,1,-Dichloroethylene (7 ug/l)	Tetrachloroethylene (5 ug/l)
Carbon tetrachloride (5 ug/l)	1,1,1-Trichloroethane (200 ug/l)	Dichloromethane (5 ug/l)
1,2-Dichloroethane (5 ug/l)	1,2-Dichloropropane (5 ug/l)	1,2,4-Trichlorobenzene (70 ug/l)
Ethylbenzene (700 ug/l)	Monochlorobenzene (100 ug/l)	1,1,2-Trichloroethane (5 ug/l)
Toluene (1000 ug/l)	Trichloroethylene (5 ug/l)	trans-1,2-Dichloroethylene (100 ug/l)
Styrene (100 ug/l)	cis-1,2-Dichloroethylene (70 ug/l)	

INORGANICS and MCLs (mg/l) collected quarterly from distribution system: NO DETECTION

Antimony (.006 mg/l)	Mercury (.002 mg/l)	Molydbenum (N/A)
Beryllium (.004 mg/l)	Nickel (0.1 mg/l)	Thallium (.002 mg/l)

Asbestos (7 Million Fibers per Liter) **collected in 1996: NO DETECTION**

SYNTHETIC ORGANIC CONTAMINANTS and MCLs (ug/l)
collected quarterly in 1994 from wells, thereafter every 4 yrs.: NO DETECTION

Alachor (2 ug/l)	Benzo(a)pyrene (0.2 ug/l)
Atrazine (3 ug/l)	Dalapon (200 ug/l)
Carbofuran (40 ug/l)	Di(2-ethylhexyl)adipate (400 ug/l)
Chlordane (2 ug/l)	Di(2-ethylhexyl)phthalate (6 ug/l)
Dibromochloropropane (0.2 ug/l)	Dinoseb (7 ug/l)
2,4-D (70 ug/l)	Diquat (20 ug/l)
Ethylene dibromide (0.05 ug/l)	Endothall (100 ug/l)
Heptachlor (0.4 ug/l)	Endrin (2 ug/l)
Heptachlor epoxide (0.2 ug/l)	Glyphosate (700 ug/l)
Lindane (0.2 ug/l)	Hexachlorobenzene (1 ug/l)
Methoxychlor (40 ug/l)	Hexachlorocyclopentadiene (50 ug/l)
Polychlorinated biphenyls (0.5 ug/l)	Oxamyl (Vydate) (200 ug/l)
Pentachlorophenol (1 ug/l)	Picloram (500 ug/l)
Toxaphene (3 ug/l)	Simazine (4 ug/l)
2,4,5-TP (50 ug/l)	2,3,7,8-TCDD (Dioxin) (.00003 ug/l)

mg/l=milligrams per liter; ug/l=micrograms per liter; MIN=minimum; MEAN=average; MAX=maximum; MCL= Maximum Contaminant Level; Limit of Detection=lowest reliable measurement; ND=not detected; N/A=not applicable; ≥=less than or equal to

Chemical Analyses of Water Samples from Kamaishi Mine

表 -5. 5. 1　既存試錐孔の採水分析結果一覧表

	KF1-1	KF1-5	KF2-2	KF2-3	KG-1
Na+ (mg/l)	4.9	4.83	8.87	8.14	14.2
K+ (mg/l)	0.49	0.46	0.63	0.41	0.69
Mg++(mg/l)	0.09	0.08	<0.02	<0.02	0.32
Ca++(mg/l)	11.3	11.3	6	6.8	6.24
Al3+(mg/l)	0.06	0.06	0.06	0.06	0.09
全Si (mg/l)	6.3	5.4	5.5	5.7	3.2
Si4+(mg/l)	5.3	5.27	4.59	5.13	3.21
全Fe (mg/l)	0.02	nd	0.04	0.02	0
Fe++(mg/l)	nd	nd	0.06	nd	nd
Li+ (mg/l)	nd	nd	nd	nd	nd
Sr++(mg/l)	0.003	0.005	0.005	0.004	0.006
Mn++(mg/l)	nd	nd	nd	nd	nd
Cl− (mg/l)	2.4	2.4	2.2	1.6	3.22
SO4−−(mg/l)	8.1	8.2	6.9	3	1.85
F (mg/l)	nd	nd	nd	nd	nd
Br−−(mg/l)	nd	nd	nd	nd	nd
I− (mg/l)	nd	nd	nd	nd	nd
S−− (mg/l)	nd	nd	nd	nd	nd
PO43−(mg/l)	0.008	0.005	0.006	0.007	0.006
全P (mg/l)	0.02	0.02	0.02	0.02	0.02
NO2− (mg/l)	nd	nd	nd	nd	0.01
NO3− (mg/l)	nd	nd	nd	nd	0.01
NH4+ (mg/l)	0.03	0.02	0.03	0.03	0.02
全N (mg/l)	0.04	0.05	0.02	0.05	0.05
TOC (mg/l)	0.48	0.53	0.36	1.31	0.8
IC (mg/l)	6.6	6.36	5.84	6.94	9.61
δ18O (‰)	-10.7	-10.7	-10.8	-10.3	-10.7
δD (‰)	-68.4	-68.8	-69.7	-65.9	-70.8
トリチウム(TR)	7.4	5.8	6.6	5.1	3.4
全菌数計数(cells/ml)	6.80E+05	3.20E+05	1.90E+05	5.10E+03	5.40E+05
従属栄養細菌(CFU/ml)	1.90E+04	1.20E+04	4.6E+04	1.80E+01	6.80E+05
鉄酸化細菌 (MPN/ml)	nd	nd	nd	nd	nd
鉄還元細菌 (MPN/ml)	nd	nd	nd	nd	nd
硫酸塩還元細菌(MPN/ml)	5.20E+02	1.10E+03	9.60E+02	nd	5.10E+00
硫黄酸化細菌(MPN/ml)	nd	nd	nd	nd	nd
メタン生成細菌(MPN/ml)	nd	nd	nd	nd	nd
亜硝酸細菌 (MPN/ml)	nd	nd	nd	nd	nd
硝酸細菌 (MPN/ml)	8.00E 01	2.00E-01	nd	nd	nd
脱窒菌細菌 (MPN/ml)	3.30E+01	1.70E+01	2.30E+00	5.00E-01	1.90E+00
O2(mg/l)	nd	nd	nd	nd	nd
N2(mg/l)	36.8	37.2	38.4	35.4	36.4
H2(mg/l)	nd	nd	nd	nd	nd
He(mg/l)	nd	nd	nd	nd	nd
CH4(mg/l)	nd	nd	nd	nd	nd
CO(mg/l)	nd	nd	nd	nd	nd
ΣCO2(mg/l)	20.41	25.46	23.35	27.77	38.44
4.3BOX(meq/l)	0.58	0.56	0.52	0.63	0.91
H2CO3(mg/l)	0.14	0.07	0.09	0.07	0.05
HCO3(mg/l)	32.55	30.96	28.57	35.78	46.31
CO3(mg/l)	0.86	1.3	0.99	1.42	2.45
水温(℃)	11.4	11.5	13.2	12.3	18.2
pH	8.9	9.12	8.89	9.11	9.5
電気伝導度(μS/cm)	64.4	64.8	65.5	119	115
酸化還元電位(mV)	242.2	104.1	249.1	119.6	92.1
溶存酸素量	0	0	0	0	0

Chemical analysis of KH-1

Chemical Analyses of Water Samples from Kamaishi Mine

分析項目	単位	KH1-2	KH1-3	KH1-4	KH1-5	変動係数(%)	定量下限
Depth 採水深度(m)		102～236	237～337	338～411	412～500		
Date 調査年月日		95.7.7	95.7.7	95.7.7	95.7.7		
Sampling section 採水区間		区間2	区間3	区間4	区間5		
EC(25℃)	μS/cm	121	124	118	163	*	
pH		10.02	10.05	10.02	10.21	*	
Eh	mV	127	125	126	101	*	
DO	mg/l.	1.2	0.1	0.8	0.0	*	
Temp. 水温	℃	13.5	13.5	13.4	13.2	*	
O_2 (DO)	mg/L	N.D	N.D	N.D	N.D	*	1.0
N_2	mg/L	25.1	25.1	24.9	25.8	*	0.5
H_2	mg/L	0.095	0.087	0.091	0.115	1.86	0.2
He	mg/L	0.202	0.199	0.19	0.183	1.92	0.1
CO	mg/L	N.D	N.D	N.D	N.D	*	0.05
CH_4	μg/L	N.D	N.D	N.D	N.D	*	0.1
ΣCO_2 (IC)	mgC/L	5.84	5.96	5.93	5.23	1.25	0.05
TOC	mg/L	0.451	0.523	0.551	0.498	0.77	0.1
Fumic acid フミン酸	mg/l.	N.D	N.D	N.D	N.D	*	0.5
Fulvic acid フルボ酸	mg/L	N.D	N.D	N.D	N.D	*	1.0
4.8BX	meq/L	0.631	0.631	0.716	0.67	0.62	0.1
T-Si	mg/L	8.23	3.22	3.73	5.21	0.56	0.1
D-Si(Si^{4+})	mg/L	7.98	3.17	3.65	5.17	0.42	0.1
Na^+	mg/L	16.9	17.5	19.8	22	0.79	0.08
K^+	mg/L	0.087	0.067	0.18	0.13	0.69	0.06
Li^+	mg/l.	N.D	N.D	N.D	N.D	*	0.09
Ca^{2+}	mg/L	2	2.1	2.2	3	0.54	0.04
Mg^{2+}	mg/L	0.031	0.015	0.027	0.017	0.91	0.08
Sr^{2+}	mg/L	N.D	N.D	N.D	N.D	*	0.01
Al^{3+}	mg/L	N.D	N.D	N.D	N.D	*	0.04
T-Fe	mg/L	N.D	N.D	N.D	N.D	*	0.001
D-Fe	mg/L	N.D	N.D	N.D	N.D	*	0.001
Fe^{2+}	mg/L	N.D	N.D	N.D	N.D	*	0.001
T-Mn	mg/L	N.D	N.D	N.D	N.D	*	0.01
D-Mn	mg/L	N.D	N.D	N.D	N.D	*	0.01
ΣS^{2-}	mg/L	N.D	N.D	N.D	N.D	*	0.9
F^-	mg/L	1.49	1.58	N.D	N.D	0.58	0.03
Cl^-	mg/L	2.08	2.09	2.51	2.05	0.14	0.09
Br^-	mg/L	N.D	N.D	N.D	N.D	*	0.07
I^-	mg/L	N.D	N.D	N.D	N.D	*	0.06
SO_4^{2-}	mg/l.	8	8.8	9.3	18.7	0.89	0.1
T-P	mg/L	0.03	0.03	0.03	0.03	1.58	0.01
PO_4-P	mg/L	0.021	0.031	0.011	0.031	0.79	0.0001
T-N	mg/L	0.09	0.07	0.08	0.09	*	*
NH_4-N	mg/L	0.08	0.004	0.078	0.081	0.52	0.005
NO_2-N	mg/L	0.005	0.007	0.005	0.004	0.98	0.005
NO_3-N	mg/L	N.D	N.D	N.D	N.D	*	0.0001
δD	‰	-77.1	-76.8	-77.9	-81.1	*	*
$\delta^{18}O$	‰	-11.6	-11.7	-11.8	-12.3	*	*
3H トリチウム	TU	0.37	N.D	N.D	N.D	*	0.3

Chemical analysis of KG-1

Chemical Analyses of Water Samples from Kamaishi Mine

分析項目	単 位	KG-788	変動係数(%)	KG-492	KG-740	KG-788	定量下限
Depth 採水深度(m)		785～791		489～495	740～747	785～791	
Fiscal year 調査年度		1995		1994			
Date 調査年月日		95年11～12月		94. 12. 22～23	94. 11. 19	95. 2. 7～20	
sampling section 採水区間		区間2		区間14	区間5	区間2	
EC(25℃)	μS/cm	105. 1	*	81. 0	105. 9	117. 7	
pH		9. 42	*	9. 97	9. 33	8. 95	
Eh	mV	381	*	333	335	452	
DO	mg/L	0. 05	*	0. 19	0. 07	0. 00	
Temp. 水温	℃	13. 0	*	12. 4	14. 6	12. 4	
O_2	mg/L	N. D	*	*	N. D	N. D	1. 0
N_2	mg/L	26. 9	1. 69	*	45. 6	43. 2	0. 5
H_2	mg/L	0. 166	1. 58	*	0. 092	0. 094	0. 2
He	mg/L	0. 303	2. 09	*	0. 047	0. 052	0. 1
CO	mg/L	N. D	*	*	N. D	N. D	0. 05
CH_4	μg/L	0. 034	2. 23	*	N. D	N. D	0. 1
ΣCO_2 (IC)	mgC/L	8. 95	0. 84	6. 97	6. 74	9. 32	0. 14
TOC	mg/L	0. 632	0. 52	0. 42	0. 23	0. 82	0. 1
Humic acid フミン酸	mg/L	N. D	*	N. D	N. D	N. D	0. 5
Fulvic acid フルボ酸	mg/L	N. D	*	N. D	N. D	N. D	1. 0
4. 3BX	meq/L	0. 861	0. 84	0. 580	0. 571	0. 921	0. 1
T-Si	mg/L	2. 30	0. 68	7. 62	4. 53	3. 11	0. 1
D-Si(Si^{4+})	mg/L	2. 24	0. 53	7. 30	4. 00	2. 99	0. 1
Na^+	mg/L	18. 6	1. 08	11. 00	17. 30	14. 70	0. 08
K^+	mg/L	0. 450	0. 86	0. 62	0. 56	0. 77	0. 05
Li^+	mg/L	N. D	*	N. D	N. D	N. D	0. 09
Ca^{2+}	mg/L	8. 35	1. 24	6. 29	7. 21	6. 80	0. 04
Mg^{2+}	mg/L	0. 205	1. 54	0. 004	0. 100	0. 336	0. 08
Sr^{2+}	mg/L	N. D	*	0. 011	0. 009	0. 009	0. 005
Al^{3+}	mg/L	N. D	*	0. 311	0. 168	0. 121	0. 04
T-Fe	mg/L	N. D	*	0. 002	0. 0035	0. 00421	0. 001
D-Fe	mg/L	N. D	*	0. 001	0. 0031	0. 00120	0. 001
Fe^{2+}	mg/L	N. D	*	0. 002	0. 002	N. D	0. 001
T-Mn	mg/L	N. D	*	N. D	N. D	N. D	0. 01
D-Mn	mg/L	N. D	*	N. D	N. D	N. D	0. 01
ΣS^{2-}	mg/L	N. D	*	N. D	N. D	N. D	0. 9
F^-	mg/L	N. D	*	0. 189	0. 353	0. 0071	0. 03
Cl^-	mg/L	2. 78	0. 22	1. 86	2. 93	3. 51	0. 09
Br^-	mg/L	N. D	*	N. D	N. D	N. D	0. 07
I^-	mg/L	N. D	*	N. D	N. D	N. D	0. 06
SO_4^{2-}	mg/L	7. 6	0. 53	8. 93	17. 1	8. 57	0. 1
T-P	mg/L	0. 03	2. 00	0. 03	0. 03	0. 03	0. 01
PO_4-P	mg/L	0. 024	0. 97	0. 021	0. 018	0. 009	0. 0001
T-N	mg/L	0. 034	*	0. 06	0. 04	0. 04	*
NH_4-N	mg/L	0. 034	1. 05	0. 069	0. 044	0. 011	0. 005
NO_2-N	mg/L	N. D	*	N. D	N. D	N. D	0. 005
NO_3-N	mg/L	N. D	*	N. D	N. D	0. 032	0. 0001
δD	‰	-71. 0	*	-73. 0	-73. 1	-67. 5	*
$\delta^{18}O$	‰	-10. 6	*	-11. 1	-10. 6	-10. 1	*
3H トリチウム	TU	3. 1±0. 1	*	2. 8±0. 1	3. 1±0. 1	4. 7±0. 1	0. 3

* not analized

This page is intentionally left blank

APPENDIX B: RESULTS OF OUT-FLOW SOLUTION IODIDE ANALYSES

KB1am -1		KC1c-FF		KC1a-alt		KC1a-unalt	
Bottle Number	Collection Date (mm/dd/yy)	Bottle Number	Collection Date (mm/dd/yy)	Bottle Number	Collection Date (mm/dd/yy)	Bottle Number	Collection Date (mm/dd/yy)
3705	09/14/1999	1833	09/29/1999	1852	08/19/1999	1801	07/08/1999
5221	05/26/1999	5800	07/12/1999	4689	09/14/1999	2615	09/14/1999
11965	06/09/1999	7993	07/23/1999	5020	10/13/1999	4442	07/06/1999
12661	07/02/1999	9237	09/14/1999	7106	06/14/1999	9640	06/30/1999
14629	06/18/1999	11043	06/14/1999	7697	05/25/1999	11080	10/27/1999
14770	08/09/1999	15589	08/31/1999	8612	07/12/1999	12556	06/14/1999
18092	07/12/1999	16649	05/25/1999	9658	05/29/1999	17601	06/25/1999
21620	06/01/1999	19438	07/19/1999	10359	07/06/1999	17712	06/04/1999
21950	06/11/1999	19460	06/21/1999	12312	05/25/1999	18753	05/28/1999
22273	07/23/1999	20185	11/24/1999	14838	08/25/1999	19048	08/02/1999
23659	07/15/1999	20615	06/25/1999	17341	06/30/1999	21517	05/31/1999
26936	08/02/1999	23229	08/02/1999	23377	06/04/1999	23485	07/15/1999
29543	06/16/1999	24131	06/07/1999	23903	07/29/1999	26659	07/23/1999
32103	06/25/1999	24392	07/29/1999	26741	06/23/1999	26914	11/24/1999
33566	06/04/1999	26347	07/02/1999	26892	06/18/1999	28553	11/10/1999
36670	07/29/1999	29703	09/23/1999	27225	06/21/1999	28964	06/18/1999
37268	09/07/1999	31557	08/25/1999	27833	09/23/1999	35668	06/07/1999
37573	10/13/1999	31596	07/05/1999	31540	09/07/1999	35915	09/29/1999
37628	05/29/1999	32195	10/13/1999	32166	08/09/1999	40168	07/02/1999
38477	06/21/1999	33582	08/09/1999	33981	05/31/1999	41471	06/16/1999
44545	06/30/1999	33843	05/26/1999	36281	07/23/1999	41870	07/19/1999
44783	07/08/1999	34024	06/11/1999	38464	10/27/1999	48643	07/05/1999
45215	07/06/1999	36925	06/04/1999	38695	05/28/1999	48782	06/01/1999
47877	05/25/1999	37355	05/27/1999	39122	06/25/1999	50258	05/26/1999
49203	06/07/1999	39213	05/29/1999	40931	11/24/1999	53067	05/25/1999
49980	05/26/1999	39586	05/25/1999	44349	06/09/1999	55292	05/26/1999
52736	10/27/1999	41069	05/29/1999	44782	06/04/1999	61678	05/29/1999
53858	08/31/1999	45861	05/26/1999	48988	05/27/1999	62465	09/07/1999
54141	05/31/1999	49785	06/28/1999	49256	07/02/1999	66673	08/09/1999
54955	07/05/1999	51725	08/19/1999	57589	07/05/1999	67853	07/12/1999
55068	05/25/1999	52834	07/08/1999	60164	08/31/1999	70384	05/25/1999
62154	08/25/1999	53854	06/03/1999	61804	05/26/1999	71095	06/21/1999
64892	05/27/1999	56268	06/18/1999	62177	07/19/1999	72202	09/23/1999
67359	11/24/1999	58375	12/08/1999	62996	08/16/1999	73957	06/04/1999
69243	11/10/1999	61020	05/28/1999	64037	07/15/1999	74307	06/11/1999
72283	05/28/1999	62370	05/26/1999	68656	05/25/1999	79253	08/16/1999
77071	07/19/1999	62648	06/16/1999	72698	06/01/1999	80078	06/23/1999
78720	06/04/1999	63883	09/07/1999	74478	06/28/1999	88078	06/09/1999
82059	06/14/1999	65637	07/06/1999	75206	06/03/1999	88950	10/13/1999
83553	06/23/1999	67308	06/30/1999	76190	06/07/1999	90026	12/08/1999
85064	12/08/1999	72090	06/04/1999	76298	05/26/1999	90874	05/25/1999
85091	09/23/1999	81645	08/16/1999	79420	06/16/1999	91770	08/31/1999
86126	06/28/1999	90785	11/10/1999	85171	06/11/1999	91865	07/29/1999
86601	08/16/1999	90842	06/09/1999	86667	11/10/1999	93636	06/28/1999
88580	06/03/1999	93849	06/23/1999	87222	07/08/1999	93665	06/03/1999
90399	09/29/1999	94341	07/15/1999	88076	09/29/1999	97204	05/26/1999
90480	05/25/1999	95024	05/25/1999	91900	05/26/1999	97921	08/25/1999
94886	08/19/1999	97494	10/27/1999	92202	12/08/1999	98362	05/27/1999
95659	05/26/1999	98731	06/01/1999	92795	08/02/1999	99660	08/19/1999

UNLV
UNIVERSITY OF NEVADA LAS VEGAS

October 19, 2000

Susan Altman
Geohydrology Department
Sandia National Laboratories
P.O. Box 5800, MS0735
Albuquerque, NM 87185-0735

Dear Dr. Altman,

The concentration of iodide in the samples received in our laboratory on June 16, 2000 were analyzed using the following High Performance Liquid Chromatographic instrumentation and conditions:

SpectraSYSTEM P4000 gradient pump
SpectraSYSTEM AS1000 autosampler
SpectraSYSTEM UV1000 detector
Column: SUPELCOSIL™ LC-ABZ Plus column
15 cm x 4.6 mm; 5-µm particle size
Mobile phase: 0.05 M KH_2PO_4 (pH of 2.7) and *methanol or *acetonitrile
(*depending on optimal separation of iodide from background interferences)
Flowrate: 1mL/minute
Injection volume: 20µL
Detection wavelength: 230nm

A summary of the iodide concentrations in each sample, along with the corresponding analysis date, are listed in Table 1. Multiple measurements were made on many of the samples to assist in addressing precision.

Please feel free to contact me if you have any questions.

Thank-You,

Irene Farnham

Irene Farnham

Harry Reid Center for Environmental Studies
4505 Maryland Parkway • Box 454009 • Las Vegas, Nevada 89154-4009
(702) 895-3382 • Telex 62048164 UNLV/MSM • FAX (702) 895-3094

Table 1. Summary of Analytical Results

Sample Name	Iodide ppm	Analysis Date
1833	0.169	13Oct00
1852	0.047	17Oct00
1852	0.040	18Oct00
2615	<0.005	18Oct00
3507	0.730	13Oct00
3705	0.715	13Oct00
4442	0.006	17Oct00
4442	0.006	18Oct00
4689	<0.005	18Oct00
5020	0.738	13Oct00
5221	16.4	07Oct00
5800	0.343	13Oct00
7106	5.58	06Oct00
7106	5.62	06Oct00b
7106	5.70	16Oct00
7993	0.164	13Oct00
9237	<0.005	18Oct00
9640	<0.005	18Oct00
9658	4.84	06Oct00
9658	4.93	06Oct00b
9658	3.59	14Oct00
9658	5.08	16Oct00
10359	0.191	13Oct00
11043	10.9	07Oct00
11043	10.9	07Oct00
11080	<0.005	18Oct00
11965	0.984	10Oct00
12312	16.8	07Oct00
12556	<0.005	17Oct00
12556	<0.005	18Oct00
12661	4.81	06Oct00
12661	4.80	06Oct00b
12661	4.92	16Oct00
12662	5.05	14Oct00
14629	2.72	06Oct00
14629	2.77	06Oct00b
14629	2.83	16Oct00
14770	2.31	14Oct00
14838	0.070	17Oct00
14838	0.067	18Oct00
15589	<0.005	18Oct00
16649	434	07Oct00
16649	435	07Oct00

Table 1. Summary of Analytical Results Continued

Sample Name	Iodide ppm	Analysis Date
17341	0.253	10Oct00
17601	<0.005	18Oct00
17712	<0.005	18Oct00
18092	1.20	16Oct00
18092	1.19	16Oct00
18753	0.156	10Oct00
19048	<0.005	18Oct00
19438	0.054	17Oct00
19438	0.051	18Oct00
19460	6.30	06Oct00
19460	6.40	16Oct00
20185	0.249	13Oct00
20615	0.365	10Oct00
20615	0.368	10Oct00
21517	0.046	17Oct00
21517	0.044	18Oct00
21620	15.1	07Oct00
21950	0.563	10Oct00
22273	2.80	14Oct00
23229	0.135	13Oct00
23377	2.99	06Oct00
23377	3.05	06Oct00b
23377	3.17	16Oct00
23485	<0.005	18Oct00
23659	1.53	16Oct00
23900	0.030	17Oct00
23903	0.027	17Oct00
23903	0.019	18Oct00
24131	10.1	06Oct00
24131	10.2	06Oct00b
24131	10.3	16Oct00
24392	0.184	13Oct00
24392	0.178	13Oct00
26347	0.384	13Oct00
26659	<0.005	18Oct00
26741	1.16	14Oct00
26892	0.967	14Oct00
26914	0.197	13Oct00
26936	4.08	14Oct00
27225	2.93	06Oct00
27225	3.02	16Oct00
27833	1.85	14Oct00
28553	<0.005	18Oct00
28964	<0.005	18Oct00

Table 1. Summary of Analytical Results Continued

Sample Name	Iodide ppm	Analysis Date
29543	2.61	10Oct00
29543	2.03	14Oct00
29703	0.724	13Oct00
31540	<0.005	18Oct00
31557	<0.005	18Oct00
31596	0.278	13Oct00
31596	0.272	13Oct00
32103	3.13	10Oct00
32103	3.15	10Oct00
32195	0.445	13Oct00
33555	0.047	17Oct00
33555	0.033	18Oct00
33566	7.94	06Oct00
33566	7.98	06Oct00b
33566	8.19	16Oct00
33582	0.041	17Oct00
33582	0.034	18Oct00
33843	47.4	07Oct00
33999	5.04	14Oct00
34024	3.49	14Oct00
35668	<0.005	18Oct00
35915	<0.005	18Oct00
36281	0.019	17Oct00
36281	0.010	18Oct00
36670	4.19	14Oct00
36925	10.0	06Oct00
36925	10.1	06Oct00b
36925	10.4	16Oct00
37268	2.22	14Oct00
37355	28.8	07Oct00
37355	29.0	07Oct00
37573	3.63	14Oct00
37628	17.1	07Oct00
38464	0.446	13Oct00
38477	2.91	10Oct00
38477	2.99	14Oct00
38477	3.03	14Oct00
38695	5.85	06Oct00
38695	5.95	06Oct00b
38695	6.11	16Oct00
39122	0.579	10Oct00
39213	20.5	07Oct00
40168	<0.005	18Oct00
40931	0.522	13Oct00

Table 1. Summary of Analytical Results Continued

Sample Name	Iodide ppm	Analysis Date
41069	9.22	06Oct00
41069	9.37	06Oct00b
41069	9.61	16Oct00
41471	<0.005	18Oct00
41870	0.952	10Oct00
44349	2.31	06Oct00
44349	2.26	06Oct00b
44349	2.43	16Oct00
44545	5.68	06Oct00
44545	5.79	06Oct00b
44545	5.93	16Oct00
44782	4.26	06Oct00
44782	4.27	06Oct00b
44782	4.43	16Oct00
44783	1.74	16Oct00
44783	1.75	16Oct00
45215	2.53	06Oct00
45215	2.75	16Oct00
45861	54.4	07Oct00
47877	23.1	07Oct00
47877	23.2	07Oct00
48643	<0.005	17Oct00
48643	<0.005	18Oct00
48782	0.034	17Oct00
48782	0.030	18Oct00
48988	6.74	06Oct00
48988	6.86	06Oct00b
48988	6.98	16Oct00
49203	5.78	06Oct00
49203	5.75	06Oct00b
49203	5.89	16Oct00
49256	0.221	10Oct00
49785	0.396	10Oct00
49785	0.396	10Oct00
49980	23.4	07Oct00
50258	0.840	10Oct00
50258	0.842	10Oct00
51725	<0.005	18Oct00
52736	2.84	14Oct00
52834	0.301	13Oct00
53852	4.58	14Oct00
53854	5.45	06Oct00
53854	5.51	06Oct00b
53854	5.60	16Oct00

Table 1. Summary of Analytical Results Continued

Sample Name	Iodide ppm	Analysis Date
54141	17.1	07Oct00
54955	5.02	06Oct00
54955	5.06	06Oct00b
54955	5.18	16Oct00
55292	0.847	10Oct00
55292	0.855	10Oct00
56268	3.90	06Oct00
56268	3.85	06Oct00b
56268	4.02	16Oct00
57589	0.266	13Oct00
58375	0.117	13Oct00
58375	0.117	13Oct00
60164	0.021	17Oct00
60164	0.017	18Oct00
61020	27.1	07Oct00
61678	0.094	10Oct00
61804	7.45	06Oct00
61804	7.50	06Oct00b
61804	7.68	16Oct00
62154	1.32	14Oct00
62177	<0.005	18Oct00
62370	36.0	07Oct00
62465	<0.005	18Oct00
62648	15.8	07Oct00
62996	<0.005	18Oct00
63883	<0.005	18Oct00
64033	0.327	13Oct00
64037	0.320	13Oct00
64892	19.5	07Oct00
65637	0.233	13Oct00
66673	<0.005	18Oct00
67308	0.381	10Oct00
67308	0.382	10Oct00
67359	1.33	14Oct00
67853	<0.005	18Oct00
68656	133	07Oct00
69243	1.89	14Oct00
70333	1.25	14Oct00
70384	1.18	10Oct00
70384	1.19	10Oct00
71095	<0.005	18Oct00
72090	2.85	06Oct00
72090	2.87	06Oct00b
72090	3.04	16Oct00

Table 1. Summary of Analytical Results Continued

Sample Name	Iodide ppm	Analysis Date
72202	0.026	17Oct00
72202	0.022	18Oct00
72283	21.2	07Oct00
72698	2.80	06Oct00
72698	2.85	06Oct00b
72698	2.95	16Oct00
73957	<0.005	17Oct00
73957	<0.005	18Oct00
74307	<0.005	18Oct00
74478	0.370	10Oct00
75206	2.61	06Oct00
75206	2.72	06Oct00b
75206	2.81	16Oct00
75206	2.75	16Oct00
76190	3.11	06Oct00
76190	3.16	06Oct00b
76190	3.28	16Oct00
76298	10.4	10Oct00
77071	2.03	14Oct00
78720	120	07Oct00
79253	<0.005	18Oct00
79420	1.45	06Oct00
79420	1.60	14Oct00
80078	<0.005	18Oct00
81645	<0.005	18Oct00
82059	11.9	07Oct00
83553	3.03	10Oct00
83553	3.11	14Oct00
83553	3.17	14Oct00
85064	1.38	14Oct00
85091	3.51	14Oct00
85171	2.23	06Oct00
85171	2.26	06Oct00b
85171	2.39	16Oct00
86126	4.36	06Oct00
86126	4.41	06Oct00b
86126	4.53	16Oct00
86601	1.72	14Oct00
86667	0.261	13Oct00
87222	0.172	13Oct00
88076	0.973	14Oct00
88078	<0.005	18Oct00
88580	6.07	06Oct00
88580	6.19	06Oct00b

Table 1. Summary of Analytical Results Continued

Sample Name	Iodide ppm	Analysis Date
88580	6.21	16Oct00
88950	<0.005	18Oct00
90026	12.1	14Oct00
90026	12.0	14Oct00
90399	3.83	14Oct00
90480	195	07Oct00
90480	196	07Oct00
90785	0.369	13Oct00
90842	6.83	06Oct00
90842	6.87	06Oct00b
90842	6.95	16Oct00
90874	64.0	07Oct00
90874	64.2	07Oct00
91770	0.124	13Oct00
91865	<0.005	18Oct00
91900	10.5	06Oct00
91900	10.5	06Oct00b
91900	10.7	16Oct00
92202	0.389	13Oct00
92795	<0.005	18Oct00
93636	<0.005	18Oct00
93665	<0.005	18Oct00
93849	1.97	16Oct00
93849	1.99	16Oct00
94341	0.181	13Oct00
94341	0.179	13Oct00
94399	0.179	13Oct00
94886	2.18	14Oct00
94886	2.14	14Oct00
95024	46.6	07Oct00
95659	16.2	07Oct00
97204	0.775	10Oct00
97204	0.778	10Oct00
97494	0.249	13Oct00
97921	<0.005	18Oct00
98362	0.280	10Oct00
98731	5.98	06Oct00
98731	5.99	06Oct00b
98731	6.11	16Oct00
99660	<0.005	18Oct00
Blank	<0.005	17Oct00
Blank	<0.005	18Oct00

APPENDIX C: ESTIMATE OF MASS DIFFUSED OUT OF THE SAMPLE BASED ON OUTFLOW-SOLUTION ANALYSES

KB1am -1

Date Experiment Started			5/25/99								Total Expected Mass (mg)		891.3	
Time Experiment Started			10:35 AM								% Mass Recovery		27.51%	
Time (minutes) between start of experiment and bottle					14						Total Mass Recovered to date (mg)		245.2	
Note I concentration of 0 indicated a concentration below the detection limit of 0.005 mg/L											Expected Initial Concentration of I (mg/L)		76300	
Shaded Areas indicate estimates											Expected Porosity of Sample		0.033	
											Volume of Sample (cm^3)		354	

Bottle	Weight (with cap) (g)		Bottle attached to test cell			Bottle removed from test cell			Weight of	Mass of	Time elapsed	M/Mo	Cumulative	Iodide Conc.
Number	dry	wet	Date	Time (hr)	Time (min)	Date	Time (hr)	Time (min)	Water (g)	Iodide (mg)	since start (days)	In Sample	Mass (mg)	(mg/L)
55068	37.338	51.823	5/25/99	n/a	n/a	n/a	n/a	n/a	14.485			1.00		
90480	37.680	333.718	5/25/99	10	49	5/25/99	16	48	296.038	58.0	0.26	0.93	58.0	196
47877	102.163	958.408	5/25/99	16	48	5/26/99	8	10	856.245	19.9	0.90	0.91	77.9	23.15
95659	35.402	335.770	5/26/99	8	10	5/26/99	14	8	300.368	4.9	1.15	0.91	82.8	16.2
5221	37.493	197.362	5/26/99	14	8	5/26/99	17	11	159.869	2.6	1.28	0.90	85.4	16.4
49980	108.476	781.810	5/26/99	17	11	5/27/99	17	27	673.334	15.8	2.29	0.89	101.2	23.4
64892	103.902	642.915	5/27/99	17	27	5/28/99	16	17	539.013	10.5	3.24	0.87	111.8	19.5
72283	103.767	604.514	5/28/99	16	17	5/29/99	16	20	500.747	10.7	4.24	0.86	122.4	21.2
37628	103.224	1008.310	5/29/99	16	20	5/31/99	12	0	905.086	15.5	6.06	0.85	137.9	17.1
54141	104.051	764.615	5/31/99	12	0	6/1/99	18	0	660.564	11.3	7.31	0.83	149.2	17.1
21620	103.420	870.252	6/1/99	18	0	6/3/99	10	58	766.832	11.6	9.02	0.82	160.9	15.1
88580	66.124	623.050	6/3/99	10	58	6/4/99	12	31	556.926	3.4	10.08	0.82	164.3	6.15
78720	37.727	74.849	6/4/99	12	31	6/4/99	16	10	37.122	4.5	10.23	0.81	168.8	120
33566	103.833	928.690	6/4/99	16	10	6/7/99	17	26	824.857	6.6	13.29	0.80	175.4	8.04
49203	103.989	623.354	6/7/99	17	26	6/9/99	17	40	519.365	3.0	15.30	0.80	178.5	5.81
11965	103.493	501.750	6/9/99	17	40	6/11/99	10	0	398.257	0.4	16.98	0.80	178.9	0.984
21950	103.772	300.818	6/11/99	10	0	6/14/99	18	34	197.046	0.1	20.33	0.80	179.0	0.563
82059	68.698	378.678	6/14/99	18	34	6/16/99	17	15	309.980	3.7	22.28	0.80	182.7	11.9
29543	68.521	558.025	6/16/99	17	15	6/18/99	11	34	489.504	1.1	24.04	0.79	183.8	2.32
14629	103.741	1080.810	6/18/99	11	34	6/21/99	17	35	977.069	2.7	27.29	0.79	186.5	2.77
38477	103.306	720.353	6/21/99	17	35	6/23/99	16	13	617.047	1.8	29.23	0.79	188.4	2.98
83553	103.143	699.446	6/23/99	16	13	6/25/99	11	54	596.303	1.9	31.05	0.79	190.2	3.10
32103	102.109	1082.810	6/25/99	11	54	6/28/99	11	46	980.701	3.1	34.05	0.78	193.3	3.14
86126	103.164	817.372	6/28/99	11	46	6/30/99	16	34	714.208	3.2	36.25	0.78	196.5	4.43
44545	102.284	735.675	6/30/99	16	34	7/2/99	14	52	633.391	3.7	38.18	0.78	200.2	5.80
12661	102.362	1035.530	7/2/99	14	52	7/5/99	12	44	933.168	4.5	41.09	0.77	204.7	4.84
54955	69.006	427.373	7/5/99	12	44	7/6/99	14	36	358.367	1.8	42.17	0.77	206.5	5.08
45215	102.145	746.773	7/6/99	14	36	7/8/99	15	3	644.628	1.7	44.19	0.77	208.2	2.64
44783	102.410	1084.520	7/8/99	15	3	7/12/99	17	3	982.110	1.7	48.27	0.76	209.9	1.75
18092	102.352	764.262	7/12/99	17	3	15-Jul	16	1	661.910	0.8	51.23	0.76	210.7	1.20

KB1am -1

Bottle	Weight (with cap) (g)		Bottle attached to test cell			Bottle removed from test cell			Weight of	Mass of	Time elapsed	M/Mo	Cumulative	Iodide Conc.
Number	dry	wet	Date	Time (hr)	Time (min)	Date	Time (hr)	Time (min)	Water (g)	Iodide (mg)	since start (days)	In Sample	Mass (mg)	(mg/L)
23659	103.189	801.197	7/15/99	16	1	7/19/99	14	58	698.008	1.1	55.18	0.76	211.8	1.53
77071	103.018	960.260	7/19/99	14	58	7/23/99	13	36	857.242	1.7	59.13	0.76	213.6	2.03
22273	102.288	897.912	7/23/99	13	36	7/29/99	16	5	795.624	2.2	65.23	0.76	215.8	2.80
36670	102.049	627.665	7/29/99	16	5	8/2/99	14	35	525.616	2.2	69.17	0.76	218.0	4.19
26936	102.266	991.858	8/2/99	14	35	8/9/99	11	43	889.592	3.6	76.05	0.75	221.6	4.08
14770	102.488	1048.180	8/9/99	11	43	8/16/99	15	30	945.692	2.2	83.20	0.75	223.8	2.31
86601	102.873	498.415	8/16/99	15	30	8/19/99	15	35	395.542	0.7	86.21	0.75	224.5	1.72
94886	102.764	864.268	8/19/99	15	35	8/25/99	10	40	761.504	1.6	92.00	0.75	226.2	2.16
62154	102.755	896.637	8/25/99	10	40	8/31/99	10	57	793.882	1.1	98.02	0.75	227.2	1.32
53852	103.015	1045.480	8/31/99	10	57	9/7/99	15	0	942.465	4.3	105.18	0.74	231.5	4.58
37268	102.270	1017.250	9/7/99	15	0	9/14/99	13	47	914.980	2.0	112.13	0.74	233.6	2.22
3705	102.436	1171.400	9/14/99	13	47	9/23/99	10	42	1068.964	0.8	121.00	0.74	234.3	0.715
85091	102.393	411.280	9/23/99	10	42	9/29/99	11	29	308.887	1.1	127.04	0.74	235.4	3.51
90399	102.384	841.390	9/29/99	11	29	10/13/99	15	24	739.006	2.8	141.20	0.73	238.3	3.83
37573	102.755	771.568	10/13/99	15	24	10/27/99	11	58	668.813	2.4	155.06	0.73	240.7	3.63
52736	102.456	799.776	10/27/99	11	58	11/10/99	11	45	697.320	2.0	169.05	0.73	242.7	2.84
69243	102.282	806.612	11/10/99	11	45	11/24/99	11	51	704.330	1.3	183.05	0.73	244.0	1.89
67359	103.092	828.442	11/24/99	11	51	12/8/99	18	0	725.350	1.0	197.31	0.73	245.0	1.33
85064	66.006	207.135	12/8/99	18	0	12/13/99	13	1	141.129	0.2	202.10	0.72	245.2	1.38

KC1c-FF

Date Experiment Started			5/25/99								Total Expected Mass (mg)		872.9	
Time Experiment Started			10:35 AM								% Mass Recovery		34.87%	
Time (minutes) between start of experiment and bottle					13						Total Mass Recovered to date (mg)		304.3	
Note I concentration of 0 indicated a concentration below the detection limit of 0.005 mg/L											Expected Initial Concentration of I (mg/L)		76300	
Shaded Areas indicate estimates											Expected Porosity of Sample		0.069	
											Volume of Sample (cm^3)		165.8	

Bottle	Weight (with cap) (g)		Bottle attached to test cell			Bottle removed from test cell			Weight of	Mass of	Time elapsed	M/Mo	Cumulative	Iodide Conc.
Number	dry	wet	Date	Time (hr)	Time (min)	Date	Time (hr)	Time (min)	Water (g)	Iodide (mg)	since start (days)	In Sample	Mass (mg)	(mg/L)
39586	35.911	45.719	5/25/99	n/a	n/a	n/a	n/a	n/a	9.808	n/a		1.00		---
16649	35.500	323.389	5/25/99	10	48	5/25/99	16	50	287.889	125.4	0.26	0.86	125.4	434.5
95024	101.739	883.956	5/25/99	16	50	5/26/99	8	10	782.217	36.6	0.90	0.81	161.9	46.6
62370	35.826	335.239	5/26/99	8	10	5/26/99	14	9	299.413	10.8	1.15	0.80	172.7	36.0
45861	35.884	181.181	5/26/99	14	9	5/26/99	17	11	145.297	7.9	1.28	0.79	180.6	54.4
33843	109.005	720.642	5/26/99	17	11	5/27/99	17	25	611.637	29.1	2.28	0.76	209.7	47.4
37355	103.968	597.806	5/27/99	17	25	5/28/99	16	17	493.838	14.3	3.24	0.74	224.0	28.9
61020	103.714	559.196	5/28/99	16	17	5/29/99	16	20	455.482	12.4	4.24	0.73	236.4	27.1
39213	103.905	931.002	5/29/99	16	20	5/31/99	12	0	827.097	17.0	6.06	0.71	253.4	20.5
41069	103.579	706.612	5/31/99	12	0	6/1/99	18	0	603.033	5.7	7.31	0.70	259.1	9.40
98731	103.360	793.706	6/1/99	18	0	6/3/99	10	56	690.346	4.2	9.01	0.70	263.2	6.03
53854	66.154	579.467	6/3/99	10	56	6/4/99	12	30	513.313	2.8	10.08	0.70	266.1	5.52
72090	35.933	69.654	6/4/99	12	30	6/4/99	16	11	33.721	0.1	10.23	0.70	266.2	2.92
36925	103.368	858.366	6/4/99	16	11	6/7/99	17	25	754.998	7.7	13.28	0.69	273.9	10.2
24131	103.347	577.308	6/7/99	17	25	6/9/99	17	41	473.961	4.8	15.30	0.68	278.7	10.2
90842	103.172	479.751	6/9/99	17	41	6/11/99	10	0	376.579	2.6	16.98	0.68	281.3	6.88
34024	103.296	908.330	6/11/99	10	0	6/14/99	18	32	805.034	2.8	20.33	0.67	284.1	3.49
11043	68.212	269.861	6/14/99	18	32	6/16/99	17	17	201.649	2.2	22.28	0.67	286.3	10.9
62648	68.378	518.357	6/16/99	17	17	6/18/99	11	35	449.979	7.1	24.04	0.66	293.5	15.8
56268	103.368	997.702	6/18/99	11	35	6/21/99	17	36	894.334	3.5	27.29	0.66	296.9	3.87
19460	103.233	670.688	6/21/99	17	36	6/23/99	16	13	567.455	3.6	29.23	0.66	300.6	6.35
93849	103.020	648.376	6/23/99	16	13	6/25/99	11	55	545.356	1.1	31.06	0.65	301.6	1.98
20615	102.903	1004.820	6/25/99	11	55	6/28/99	11	47	901.917	0.3	34.05	0.65	302.0	0.366
49785	102.000	759.773	6/28/99	11	47	6/30/99	16	33	657.773	0.3	36.25	0.65	302.2	0.396
67308	103.046	680.541	6/30/99	16	33	7/2/99	14	52	577.495	0.2	38.18	0.65	302.5	0.382
26347	103.137	960.630	7/2/99	14	52	7/5/99	12	45	857.493	0.3	41.09	0.65	302.8	0.384
31596	68.597	397.280	7/5/99	12	45	7/6/99	14	37	328.683	0.1	42.17	0.65	302.9	0.275
65637	103.182	698.353	7/6/99	14	37	7/8/99	15	3	595.171	0.1	44.19	0.65	303.0	0.233
52834	102.421	1006.245	7/8/99	15	3	7/12/99	17	4	903.824	0.3	48.27	0.65	303.3	0.301
5800	101.826	738.072	7/12/99	17	4	7/15/99	16	2	636.246	0.2	51.23	0.65	303.5	0.343

KC1c-FF

Bottle	Weight (with cap) (g)		Bottle attached to test cell			Bottle removed from test cell			Weight of	Mass of	Time elapsed	M/Mo	Cumulative	Iodide Conc.
Number	dry	wet	te (mm/dd/	Time (hr)	Time (min)	te (mm/dd/	Time (hr)	Time (min)	Water (g)	Iodide (mg)	since start (days)	In Sample	Mass (mg)	(mg/L)
94341	101.852	779.149	7/15/99	16	2	7/19/99	14	59	677.297	0.1	55.18	0.65	303.6	0.180
19438	102.361	892.491	7/19/99	14	59	7/23/99	13	36	790.130	0.0	59.13	0.65	303.7	0.053
7993	102.490	834.816	7/23/99	13	36	7/29/99	16	4	732.326	0.1	65.23	0.65	303.8	0.164
24392	102.862	584.595	7/29/99	16	4	8/2/99	14	34	481.733	0.1	69.17	0.65	303.9	0.181
23229	102.087	919.746	8/2/99	14	34	8/9/99	11	44	817.659	0.1	76.05	0.65	304.0	0.135
33582	102.864	971.955	8/9/99	11	44	8/16/99	15	30	869.091	0.0	83.20	0.65	304.0	0.037
81645	102.835	466.542	8/16/99	15	30	8/19/99	15	35	363.707	0.0	86.21	0.65	304.0	0
51725	103.072	800.037	8/19/99	15	35	8/25/99	10	40	696.965	0.0	92.00	0.65	304.0	0
31557	103.219	829.975	8/25/99	10	40	8/31/99	10	58	726.756	0.0	98.02	0.65	304.0	0
15589	102.880	966.952	8/31/99	10	58	9/7/99	15	0	864.072	0.0	105.18	0.65	304.0	0
63883	102.920	942.300	9/7/99	15	0	9/14/99	13	47	839.380	0.0	112.13	0.65	304.0	0
9237	102.678	1081.680	9/14/99	13	47	9/23/99	10	42	979.002	0.0	121.00	0.65	304.0	0
29703	102.671	385.613	9/23/99	10	42	9/29/99	11	29	282.942	0.2	127.04	0.65	304.2	0.724
1833	102.796	780.467	9/29/99	11	29	10/13/99	15	24	677.671	0.1	141.20	0.65	304.3	0.169
32195	102.560	713.578	10/13/99	15	24	10/27/99	11	58	611.018	0.3	155.06	0.65	304.6	0.445
97494	103.017	742.731	10/27/99	11	58	11/10/99	11	45	639.714	0.2	169.05	0.65	304.8	0.249
90785	102.285	748.762	11/10/99	11	45	11/24/99	11	51	646.477	0.2	183.05	0.65	305.0	0.369
20185	103.113	770.166	11/24/99	11	51	12/8/99	18	0	667.053	0.2	197.31	0.65	305.2	0.249
58375	65.510	306.402	12/8/99	18	0	12/13/99	13	1	240.892	0.0	202.10	0.65	305.2	0.117

KC1a-alt

Date Experiment Started			5/25/99								Total Expected Mass (mg)		232.0	
Time Experiment Started			1:40 PM								% Mass Recovery		4.78%	
Time (minutes) between start of experiment and bottle attacheme						17					Total Mass Recovered to date (mg)		11.1	
Note I concentration of 0 indicated a concentration below the detection limit of 0.005 mg/L											Expected Initial Concentration of I (mg/L)		76300	
Shaded Areas indicate estimates											Expected Porosity of Sample		0.032	
											Volume of Sample (cm^3)		95	

Bottle	Weight (with cap) (g)		Bottle attached to test cell			Bottle removed from test cell			Weight of	Mass of	Time elapsed	M/Mo	Cumulative	Iodide Conc.
Number	dry	wet	Date	Time (hr)	Time (min)	Date	Time (hr)	Time (min)	Water (g)	Iodide (mg)	since start (days)	In Sample	Mass (mg)	(mg/L)
7697	37.513	41.623	5/25/99	n/a	n/a	n/a	n/a	n/a	4.110			1.00		---
68656	37.561	245.015	5/25/99	13	57	5/25/99	17	45	207.454	27.7	0.17	0.88	27.7	133
12312	102.208	959.792	5/25/99	17	45	5/26/99	8	37	857.584	14.4	0.79	0.82	42.1	16.8
61804	37.421	335.530	5/26/99	8	37	5/26/99	14	10	298.109	2.3	1.02	0.81	44.4	7.54
76298	37.563	185.804	5/26/99	14	10	5/26/99	17	38	148.241	1.5	1.17	0.80	45.9	10.4
91900	108.923	831.901	5/26/99	17	38	5/27/99	17	48	722.978	7.7	2.17	0.77	53.6	10.6
48988	103.613	679.322	5/27/99	17	48	5/28/99	16	43	575.709	4.0	3.13	0.75	57.5	6.86
38695	104.016	601.909	5/28/99	16	43	5/29/99	16	20	497.893	3.0	4.11	0.74	60.5	5.97
9658	103.515	1065.420	5/29/99	16	20	5/31/99	12	21	961.905	4.4	5.95	0.72	65.0	4.61
33981	103.321	719.503	5/31/99	12	21	6/1/99	18	0	616.182	3.1	7.18	0.71	68.1	5.040
72698	103.923	902.432	6/1/99	18	0	6/3/99	11	27	798.509	2.3	8.91	0.70	70.4	2.87
75206	66.472	615.509	6/3/99	11	27	6/4/99	12	28	549.037	1.5	9.95	0.69	71.9	2.72
23377	37.403	98.635	6/4/99	12	28	6/4/99	16	36	61.232	0.2	10.12	0.69	72.1	3.07
44782	104.782	920.890	6/4/99	16	36	6/7/99	17	57	816.108	3.5	13.18	0.67	75.6	4.32
76190	103.513	627.445	6/7/99	17	57	6/9/99	18	13	523.932	1.7	15.19	0.67	77.3	3.18
44349	103.359	519.040	6/9/99	18	13	6/11/99	10	0	415.681	1.0	16.85	0.66	78.2	2.33
85171	103.607	987.385	6/11/99	10	0	6/14/99	18	58	883.778	2.0	20.22	0.65	80.3	2.29
7106	67.131	380.738	6/14/99	18	58	6/16/99	17	41	313.607	1.8	22.17	0.65	82.0	5.63
79420	68.055	556.479	6/16/99	17	41	6/18/99	12	0	488.424	0.7	23.93	0.64	82.8	1.53
26892	103.950	1076.240	6/18/99	12	0	6/21/99	17	59	972.290	0.9	27.18	0.64	83.7	0.967
27225	103.099	724.640	6/21/99	17	59	6/23/99	16	40	621.541	1.9	29.13	0.63	85.6	2.98
26741	102.809	685.549	6/23/99	16	40	6/25/99	12	17	582.740	0.7	30.94	0.63	86.3	1.16
39122	102.172	1067.770	6/25/99	12	17	6/28/99	12	16	965.598	0.6	33.94	0.63	86.8	0.579
74478	102.388	810.921	6/28/99	12	16	6/30/99	16	59	708.533	0.3	36.14	0.62	87.1	0.370
17341	103.048	709.240	6/30/99	16	59	7/2/99	15	16	606.192	0.2	38.07	0.62	87.2	0.253
49256	102.078	1015.880	7/2/99	15	16	7/5/99	12	46	913.802	0.2	40.96	0.62	87.4	0.221
57589	68.285	416.786	7/5/99	12	46	7/6/99	15	3	348.501	0.1	42.06	0.62	87.5	0.266
10359	103.031	735.032	7/6/99	15	3	7/8/99	15	16	632.001	0.1	44.07	0.62	87.6	0.191
87222	103.076	1072.690	7/8/99	15	16	7/12/99	17	26	969.614	0.2	48.16	0.62	87.8	0.172

KC1a-alt

Bottle	Weight (with cap) (g)		Bottle attached to test cell			Bottle removed from test cell			Weight of	Mass of	Time elapsed	M/Mo	Cumulative	Iodide Conc.
Number	dry	wet	Date	Time (hr)	Time (min)	Date	Time (hr)	Time (min)	Water (g)	Iodide (mg)	since start (days)	In Sample	Mass (mg)	(mg/L)
8612	102.268	780.931	7/12/99	17	26	7/15/99	16	38	678.663	0.0	51.12	0.62	87.8	
64037	102.302	802.215	7/15/99	16	38	7/19/99	15	26	699.913	0.2	55.07	0.62	88.0	0.320
62177	102.268	935.138	7/19/99	15	26	7/23/99	13	36	832.870	0.0	59.00	0.62	88.0	0
36281	102.430	872.323	7/23/99	13	36	7/29/99	16	45	769.893	0.0	65.13	0.62	88.0	0.014
23903	102.007	607.748	7/29/99	16	45	8/2/99	15	8	505.741	0.0	69.06	0.62	88.1	0.023
92795	103.234	960.937	8/2/99	15	8	8/9/99	12	15	857.703	0.0	75.94	0.62	88.1	0
32166	102.457	1012.760	8/9/99	12	15	8/16/99	15	30	910.303	0.0	83.08	0.62	88.1	
62996	103.528	483.800	8/16/99	15	30	8/19/99	16	14	380.272	0.0	86.11	0.62	88.1	0
1852	103.576	832.813	8/19/99	16	14	8/25/99	10	40	729.237	0.0	91.88	0.62	88.1	0.044
14838	102.546	861.772	8/25/99	10	40	8/31/99	10	59	759.226	0.1	97.89	0.62	88.1	0.069
60164	103.149	1003.800	8/31/99	10	59	9/7/99	14	30	900.651	0.0	105.03	0.62	88.2	0.019
31540	103.331	977.056	9/7/99	14	30	9/14/99	14	20	873.725	0.0	112.03	0.62	88.2	0.000
4689	102.182	1121.600	9/14/99	14	20	9/23/99	10	43	1019.418	0.0	120.88	0.62	88.2	0.000
27833	103.255	399.937	9/23/99	10	43	9/29/99	12	9	296.682	0.5	126.94	0.62	88.7	1.85
88076	103.147	803.796	9/29/99	12	9	10/13/99	16	9	700.649	0.7	141.10	0.61	89.4	0.973
5020	102.439	735.977	10/13/99	16	9	10/27/99	11	56	633.538	0.5	154.93	0.61	89.9	0.738
38464	102.448	763.084	10/27/99	11	56	11/10/99	11	44	660.636	0.3	168.92	0.61	90.2	0.446
86667	102.235	768.015	11/10/99	11	44	11/24/99	11	51	665.780	0.2	182.92	0.61	90.3	0.261
40931	102.369	787.532	11/24/99	11	51	12/8/99	18	0	685.163	0.4	197.18	0.61	90.7	0.522
92202	66.173	315.442	12/8/99	18	0	12/13/99	13	1	249.269	0.1	201.97	0.61	90.8	0.389

KC1a-unalt

Date Experiment Started			5/25/99								Total Expected Mass (mg)		310.3	
Time Experiment Started			1:40 PM								% Mass Recovery		4.93%	
Time (minutes) between start of experiment and bottle a					18						Total Mass Recovered to date (mg)		15.3	
Note I concentration of 0 indicated a concentration below the detection limit of 0.005 mg/L											Expected Initial Concentration of I (mg/L)		76300	
Shaded Areas indicate estimates											Expected Porosity of Sample		0.031	
											Volume of Sample (cm^3)		131.2	

Bottle	Weight (with cap) (g)		Bottle attached to test cell			Bottle removed from test cell			Weight of	Mass of	Time elapsed	M/Mo	Cumulative	Iodide Conc.
Number	dry	wet	Date	Time (hr)	Time (min)	Date	Time (hr)	Time (min)	Water (g)	Iodide (mg)	since start (days)	In Sample	Mass (mg)	(mg/L)
53067	37.828	42.525	5/25/99	n/a	n/a	n/a	n/a	n/a	4.697			1.00		
90874	37.414	173.608	5/25/99	13	58	5/25/99	17	44	136.194	8.7	0.17	0.97	8.7	64.1
70384	102.816	962.929	5/25/99	17	44	5/26/99	8	37	860.113	1.0	0.79	0.97	9.8	1.18
55292	35.860	335.067	5/26/99	8	37	5/26/99	14	11	299.207	0.3	1.02	0.97	10.0	0.851
97204	37.515	222.894	5/26/99	14	11	5/26/99	17	37	185.379	0.1	1.16	0.97	10.2	0.776
50258	109.481	797.416	5/26/99	17	37	5/27/99	17	49	687.935	0.6	2.17	0.97	10.7	0.841
98362	103.875	652.513	5/27/99	17	49	5/28/99	16	43	548.638	0.2	3.13	0.96	10.9	0.280
18753	103.881	590.402	5/28/99	16	43	5/29/99	16	20	486.521	0.1	4.11	0.96	11.0	0.156
61678	103.262	1046.990	5/29/99	16	20	5/31/99	12	21	943.728	0.1	5.95	0.96	11.1	0.094
21517	103.137	755.378	5/31/99	12	21	6/1/99	18	0	652.241	0.0	7.18	0.96	11.1	0.045
48782	103.304	897.700	6/1/99	18	0	6/3/99	11	29	794.396	0.0	8.91	0.96	11.1	0.032
93665	66.090	602.782	6/3/99	11	29	6/4/99	12	19	536.692	0.0	9.94	0.96	11.1	0
73957	35.754	106.934	6/4/99	12	19	6/4/99	16	37	71.180	0.0	10.12	0.96	11.1	0
17712	103.404	919.880	6/4/99	16	37	6/7/99	17	58	816.476	0.0	13.18	0.96	11.1	0
35668	103.429	629.115	6/7/99	17	58	6/9/99	18	14	525.686	0.0	15.19	0.96	11.1	0
88078	103.992	522.154	6/9/99	18	14	6/11/99	10	0	418.162	0.0	16.85	0.96	11.1	0
74307	103.608	993.578	6/11/99	10	0	6/14/99	18	59	889.970	0.0	20.22	0.96	11.1	0
12556	66.730	382.802	6/14/99	18	59	6/16/99	17	42	316.072	0.0	22.17	0.96	11.1	0
41471	68.669	560.293	6/16/99	17	42	6/18/99	11	59	491.624	0.0	23.93	0.96	11.1	0
28964	103.132	1083.080	6/18/99	11	59	6/21/99	17	58	979.948	0.0	27.18	0.96	11.1	0
71095	103.269	729.839	6/21/99	17	58	6/23/99	16	41	626.570	0.0	29.13	0.96	11.1	0
80078	103.386	691.858	6/23/99	16	41	6/25/99	12	17	588.472	0.0	30.94	0.96	11.1	0
17601	102.100	1078.970	6/25/99	12	17	6/28/99	12	15	976.870	0.0	33.94	0.96	11.1	0
93636	102.246	817.355	6/28/99	12	15	6/30/99	16	58	715.109	0.0	36.14	0.96	11.1	0
9640	102.412	718.689	6/30/99	16	58	7/2/99	15	16	616.277	0.0	38.07	0.96	11.1	0
40168	101.970	1031.600	7/2/99	15	16	7/5/99	12	47	929.630	0.0	40.96	0.96	11.1	0
48643	68.979	423.399	7/5/99	12	47	7/6/99	15	2	354.420	0.0	42.06	0.96	11.1	0
4442	102.342	745.797	7/6/99	15	2	7/8/99	15	16	643.455	0.0	44.07	0.96	11.1	0.006
1801	102.970	1093.310	7/8/99	15	16	7/12/99	17	26	990.340	0.0	48.16	0.96	11.1	
67853	103.158	796.096	7/12/99	17	26	7/15/99	16	39	692.938	0.0	51.12	0.96	11.1	0

KC1a-unalt

Bottle	Weight (with cap) (g)		Bottle attached to test cell			Bottle removed from test cell			Weight of	Mass of	Time elapsed	M/Mo	Cumulative	Iodide Conc.
Number	dry	wet	Date	Time (hr)	Time (min)	Date	Time (hr)	Time (min)	Water (g)	Iodide (mg)	since start (days)	In Sample	Mass (mg)	(mg/L)
23485	102.358	816.699	7/15/99	16	39	7/19/99	15	27	714.341	0.0	55.07	0.96	11.1	0
41870	102.111	954.215	7/19/99	15	27	7/23/99	13	36	852.104	0.8	59.00	0.96	11.9	0.952
26659	102.986	889.861	7/23/99	13	36	7/29/99	16	44	786.875	0.0	65.13	0.96	11.9	0
91865	102.253	618.388	7/29/99	16	44	8/2/99	15	8	516.135	0.0	69.06	0.96	11.9	0
19048	103.248	979.924	8/2/99	15	8	8/9/99	12	15	876.676	0.0	75.94	0.96	11.9	0
66673	102.672	1032.910	8/9/99	12	15	8/16/99	15	30	930.238	0.0	83.08	0.96	11.9	0
79253	103.533	491.999	8/16/99	15	30	8/19/99	16	14	388.466	0.0	86.11	0.96	11.9	0
99660	103.495	848.194	8/19/99	16	14	8/25/99	10	40	744.699	0.0	91.88	0.96	11.9	0
97921	102.888	877.860	8/25/99	10	40	8/31/99	11	0	774.972	0.0	97.89	0.96	11.9	0
91770	102.819	1025.840	8/31/99	11	0	9/7/99	14	30	923.021	0.1	105.03	0.96	12.1	0.124
62465	103.599	999.225	9/7/99	14	30	9/14/99	14	20	895.626	0.0	112.03	0.96	12.1	0
2615	102.711	1147.780	9/14/99	14	20	9/23/99	10	43	1045.069	0.0	120.88	0.96	12.1	0
72202	102.642	406.728	9/23/99	10	43	9/29/99	12	9	304.086	0.0	126.94	0.96	12.1	0.024
35915	102.243	822.332	9/29/99	12	9	10/13/99	16	9	720.089	0.0	141.10	0.96	12.1	0
88950	102.404	756.223	10/13/99	16	9	10/27/99	11	56	653.819	0.0	154.93	0.96	12.1	0
11080	102.301	783.282	10/27/99	11	56	11/10/99	11	44	680.981	0.0	168.92	0.96	12.1	0
28553	102.429	790.724	11/10/99	11	44	11/24/99	11	51	688.295	0.0	182.92	0.96	12.1	0
26914	102.497	812.190	11/24/99	11	51	12/8/99	18	0	709.693	0.1	197.18	0.96	12.2	0.197
90026	65.377	322.299	12/8/99	18	0	12/13/99	13	1	256.922	3.1	201.97	0.95	15.3	12.0

DISTRIBUTION

Federal Agencies

1 Elizabeth O'Malley
US Department of Energy, EM-54
International Technology Exchange Staff
Cloverleaf
19901 Germantown Road
Germantown, MD 20874

Universities

1 Irene Farnham
Harry Reid Center for Environmental Studies
University of Nevada Las Vegas
4505 Maryland Parkway
Box 454009
Las Vegas, Nevada 89154-4009

Foreign Addresses

20 Masahiro Uchida
Japan Nuclear Cycle Development Institute
Tokai Works
4-33 Muramatsu, Tokai-mura, Ibaraki-ken
JAPAN 319-1194

1 Mikazu Yui
Japan Nuclear Cycle Development Institute
Tokai Works
4-33 Muramatsu, Tokai-mura, Ibaraki-ken
JAPAN 319-1194

5 Masao Shiotsuki
Japan Nuclear Cycle Development Institute
4-49 Muramatsu, Tokai-mura, Ibaraki-ken
JAPAN 319-1184

1 Kunio Ota
Japan Nuclear Cycle Development Institute
Tono Geoscience Center
959-31 Jorinji, Izumi, Tokishi
JAPAN 509-5102

1 Kenji Amano
Japan Nuclear Cycle Development Institute
Tono Geoscience Center
59-31 Jorinji, Izumi, Tokishi
JAPAN 509-5102

Internal

1	MS-0701	P. Davies, 6100
1	MS-0701	W. Cieslak, 6100
1	MS-0735	E. Webb, 6115
15	MS-0735	S. Altman, 6115
1	MS-0735	B. Chambers, 6115
1	MS-0735	S. McKenna, 6115
5	MS-0735	V. Tidwell, 6115
1	MS-0771	M. Chu, 6800
1	MS-0771	S. Pickering, 6800
1	MS-0972	C. Boney, 5735
12	MS-0731	NWM Library
1	MS-9018	Central Technical Files, 8945-1
2	MS-0899	Technical Library, 9616
1	MS-0612	Review & Approval Desk, 9612 For DOE/OSTI